THE
PHYSICAL REVIEW
A journal of experimental and theoretical physics established by E. L. Nichols in 1893

SECOND SERIES, VOL. 63, NOS. 3 AND 4 FEBRUARY 1 AND 15, 1943

Radioactive Isotopes of Lanthanum

KATHERINE E. WEIMER, M. L. POOL, AND J. D. KURBATOV
The Ohio State University, Columbus, Ohio

(Received December 11, 1942)

The radioactive isotope La^{140}, known to be produced by deuteron and slow neutron bombardments of lanthanum is found to have a half-life of 40.0±0.3 hours. This isotope has now been produced by the reaction $Ce^{140}(n, p)La^{140}$. Evidence for the occurrence of a *d, y* reaction has been obtained through the formation of La^{140} by the reaction $Ba^{138}(d, y)La^{140}$. The 40-hour isotope decays with the emission of 1.41±0.05-Mev electrons and 2.00±0.05-Mev gamma-rays. Deuteron and also proton bombardments of barium produce a new radioactive isotope of lanthanum of half-life 17.5±0.5 hours. This activity decays by the process of *K*-electron capture with the emission of x-rays identified as the characteristic *K* radiation of barium. The presence of a 0.88±0.1-Mev gamma-ray of low intensity indicates that the resulting barium nucleus may also be left in an excited state. This 17.5-hour activity is assigned to La^{137}.

INTRODUCTION

ARTIFICIAL radioactivity in lanthanum was first induced by a slow neutron activation of the oxide, from which a 45.6±4.8-hour activity, assigned to La^{140}, was obtained.[1] The determinations of the half-life of the lanthanum activity produced by different nuclear processes and described by several investigators vary to a rather large extent, namely, from 31 hours to 46 hours.[2–6]

It is the purpose of this paper to investigate more accurately the La^{140} period and in addition to describe a new 17.5-hour period found in lanthanum after activation of barium with deuterons and protons.

EXPERIMENTAL

All bombardments were carried out in the 42-inch cyclotron of The Ohio State University. The bombarding particles used were approximately 20-Mev alpha-particles, 10-Mev deuterons, 5-Mev protons, slow neutrons produced by the Be+*d* reaction, and fast neutrons from the Li+*d* reaction. Chemical separations were made after all activations except those with slow neutrons.

In all bombardments of lanthanum and cerium, Hilger H.S. brand oxides were used while, in the barium activations, Hilger "Specpure" barium chloride was used. A spectroscopic analysis accompanying the material revealed the following maximum impurities:

Lanthanum oxide, 99.9 percent, Lab No. 6404—very slight traces of Na, Mg, Ca, Bi, Sm; Gd, 0.015 percent; Nd, 0.1 percent.

Cerium oxide, 99.99 percent, Lab No. 6401—traces of Mg and Gd.

[1] J. K. Marsh and S. Sugden, Nature **136**, 102 (1935).
[2] M. L. Pool and L. L. Quill, Phys. Rev. **53**, 437 (1938).
[3] O. Hahn and F. Strassmann, Naturwiss. **27**, 11 (1939).
[4] O. Hahn and F. Strassmann, Naturwiss. **28**, 54 (1940).
[5] W. G. Chlopin, M. A. Passwik-Chlopin, and N. F. Wolkov, Nature **144**, 595 (1936).
[6] G. N. Glasoe and J. Steigman, Phys. Rev. **58**, 1 (1940).

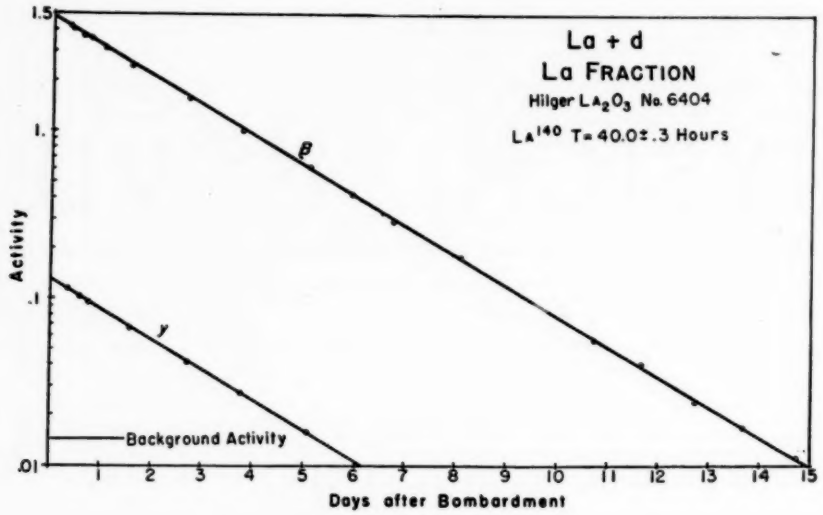

FIG. 1. Decay curve for lanthanum fraction from La+*d*.

Barium chloride, 99.98 percent, Lab No. 8442 —Ca, 0.0015 percent; Fe, 0.005 percent; Mg, less than 0.001 percent; Na, about 0.001 percent; Pb, 0.01 percent; and Sr, absent.

The other source of barium used was a special grade of the nitrate prepared by a modification of the method used in preparing barium for atomic weight determinations. Spectroscopic analysis of this material revealed that it was of a high degree of purity. Hilger cesium chloride was also bombarded in the course of the work.

Measurements of the radioactivity were made on a Wulf unifilar electrometer with an ionization chamber containing two atmospheres of freon, or, in some cases, on another Wulf unifilar electrometer with an ionization chamber having a 0.25-mil aluminum window and containing air at atmospheric pressure. The latter chamber was used in the detection of soft beta-radiation.

For the study of the emitted radiations, a Wilson cloud chamber of 15-cm diameter and a 180° focusing type magnetic spectrometer with a radius of curvature of 16 cm were available.

THE 40-HOUR PERIOD

A very intense 40.0-hour lanthanum activity emitting electrons and gamma-rays, was produced by the deuteron bombardment of the lanthanum oxide. The procedure used for the purification of lanthanum after activation was identical with that described for praseodymium.[7] Since the decay curve of the deuteron-activated lanthanum, shown in Fig. 1, was linear through 11 half-lives, a very reliable evaluation of the period could be made. From an average of three such determinations, the half-life was found to be 40.0±0.3 hours.

Activation of lanthanum with slow neutrons gave a value of 39.8 hours for the period of La^{140}. Although the activity produced in this case was weak compared to that produced by the deuteron bombardment, it yet was easily followed through several half-lives.

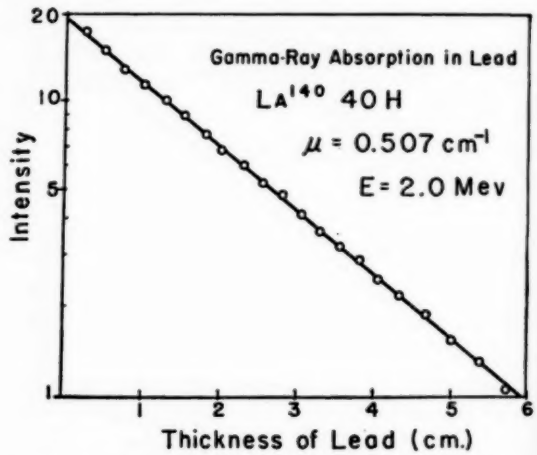

FIG. 2. Gamma-ray absorption in lead of 40-hour lanthanum.

[7] J. W. DeWire, M. L. Pool, and J. D. Kurbatov, Phys. Rev. **61**, 564 (1942).

After cerium was bombarded with fast neutrons a lanthanum fraction was separated from the cerium. The activity of the lanthanum fraction also decayed with a 40-hour period. This activity was likewise weak compared to that obtained by deuteron bombardment. The new reaction, $Ce^{140}(n,p)La^{140}$ seemed therefore to be established.

An energy of 2.0 Mev for the gamma-rays emitted by the 40-hour period has been determined by absorption in lead. Measurements, as shown in Fig. 2, made with a very strong source gave a single absorption coefficient of 0.507 ± 0.005 cm^{-1}, corresponding to an energy of 2.00 ± 0.05 Mev.

From aluminum absorption measurements, shown in Fig. 3, and from a beta-ray spectrum, shown in Fig. 4, taken with the magnetic spectrometer, the maximum energy of the beta-particles was estimated to be 1.41 ± 0.05 Mev. A tail of high energy Compton recoil electrons produced by the 2.0-Mev gamma-rays was observed in both cases.

In Fig. 5, a section of the periodic table is reproduced showing the assignments of and the reactions producing the various radioactive isotopes in the lanthanum region.

THE 17.5-HOUR PERIOD

A new radioactive isotope of lanthanum with a half-life of 17.5 hours has been found to be produced by bombardments of barium with 10-Mev deuterons. From the lanthanum fractions of these bombardments, complex decay curves were obtained; a portion of one is shown in Fig. 6. The longer period was observed to be 40 hours. Upon subtraction of this activity from the original curve, a period of 17.5 ± 0.5 hours resulted. Proton bombardment of barium gave only a 17.5-hour activity in the lanthanum fraction.

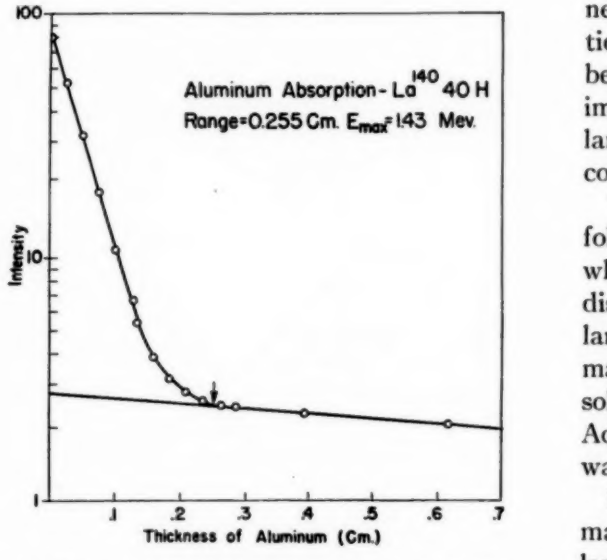

FIG. 3. Beta-ray absorption in aluminum of 40-hour lanthanum.

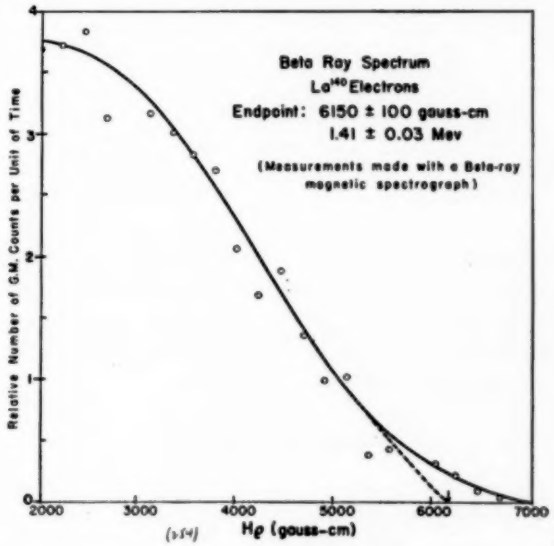

FIG. 4. Beta-ray spectrum of 40-hour lanthanum.

In order to observe the 17.5-hour period a careful separation of barium and lanthanum is necessary because of the very strong beta-radiation emitted by Ba^{139} of 85.6-minute period. It has been found that even 0.01 percent of this activity immediately after bombardment, if left in the lanthanum fraction, is sufficient to mask the correct evaluation of the 17.5-hour period.

The chemical procedures were arranged in the following manner: Bombarded barium chloride, which was contained in a platinum holder, was dissolved in nitric acid with the addition of lanthanum oxide. The radioactive chlorine was mainly removed by evaporation and the nitrate solution was converted into a chloride solution. Added platinic acid was reduced and platinum was filtered off.

Separation of barium and lanthanum was first made with ammonium hydroxide. Precipitated lanthanum was dissolved and reprecipitated as an oxalate in presence of stabilizers for active

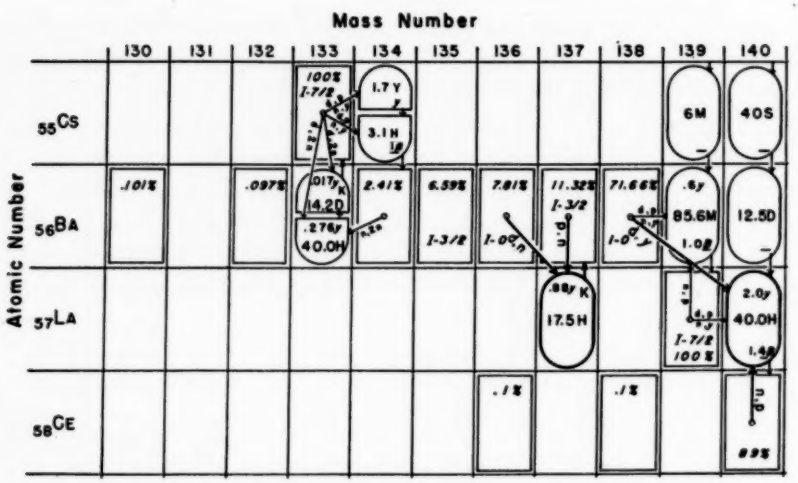

FIG. 5. Isotopic chart of the lanthanum region.

impurities other than those of the rare-earth group. Separate purification of lanthanum was performed from phosphoric acid to remove radioactive phosphorus, which was present because of the $Cl^{35}(n, \alpha)P^{32}$ reaction.

K-Electron Capture

The radiation from the 17.5-hour period consisted entirely of x-rays and gamma-rays as evidenced in the aluminum absorption curve of Fig. 7 and in the copper absorption curve of Fig. 8. Because of the presence of a low intensity gamma-ray, a gradual bending of these curves was observed. Upon subtraction of the activity of the gamma-ray in each case, new curves were obtained, from which were determined mass absorption coefficients of 0.86 cm^2/g in aluminum and of 9.11 cm^2/g in copper. These coefficients corresponded, respectively, to x-ray wave-lengths of 0.367A and 0.389A, or to an average wave-length of 0.378 ± 0.011A. The close agreement of this wave-length with the estimated mean wave-length, 0.376A, of the *K* series for barium, suggested at once that the radioactive lanthanum might be decaying by the process of *K*-electron capture.

The deuteron bombardment of barium could, however, give rise to a radioactive isotope of the stable La^{139}, which would then decay to the ground state by the emission of a gamma-ray. A possibility therefore exists that the x-rays observed might arise from the internal conversion of this gamma-ray. As the *K*-radiation produced in this case would be that of lanthanum while in the case of *K* capture it would be that of barium, a more refined measurement of the wave-length of these x-rays should make it possible to distinguish between the two processes.

Critical Absorption

The most widely used method for the determination of the wave-length of the x-rays emitted by radioactive substances is provided by critical absorption. From the data in Table I, it may be seen that tellurium should absorb the x-radiation from both barium and lanthanum strongly, but that iodine should absorb only about 20 percent of the barium x-rays as compared with 74 percent of the lanthanum x-rays. In addition, if the *K* radiation were that of lanthanum, the iodine

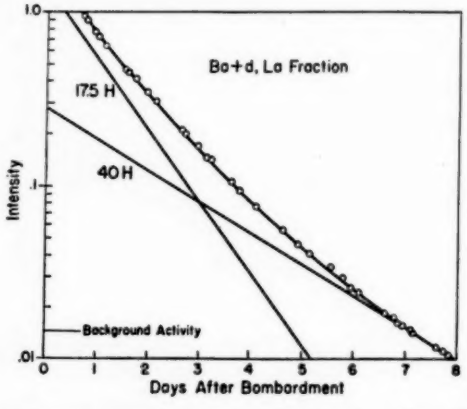

FIG. 6. Decay curve for lanthanum fraction from Ba+*d*.

absorption curve should reveal the presence of the two principal lines of the K series, one of which ($K\alpha_1$) would be absorbed and the other ($K\alpha_2$), transmitted.

Filters of powdered tellurium metal and of sodium iodide were therefore prepared for the purpose of determining the mass absorption coefficients of the x-rays in the two substances. The main source of error in measurements of this kind lies in the difficulty in preparing thin filters of uniform thickness.[8] An estimate of this error, for an extreme case, was made by measuring the absorption coefficients for the x-rays emitted by the 17.5-hour isotope with tin foils of 9.8 mg/cm² and with filters of 30-mesh tin powder. The coefficient obtained with the foils was 28.9 cm²/g, which is very nearly the true value, while with the powder, it was found to be only 12.6 cm²/g.

The x-rays from the 17.5-hour activity had a mass absorption coefficient, in tellurium, of 18 cm²/g. A correction, which was estimated from the tin absorption measurements just described, was made necessary by the fact that the thin filters of tellurium metal used were not homogeneous. The value of the absorption coefficient in tellurium then obtained was approximately 30 cm²/g, showing that the x-rays were strongly absorbed by the metal. This strong absorption was to be expected for either barium or lanthanum x-rays.

In iodine, a single mass absorption coefficient of 8.5 cm²/g was found for the x-rays from the 17.5-hour period. Correction for inhomogeneity was relatively small in this case. Barium x-rays would give a simple absorption curve in iodine, corresponding to a mass absorption coefficient estimated to be approximately 11.7 cm²/g. The observed value, 8.5 cm²/g, is in satisfactory agreement with this estimated coefficient. As the iodine was relatively transparent to the x-rays, the possibility that the K radiation was that of lanthanum seemed definitely excluded.

TABLE I. Data on K series lines of barium and lanthanum

K series line	$K\alpha_2$	$K\alpha_1$	$K\beta_1$	$K\beta_2$
Fraction of total intensity	0.26	0.53	0.16	0.05
Ba wave-length (A)	0.38899	0.38443	0.34022	0.33222
La wave-length (A)	0.37466	0.37004	0.32726	0.31966

Critical absorption limits: Te, 0.38926A; I, 0.37244A.

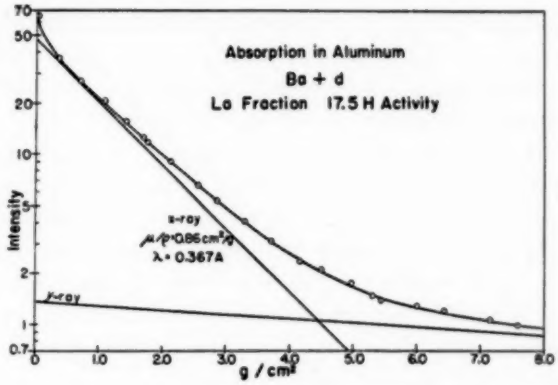

FIG. 7. Aluminum absorption curve for 17.5-hour lanthanum.

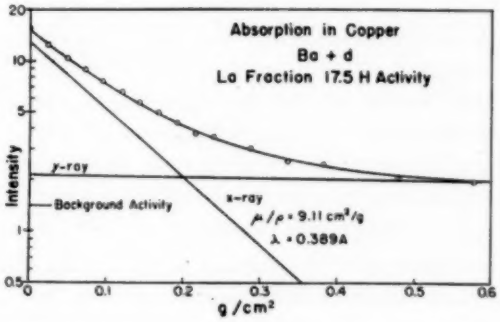

FIG 8. Copper absorption curve for 17.5-hour lanthanum.

The evidence from these critical absorption measurements, therefore, leads to the conclusion that the x-rays are those of barium and that, consequently the 17.5-hour isotope decays by the process of K-electron capture.

The 0.88-Mev Gamma-Ray

The gamma-ray observed in the aluminum and copper absorption measurements was also found to decay with a half-life of 17.5 hours. From lead absorption measurements, the energy of this penetrating radiation was determined to be 0.88 ± 0.1 Mev. Should this gamma-ray be internally converted, electrons of approximately 0.84 Mev would be produced. As no such electrons were observed, the possibility that the x-rays might arise from the internal conversion of this gamma-ray has been excluded independently of

[8] A. H. Compton and S. K. Allison, *X-Rays in Theory and Experiment* (D. Van Nostrand Company, Inc., New York, 1935), second edition, p. 517.

the indentification of the K x-rays as those of barium.

No positrons were observed in any of the cloud-chamber photographs taken of the 17.5-hour activity. This would indicate that K-electron capture is a very much more probable type of disintegration for this isotope than positron emission. The absence of annihilation radiation also confirmed the failure to observe positrons.

The number of x-rays relative to the number of gamma-rays is about 50 which means that in about two percent of the capture processes the barium nucleus is left in an excited state.

Assignment

The assignment of the 17.5-hour period has been made to La^{137} as illustrated in Fig. 5. Bombardments of cesium with alpha-particles and of lanthanum with fast neutrons failed to produce any activity in the lanthanum fractions other than a small amount of the 40-hour activity in the latter case. It seems therefore unlikely that the 17.5-hour activity can be due to either La^{136} or La^{138}. It is improbable that the lighter and less abundant isotopes of barium would produce an activity as intense as was obtained. In view of these considerations, the activity was assigned to La^{137}, which is probably produced by the reactions $Ba^{136}(d, n)La^{137}$ and $Ba^{137}(p, n)La^{137}$.

EVIDENCE FOR A d, y REACTION

A weak 40-hour period was observed in the lanthanum fractions from the deuteron bombardments of barium. The decay curve for one such fraction, shown in Fig. 6, has already been considered. It was found that the ratio of the intensity of the total radiation for this 40-hour activity to that of the gamma-radiation alone was of the same order of magnitude as that obtained previously for the 40-hour activity of La^{140}.

The activity of the 17.5-hour lanthanum calculated for an infinite bombardment, relative to that calculated for this 40-hour period remained practically constant in each of the several deuteron activations of barium. As the spectroscopic analysis for both sources of barium used in the bombardments showed the complete absence of lanthanum, there was no possibility of producing the 40-hour activity by a d, p reaction from a lanthanum impurity. It therefore seems reasonably certain that the reaction $Ba^{138}(d, y)La^{140}$ does take place.

There are only a few cases where an activity can be produced unequivocally by a d, y reaction. In general, the distribution of the stable isotopes is such that the more probable d, n or $d, 2n$ reactions will occur with a consequent masking of any contribution made by a d, y reaction.

The probability that the d, y reaction will occur in this particular case, relative to the occurrence of the d, n reaction was calculated to be 1 to 1300.

It is a pleasure to acknowledge the support received from Mr. Julius F. Stone and from The Ohio State University Development Fund. Acknowledgment is also made of the valuable assistance obtained through W.P.A. cyclotron project No. 65-1-42-89.

A Simple Method for the Investigation of Secondary Electrons Excited by γ-Rays and the Interference of These Electrons with Measurements of Primary β-Ray Spectra

LISE MEITNER
Forskningsinstitutet för Fysik, Stockholm, Sweden
(Received December 17, 1942)

It has been shown that the special directional distribution of the Compton electrons can be used to obtain their absorption curve and therefore their upper limit of energy without employing coincidence measurements. This fact has to be taken into account when inspecting primary β-spectra by absorption measurements. It has been found that the complexity of the primary β-ray spectrum of Fe^{59} reported by Livingood and Seaborg is apparently due to the interference of secondary electrons. Some problems connected with the directional distribution of the Compton electrons and concerning the efficiency of γ-counters are discussed.

IN a paper[1] dealing with the β- and γ-rays emitted by Sc^{46} we had found that under certain experimental conditions the secondary electrons excited by the γ-rays may be observed quite easily without using coincidence arrangement and it was pointed out that this fact has to be taken into account, when inspecting primary β-ray spectra by absorption measurements. It was also briefly mentioned that, in case only light elements such as Al are used, the presence of the secondary electrons is due to the special directional distribution of the Compton electrons, the greater part of these electrons moving at large angles relative to the direction of the γ-rays by which they are produced. So if the radioactive source is placed at some distance from a thin-walled aluminum counter the Compton electrons excited near the source and reaching the counter may be due in a large part to γ-rays which do not enter the counter at all. If the solid angle which the source subtends at the counter, is much smaller than π, a larger number of these electrons will enter into the counter than would correspond to the saturation number excited by the γ-rays impinging on the counter. Hence if absorbing foils of Al are inserted directly in front of the counter, one can obtain the absorption curve of these secondary electrons and in this way determine the energy of the respective γ-rays.

Of course, one can produce a surplus of secondary electrons as well by placing a lead absorber in front of the source and measure the absorption of the secondary electrons excited in the lead by inserting the absorbing Al foils in front of the counter. In this case one gets in addition to the surplus of Compton electrons an excess of photoelectrons as no comparable photoeffect takes place either in the wall of the counter or in the foils inserted in front of the counter.

The correctness of these statements has been proved by a series of experiments, a detailed report of which is to be published in the issues of the Academy of Sciences of Stockholm.

Here I shall mention only some of the main points.

To prove that actually the directional distribution of the Compton electrons can provide an excess of secondary electrons entering the counter the following experiment was carried out. A thick layer of metallic thorium emitting practically only the β- and γ-rays belonging to Th C +C″ was placed at 18-cm distance from a thin-walled aluminum counter. The source was covered with aluminum plates of 4-mm total thickness in order to cut off the primary β-rays and to get at the same time secondary electrons excited in the Al by the γ-rays. Two sets of measurements were made: first the Al plates placed in front of the source were 1.2×3.2 cm, secondly the plates had an area of 5×10 cm.

In the first case the activity found amounted to 184/min. When 4.1-mm Al (corresponding to the maximum range of the secondary electrons) was inserted directly in front of the counter, in order to absorb all the secondary electrons coming from the source, the activity obtained

[1] L. Meitner, Arkiv f. Mat. Astron. och Fysik, Stockholm **28B**, No. 14 (1942).

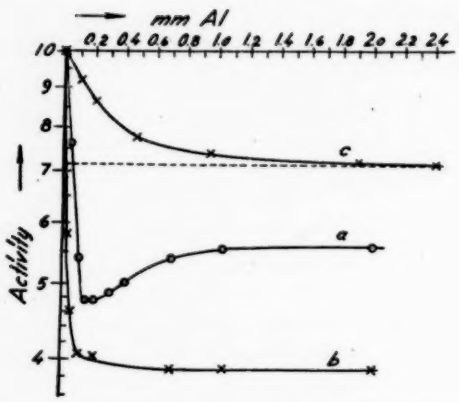

FIG. 1. Absorption curves of primary and secondary electrons of Sc^{46}.

was 146/min. In the second case the activity found with no absorber was 216/min., with 4.1-mm Al in front of the counter the rate was 147/min. The equality of the two values found with 4.1-mm Al in front of the counter proves that the surplus of activity obtained with the larger Al plates in front of the source and no absorber in front of the counter is actually due to additional excited Compton electrons (as is to be expected from their directional distribution) and is not produced by scattered γ-rays.

As to the entering of the secondary electrons into the measurements of the primary electrons there are two cases to be distinguished.

(1) The primary β-rays of the substance to be investigated have an upper limit of energy much lower than the maximum energy of the secondary electrons coupled with the emitted γ-rays. If the source is a thin layer, one will find, with the absorbers inserted closely in front of the source, that beyond the end of the primary β-ray spectrum an increase of the activity takes place because of the increasing number of excited electrons with increasing thickness of the aluminum absorbers. With the absorbers inserted in front of the counter the interference of the secondary electrons will be much smaller, because the γ-rays are not impinging at large angles upon the counter or upon the absorbing foils.

If the source is a thick layer, the absorption curve obtained with the absorbing foils in front of the source will, beyond the range of the primary β-rays, exhibit a constant value, as far, of course, as the absorption of the γ-rays is negligible and as far as the total thickness of the inserted absorbers is small in comparison with the distance between source and counter. Otherwise the surplus of Compton electrons reaching the counter decreases with increasing thickness of the absorbing foils, since more and more of these electrons are produced nearer to the counter. If the absorbing foils are placed in front of the counter, one gets in addition to the absorption curve of the primary β-rays the absorption curve of the secondary electrons.

Therefore in the case of a thick layer the curve for the primary β-rays is least disturbed by secondary electrons, if the absorbing foils are inserted as closely as possible in front of the source. At any rate if the two curves obtained with the absorbing foils in front of the source in comparison with those in front of the counter display differences in the ranges, one can conclude that there are secondary electrons entering into the measurements.

(2) The maximum energy of the secondary electrons is smaller than the upper limit of the primary β-ray spectrum. In this case the secondary electrons do not interfere with the determination of the upper energy limit for the primary β-rays. By absorbing the latter in Al foils inserted in front of the source, one can obtain the absorption curve of the secondary electrons (excited in the foils close to the source) by putting absorbing foils in front of the counter.

The following figures give some examples of the procedure described.

Figure 1 relates to experiments carried out with Sc^{46}. For the curves *a* and *b* we used a small and rather thin layer of Sc^{46} (as Sc_2O_3) supported by an Al sheet of 0.1-mm thickness. The source was placed at 5.5-cm distance from the Al counter. To exclude as far as possible scattering from the surroundings the counter was mounted on a plate of ebonite and no other material but wood was employed in the neighborhood of source and counter.

Curve *a* was obtained with the absorbing foils inserted in front of the source, curve *b* represents the measurements with the absorbers put in front of the counter. The absorbing foils were in both cases just sufficiently large to cover the source or the counter.

Curve *a* shows, beyond the end of the primary β-ray spectrum ($R=0.24$ mm Al, we take into

account the thickness of the counterwall), an increase of the intensity due to the formation of secondary electrons by the strong γ-line of 1.5-Mev energy.

Curve *b* exhibits in addition to the steep slope corresponding to the absorption of the primary β-rays a slight indication of a much flatter slope caused by a small number of additional secondary electrons. This number of secondary electrons excited in the thin layer of Sc_2O_3 itself did by chance nearly correspond to the saturation number of Compton electrons excited in the wall of the counter by the impinging γ-rays. It may be mentioned that without the interference of the secondary electrons curve *a* should begin with a steeper slope than curve *b*, because the scattering of the (primary) β-rays is more important in the former case than in the latter.

From the difference between the terminal values of both curves one can compute the excess of Compton electrons produced in Al placed closely to the source over the number produced in the Al when inserted in front of the counter. It amounted to 57 percent.

Curve *c* exemplifies the determination of the range of secondary electrons. The source was a sample of Sc^{46} [as $Sc_2(OH)_3$] which filled a glass tube of 0.8-mm thickness, surrounded by 0.5-mm Al. It was placed at 9-cm distance from the counter and the absorbing foils were inserted in front of the counter. All the electrons are, of course, of secondary origin. From the curve *c* (the dotted line represents the absorption of the γ-rays in Al) one deduces a range of 2.0 mm in Al, corresponding to a maximum energy of the electrons of 1.3 Mev, in very good agreement with the value to be expected from the γ-energy of 1.5 Mev.

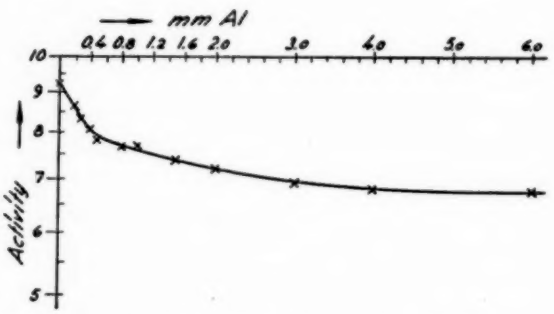

FIG. 2. Absorption curve of secondary electrons of the gamma-rays of ThC″.

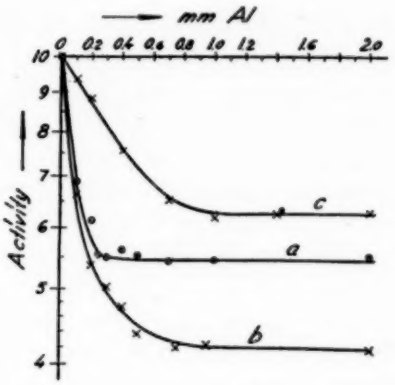

FIG. 3. Absorption curves of primary and secondary electrons of Fe^{59}.

In order to establish that this simple method can be used as well when more than one γ-line is present, experiments were carried out with the three γ-lines of 0.537-, 0.592-, and 2.65-Mev energy emitted by Th C″. Here the primary β-particles have an upper limit of energy larger, in fact comparable with the maximum energy of the secondary electrons excited by the γ-rays. The source, a thick sample of metallic Th was arranged at 18-cm distance from the counter, so that the rays were impinging nearly parallel upon the counter. The source was covered with 0.75-mm Pb+4-mm Al. The photoelectrons excited in the lead are absorbed in the Al and only Compton electrons excited in the Al reach the counter. Lead was chosen in order to absorb the γ-line of 0.24 Mev belonging to Th B and emerging at a small rate from the thick Th sample.

The curve of Fig. 2 relates to these measurements. It shows clearly a form different from that of curve *c* of Fig. 1, exhibiting two groups of secondary electrons with ranges of about 0.36-mm and of 4.2-mm Al. The energy corresponding to a range of 0.36 mm Al can only be estimated as lying between 0.4 and 0.45 Mev. The energy corresponding to a range of 4.2-mm Al is 2.40 Mev. The values to be expected from the γ-energies of 0.592 and 2.65 Mev are 0.41 and 2.42 Mev, respectively. The agreement of the measurements with these values is therefore rather good.

Measurements with Pb in front of the source instead of Al gave practically the same results.

THE PRIMARY β-SPECTRUM OF Fe^{59}

By investigating the β- and γ-rays of Fe^{59} we found an example where the complexity of the primary β-spectrum reported by Livingood and Seaborg[2] apparently has to be explained by the interference of secondary electrons. The authors found by inspecting the β-ray spectrum that most of the primary β-particles have a maximum range of 0.09 g/cm² Al while a small number extends to 0.35 g/cm² Al. In addition there is emitted a γ-line of about 1-Mev energy.

By carrying out experiments of the above described procedure with Fe^{59} the curves of the Fig. 3 were obtained.

The Fe^{59} was a thick layer of metallic iron. It was supported by a sheet of wood and placed at 8-cm distance from the counter. For the measurements given in curve *c* of Fig. 3 the source was covered with 4-mm Pb, because there was present a weak γ-radiation of about 0.25 Mev which I could not identify. It may be mentioned that for γ-rays of 1-Mev energy the energy of the photoelectrons excited in the *K* level of Pb is practically the same as the maximum energy of the Compton electrons. The absorbing Al foils were, of course, inserted in this set of measurements in front of the counter.

From the curve *a*, which was obtained with the absorbers in front of the source, one deduces for the primary β-particles a range of 0.36-mm Al corresponding to 0.098 g/cm², a value somewhat larger than that one found by Livingood and Seaborg. There is no indication of a second β-group.

Curve *b* exhibits in addition to the absorption of the primary β-rays a flatter slope due to the presence of the secondary electrons, the range of which is 1.1-mm Al or 0.30 g/cm². The same value is found in curve *c*, where, of course, only secondary electrons enter into the measurements. So the conclusion that Fe^{59} emits a single primary β-group is supported also by the measurements given in curve *c*.

The fact that the surplus of Compton electrons to be expected from their directional distribution is found in the described experiments, proves that the original directional distribution is not much disturbed by the scattering of the electrons when passing through the aluminum foils. It is, however, possible to investigate this point in a different way. Since no Compton electrons are excited at directions forming angles larger than $\pi/2$ with the incident γ-radiation, the back wall of the counter will have a noticeable influence only if it gives rise to an appreciable scattering of the Compton electrons. Hence the following experiment was carried out with γ-rays of about 1-Mev energy.

The wall of the counter facing the source was covered with 2-mm Al in order to insure that no secondary electron coming from the source entered into the counter. The intensity of the radiation was measured first when the back wall of the counter was not screened by any foils, secondly, when different foils of Al were placed closely to the back wall. If the Compton electrons excited in the back wall are noticeably scattered in Al, a large increase of the intensity is to be expected with increasing thickness of the foils inserted behind the back wall of the counter.

The values obtained with no Al, 0.1- and 0.5-mm Al, respectively, were $I_0 = 52$/min., $I_{0.1} = 53.7$/min., and $I_{0.5} = 56.6$/min. The increase is very small proving that the scattering in Al is not important and does not change the original directional distribution at a large rate.

If instead of the Al foils a Pb foil of 0.11-mm thickness corresponding to 0.4-mm Al was inserted closely to the back wall of the counter, the activity found amounted to 67/min. This large increase is due partly to the photoelectrons excited in the lead having originally an isotropic distribution, partly to the fact that the scattering of the (Compton) electrons is much more important in lead than in aluminum.

These results are of some significance when computing for different γ-energies the efficiency of γ-counters made of different materials. As long as a γ-radiation does not noticeably excite photoelectrons in the counter material and as long as the scattering of the (Compton) electrons is not important, the back wall of the counter does not contribute to the activity at the same rate as the front wall, as it was supposed usually.

The author wishes to express her sincere gratitude to Professor N. Bohr and Professor J. Jacobsen (Copenhagen) for the irradiation of the substances used in this work.

Acknowledgment is also made for a grant given by the Academy of Sciences of Stockholm.

[2] J. J. Livingood and G. T. Seaborg, Phys. Rev. **54**, 51 (1938).

Direct Determination of the Charge of the β-Particle[1]

YARDLEY BEERS*
Palmer Physical Laboratory, Princeton University, Princeton, New Jersey
(Received December 18, 1942)

The charge of radium E β-particles was measured by first measuring the charge carried per second by a magnetically analyzed beam and then, after the beam had been reduced by a known fraction by the decay of the source, by counting the number of particles per second in the beam. The average value obtained was $-4.80_0 \pm 0.03_5 \times 10^{-10}$ e.s.u. in agreement with the accepted value of the charge of the electron. Also a half-life of 4.99_0 days for radium E was observed. No dependence of either the charge or the half-life upon $H\rho$ was detected.

INTRODUCTION

THE method of this experiment[2] is to measure the current carried by a beam of radium E β-particles emerging from a β-ray spectrometer by means of a Faraday collector and a vacuum tube electrometer and then to replace the collector by a Geiger counter and to count the number of particles emerging per second. This is a modification of the method which has been used to measure the charge of the alpha-particle.[3] Until recent developments in Geiger counter technique it has not been possible to determine the charge of the β-particle in this way, but instead the first experiment of this type on β-particles[4] was performed to measure the efficiency of the counter for β-rays.

Because it was necessary to have a current larger than 5×10^{-15} ampere (3×10^4 electronic charges per second) for accurate current measurements while it was not possible to measure accurately counting rates greater than 300 per sec., for the counting measurements it was necessary to reduce the strength of the beam by a known fraction by allowing the source to decay for nearly ten half-lives. The amount of the decay could not be calculated accurately over such a long period of time from the known half-life of radium E because of impurities of radium D. Therefore the spectrometer was equipped with a second exit slit and set of baffles similar to the first ones through which the beam could be sent by reversing the magnetic field into an ionization chamber which could be connected to the vacuum tube electrometer. (See Fig. 1.) At the times of the collector current and counting measurements the corresponding ionization currents (I_S and I_W, respectively) were observed, these being measures of the relative strengths of the source. Then if e is the charge of the β-particle, I_F the collector current, and n' the number of counts per second,

$$I_F = n'e(I_S/I_W) \quad \text{or} \quad e=(I_F/I_S)/(n'/I_W) \quad (1)$$

(I_F, I_S, I_W, and n' are all measured at the same value of the magnetic field).

The collector current and both ionization currents were measured by means of an electrometer tube and the null method of Townsend,[5] in which the grid is maintained at zero potential by inducing upon it through a condenser a charge equal in magnitude but opposite in sign to that being measured. The current is given by the product of the condenser capacity C and the rate of change of potential V' supplied to the condenser such that the grid is maintained at zero potential. A condenser C_1 of small but very accurately known capacity was used for measurements of the small currents I_F and I_W, and a large condenser C_3 was used for the "strong" ionization current I_S. Hence Eq. (1) becomes

$$e=C_1\left(\frac{C_1}{C_3}\right)\frac{V_F'/V_S'}{n'/V_W'}, \quad (2)$$

* Now at Massachusetts Institute of Technology, Cambridge, Massachusetts.

[1] This paper contains a portion of a dissertation submitted to the faculty of Princeton University in partial fulfillment of the requirements for the degree of Doctor of Philosophy. Further information concerning this work can be obtained by consulting the complete dissertation, a copy of which is available for inter-library loan at the Princeton University Library.

[2] A preliminary report of this work has been published previously: R. Ladenburg and Y. Beers, Phys. Rev. **58**, 757 (1940).

[3] E. Schopper, Zeits. f. Physik **93**, 1 (1934); **94**, 649 (1935).

[4] A. F. Kovarik, Phys. Rev. **13**, 272 (1919).

[5] J. S. Townsend, Phil Mag. **6**, 603 (1903); H. G. S. Mosely, Proc. Roy. Soc. **87**, 230 (1912).

where the subscripts F, S, and W refer, as before, to the collector current and to the "strong" and "weak" ionization currents, respectively. It is to be noted that the absolute value of C_3 is not involved but only its ratio to C_1.

APPARATUS

The double β-ray spectrometer, Faraday collector, and the ionization chamber are illustrated in Fig. 1. The sides of the spectrometer were made of Armco iron blocks 18 cm×12 cm×1 in. which became the actual pole pieces when the apparatus was placed in position. These were held 6 cm apart by a brass frame which contained the entrance slit (4×15 mm), the two exit slits (2×40 mm), and the aluminum baffle system. These were designed to give as large an intensity as possible and still restrict the emerging beam to within 30 degrees to the normal of the exit slit so that the beam could easily be trapped in either the collector or counter. The radius of the trajectory was about 3 cm. The spectrometer and Faraday collector were evacuated to a pressure less than 10^{-4} mm Hg by means of a diffusion pump.

The magnetic field was measured by means of a flip coil and fluxmeter, the calibration of which could be checked with a mutual inductance. Because of uncertainty in the average radius, the absolute values of $H\rho$ given herein may be in error as much as 10 or 15 percent, but the results of this experiment depend only upon the accuracy of reproducing the magnetic field which is estimated to be about $\frac{1}{2}$ percent. As most of the measurements were made near the maximum of the spectrum, small errors in reproducing the field produced little effect upon the results.

The Faraday collector F (see Fig. 1) consisted of a rectangular box which, except for the bottom, was made of aluminum. In the bottom ($\frac{1}{16}$" brass) was cut a slit 9 mm ×48 mm. The inside surfaces were covered by graphite or soot. This box was suspended from the roof of a larger box by amber insulators so that its bottom was less than 2 mm above the exit slit of the spectrometer. The outer box served as an electrical shield, and it was made air-tight with wax so that it could be evacuated. Rough estimates of the efficiency of collecting β-particles entering the collector based upon consideration of the solid angle subtended by the slit

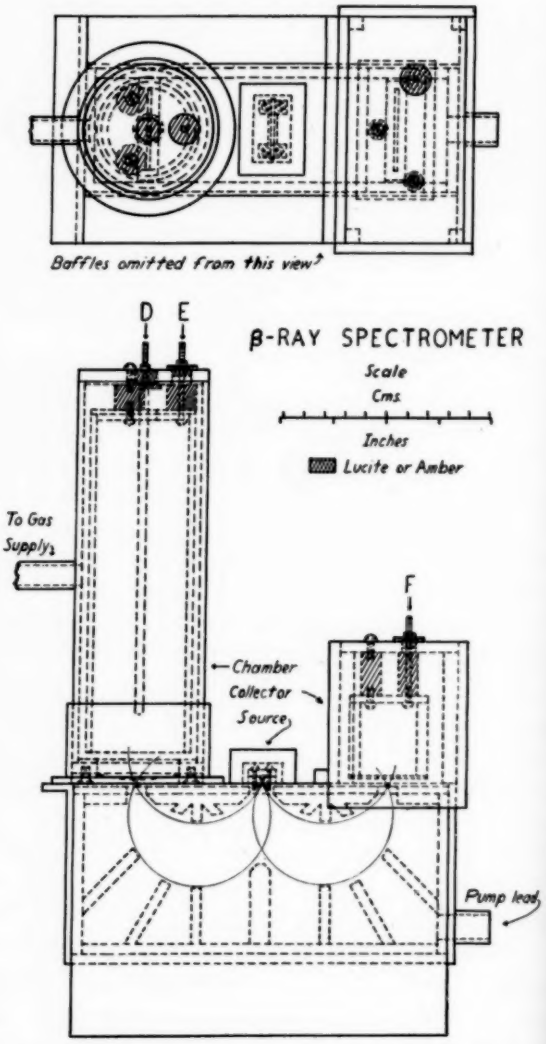

FIG. 1. Double β-ray spectrometer with Faraday collector and ionization chamber.

at the opposite wall and of the reflection coefficient of the surfaces[6] indicate that it was at least 99.5 percent.

The ionization chamber (see Fig. 1) consisted of a copper cylinder 2" in diameter and 18 cm long closed at its lower end by a copper gauze with a $\frac{1}{4}$" copper rod mounted coaxially. These were supported from the interior of an air-tight brass cylindrical case by amber insulators. For admitting the beam there was in the bottom of this case a hole $1\frac{1}{2}$" in diameter covered by an 0.1-mm aluminum foil which was held between two flat brass rings with Apiezon Q as a gasket. The foil could withstand a pressure difference of

[6] B. F. J. Schonland, Proc. Roy. Soc. **A108**, 187 (1925).

at least four atmospheres, and when the chamber was mounted in place with the spectrometer previously evacuated, it could be evacuated for filling. The pressure of the gas (argon) was measured by the aid of an open ended mercury manometer 2 meters long. The concentration of the gas (P/T) was maintained between 7.00 and 8.00 mm Hg/degree absolute (about 3 atmospheres). All measurements were corrected to a standard concentration of 7.50 mm Hg/degree absolute by use of some empirical correction factors found by determining the dependence of the ionization current due to a constant source upon gas concentration. The voltage upon the chamber was supplied by a 750-volt bank of "B" batteries. With the strongest source ever used, a reduction in the voltage to 400 volts caused the current to decrease by a factor of 0.997 ± 0.003 as a probable error, indicating that the systematic error in the final results due to imperfect saturation was very small, not more than 0.2 percent. The background current was about 4×10^{-15} ampere. The largest source of experimental error in the "weak source" measurements was due to fluctuations in this background current, mainly due to alpha-particle contamination of the chamber. Numerous precautions were taken to reduce this contamination to a minimum. The probable error in a determination of the background lasting for 450 seconds was 3.4×10^{-16} ampere.

The Faraday collector and ionization currents were measured by means of a vacuum tube electrometer employing a Western Electric D-96475 tube in a modified Barth circuit.[7] In order to reduce the grid (background) current, the entire grid circuit was placed in an evacuated shield. This current varied between $+6$ and $+12 \times 10^{-16}$ ampere, and the largest source of experimental error in the Faraday collector measurements was due to fluctuations in it. The probable error in a determination of the grid current which required 450 seconds was 5.8×10^{-17} ampere and seemed to be independent of the magnitude of the current. To obtain the most stable operating conditions, the electrometer circuit ran 24 hours a day, and the storage battery which supplied the power was charged by a trickle charger with an Acme-Delta voltage stabilizer on its input.

[7] D. B. Penick, Rev. Sci. Inst. **6**, 115 (1935).

This electrometer was operated according to the null method of Townsend,[5] as mentioned in the introduction. An especial advantage of this method is that the capacity of the grid and its circuit are not directly involved.

The three cylindrical condensers used with this electrometer were equipped with special shielding[1] so that the capacity between the lead wires was eliminated. The smallest of these condensers (referred to as C_1) was a primary standard of 11.77 ± 0.03 micromicrofarads. The largest condenser (referred to as C_3) was designed to have high capacity rather than to have high accuracy as a primary standard. Only the ratio of its capacity to that of C_1 is involved in the final result, as is explained in the introduction. This ratio was obtained by using both condensers to measure the same steady current and was equal to the reciprocal of the ratio of the corresponding rates of change of potential. In this way a value of 364.3 micromicrofarads was found for the capacity of C_3. C_1 was also compared by this same method with another primary standard C_2 and was found to be in excellent agreement with it. The value of C_2 found from its geometry was in good agreement with the calibration by the National Bureau of Standards.

The counters were made of 1″ diameter brass tubing. On one side was milled a flat place, in the center of which was cut a slit 48 mm $\times$ 6 mm over which was waxed a 4.65 mg/cm^2 aluminum foil. Into the ends were waxed closed glass tubes supporting the counter wire of 3-mil tungsten which was kept taut by a spring. To obtain a more uniform field the ends of the wire were shielded by $\frac{1}{4}$″ glass tubes which extended into the cylinder for 1″. These counters were normally filled by a mixture of 9 cm Hg of argon and 1 cm of alcohol and were self-extinguishing.[8] Only Apiezon wax was used as this absorbed alcohol very slowly, if at all. In the principal experiments no counter was used for more than a total of six million counts or later than ten days after its previous filling. Usually before filling the wires were heated in vacuum by passing a current of one ampere for several periods of a second or two. Only those counters with an essentially flat region in their plateaus were used; otherwise the measured counting rate could have no unambiguous

[8] A. Trost, Zeits. f. Physik **105**, 399 (1937).

connection with the true number of particles entering the counter. The absolute efficiency of these counters will be discussed later. The circuit consisted of a two-stage amplifier followed in turn by a pulse sign discriminator,[9] a vacuum scale of eight,[9] a thyratron scale of eight,[10] and a Cenco recorder. The method which was used to correct for losses in the counting rate due to the resolving time of the counter has been described elsewhere and will not be discussed here.[11] The radium E sources (practically free of radium D but containing radium F) were deposited upon 40-mil nickel wires from a solution containing about 7 millicuries of radium D and its products, which had been prepared previously in this laboratory from old radon tubes. The deposit was restricted to a portion of the wire 1 cm long by covering other portions with collodion. For work with the Faraday collector the source strength was usually 2 to 3 millicuries. The procedure used in depositing the sources was the usual one[12] but it should be mentioned that the process apparently depends critically upon the constitution of the wire. Pure nickel from Baker and Company of Newark, New Jersey gave very good results, but some wire from another manufacturer gave hardly any yield at all.

No difficulty was caused by the presence of radium F (polonium) in the source because the alpha-rays were prevented from entering the detecting devices by the magnetic spectrometer, and the gamma-rays were too weak to be observed when the source and counter were mounted in their normal positions.

FOIL CORRECTIONS; INFLUENCE OF SCATTERING AND OF SECONDARY ELECTRONS

The slit on the counter and the exit slit of the spectrometer were each covered by a 4.65-mg/cm² aluminum foil. A certain fraction of the beam is lost when the counter is used which is not lost with the Faraday collector (unless an equivalent amount of foils is placed in front of the collector). Therefore, if n' of formulae (1) and (2) is

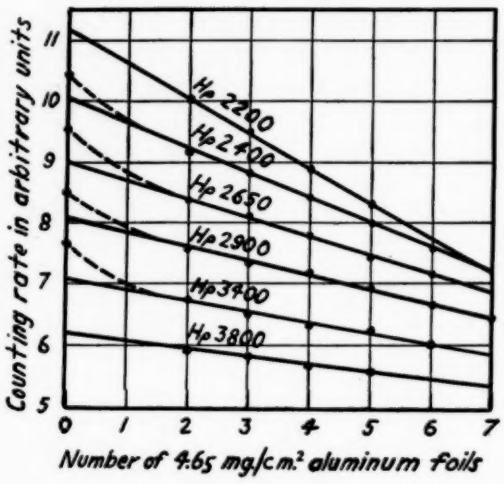

FIG. 2. Foil correction data. The counting rate is plotted against increasing foil thickness as extra foils are placed in front of the counter. The Geiger counter data are extrapolated to zero thickness (solid lines). Also is indicated (dashed lines) the behavior at small thicknesses as inferred from the Faraday collector measurements.

to be construed to be the observed counting rate (corrected, however, for resolving time losses), its value must be multiplied by a correction factor J.

One value of J (hereafter called J_g) can be found by placing additional foils between the counter and the spectrometer slit and measuring the corresponding counting rates due to a constant source. In Fig. 2 are plotted such data for the values of $H\rho$ which were of interest in the present work. Each point represents the average of two values involving 60,000 or more counts each. These data are well represented by straight lines which have been extrapolated to zero foil thickness (solid lines). The correction factor J_g is found by dividing the extrapolated value of the counting rate for zero foil thickness by the value for 2 foils.

Another value (hereafter denoted J_F) of this correction factor can be found by measuring the current from a constant source, first with no foils and secondly with two foils (connected electrically to ground) in front of the Faraday collector. J_F is given by dividing the first of these quantities by the second. Values of J_F (somewhat less accurate than the corresponding J_g values) were obtained at four of the same values of $H\rho$. These turned out to be consistently larger than the corresponding J_g values, the discrepancies being too large to be accounted for by errors in the

[9] H. Lifschutz and J. L. Lawson, Rev. Sci. Inst. **9**, 83 (1938); H. Lifschutz, Rev. Sci. Inst. **10**, 21 (1939).
[10] J. Giarratana, Rev. Sci. Inst. **8**, 390 (1937).
[11] Y. Beers, Rev. Sci. Inst. **13**, 72 (1942).
[12] O. Erbacher and K. Phillip, Zeits. f. Physik **51**, 309 (1928); W. F. Libby and D. D. Lee, Phys. Rev. **55**, 252 (1939).

measurements. It can be inferred that the behavior at small foil thicknesses must be according to the broken line curves of Fig. 2 and not according to the extrapolations of the straight lines.

There are two possible causes for a discrepancy between the values found by these two methods. If there are any secondaries ejected from the foil, these will be recorded separately by the collector but not by the counter, and J_f will be smaller than J_θ. On the other hand, if there are some very low energy particles emerging from the spectrometer after having been scattered therein, these are completely stopped in the first one or two foils, and will cause J_f to be larger than J_θ. The latter process gives the observed sign of the discrepancy, and it must be concluded that this is the predominant one. Therefore, it can be concluded that the value found with the collector (J_F) is the more reliable. Instead of attempting to measure this quantity accurately, however, there was employed in the final experiment the much simpler procedure of placing in front of the collector during the measurements of I_F a foil thickness equal to that used with the counter. Then the measured values of I_F and n' were used for the calculation of the charge, and no numerical correction was necessary.

Evidence for scattering was found by photographing the beam at a known distance from the exit slit. A slight indication that the beam was not confined entirely to within thirty degrees to the normal was detected. Particles emerging at large angles cause the measured value of the charge to be too large, for while they fail to enter the counter and are not recorded by it, they may be recorded by the collector even though they strike the outside surface.

Secondary electrons, if ejected from the foil into the collector, make the collector current too large, while secondaries ejected from the collector produce a reverse effect. Because of the large stray magnetic field, it is not to be expected that either effect is large, and the number of secondaries leaving the collector must be relatively very small because of solid angle considerations. To investigate the possibility of errors due to these sources an experiment was performed in which the foils were insulated from the spectrometer and in which various potentials were applied to them. The application of a positive potential gave no detectable effect, while negative potentials of 45 and 200 volts both gave an increase in current of about one percent, slightly greater than the probable error, which indicated that there might be secondaries of this amount being emitted from the foil in excess of those emitted from the collector.

As the pressure was normally 10^{-4} mm Hg or less it was unlikely that a large error could have been caused by the production of ion pairs. A rough calculation based on the specific ionization of β-particles, the length of path, and the pressure indicated that the probability that a β-particle produced one ion pair was about 0.01 percent. Also an experiment was performed in which the pressure was raised to 5×10^{-2} mm Hg with no appreciable change in collector current.

THE ABSOLUTE EFFICIENCY OF COUNTERS

The absolute efficiency of a counter has been shown to obey the following theoretical formula based upon an analogy with the mean free path theory of statistical mechanics. (The mean free path for producing a primary ion pair is the reciprocal of the primary specific ionization.)

$$E=100(1-e^{-KP}), \tag{3}$$

where

$$K=(\omega s d T_0/P_0 T), \tag{4}$$

s = number of primary ion pairs produced per unit path at standard pressure P_0 and temperature T_0; P and T are the pressure and temperature, respectively, of the gas in the counter; d = path of the particle in the counter; ω = probability that a primary ion pair causes the counter to discharge.

Some workers[13–15] have assumed that ω was equal to unity and have used the measured efficiencies of Geiger counters for determining the primary specific ionizations of the gas, while other workers[16] find that ω must be considerably less than unity if their data are to be consistent with values of s obtained by independent methods. All are agreed, however, upon a dependence of the efficiency on pressure of the type given by Eq. (3).

[13] W. E. Danforth and W. E. Ramsey, Phys. Rev. **49**, 854 (1936).
[14] M. Cosyns, Bull Tech. Ass. Ing. Brux. 173–265 (1936).
[15] T. Graf, J. de phys. et rad. [7], **10**, 513 (1939).
[16] J. DeVries and G. J. Sizoo, Physica **6**, 593 (1939) and references quoted therein.

If one assumes ω is unity and uses the following values: $s=29.4$ per cm at $P_0=76$ cm Hg (see reference 14), $d=1.9$ cm, $P=9$ cm Hg, and $T=T_0$ (assumed), the efficiency of the counters used in this work is calculated to be 99.94 percent.

For checking the absolute efficiency experimentally a method of comparing counters having different pressures was used. If two counters are used to measure the same beam of particles, the measured counting rates are proportional to their efficiencies. If E and E_α refer, respectively, to the efficiencies of two counters which have pressures of P and αP but which are identical otherwise,

$$E_\alpha/E=(1-e^{-\alpha KP})/(1-e^{-KP}). \qquad (5)$$

In practice e^{-KP} is a very small quantity and if α is roughly 2 or greater, this ratio becomes $1+e^{-KP}$ approximately.

Several comparisons were made of the efficiencies of counters having 1.1 cm Hg alcohol vapor in addition to 4.7, 9, and 12 cm argon, respectively. While these did not agree within the probable error there was no systematic dependence of efficiency upon pressure. The largest discrepancy was observed in one experiment in which a counter containing 9 cm argon gave a counting rate 2 percent greater than the others. Even if such a large change in efficiency could be shown to be attributed to changing the argon pressure from 4.7 cm Hg (P) to 9 cm Hg (αP), e^{-KP} must be not larger than 2 percent and the efficiencies of the higher pressure counters must be at least 99.9 percent except for the "inherent error" (that is, discrepancies between the counters which cannot be attributed to a change in pressure).

The "inherent error" was further investigated by comparing a number of counters all having the same pressure (9 cm Hg of argon and 1.1 cm Hg of alcohol), and these were found to disagree by amounts large enough to account entirely for the discrepancies observed with the counters having different pressures. Comparison of the five counters used in the final experiment of the charge of the β-particle showed that a probable "inherent" error of 1.2 percent should be assigned to each counter. This result was in agreement with earlier experiments of this type. Therefore, such errors are included in the summary of errors. (See Table III.) Otherwise, the counters are considered to have perfect efficiency.

The explanation of this "inherent" error is by no means clear, and this matter could bear further investigation. Undoubtedly some of it is connected with the fact that no counter has a perfectly "flat" plateau and that there is some uncertainty in selecting the correct operating voltage. A small amount of it may be due to temperature effects in the counter and in the voltmeter used to measure the counter voltage.

PROCEDURE

Altogether three separate sets of experiments upon the charge of the β-particle were carried out. The first two of these, especially the first set which was very rough, are to be regarded as preliminary experiments. The procedure of the final experiment, now to be described, was based upon the experience gained from the other two.

Separate sets of measurements were taken at each of five values of $H\rho$, and therefore five nearly independent values were obtained. A source of radium E having an original strength of roughly 3 millicuries was used. The Faraday collector measurements (with foils in front of the collector) were carried out during the first six days. The individual values at each $H\rho$ were corrected to their average time by the use of an assumed half-life of 5.00 days, and the corrected values were then averaged together. The ionization current was measured at intervals of about every three days until the currents were too small to be measured conveniently with the large condenser (C_3), 25 days after the start of the experiment. These values were corrected for decay to the average time of the corresponding set of collector measurements and then were averaged together. Various values of the half-life, differing only very slightly from 5.00 days, were tried until one was found which gave a minimum probable error in the average value, and the corresponding average value of I_S was divided into the average value of I_F to give the quantity I_F/I_S [see Eq. (1)].

While this quantity was obtained by determining average values of I_F and I_S and by calculating their quotient, the analogous "weak source" quantity, n'/I_W, was measured directly

by making practically simultaneous observations upon n' and I_W, and the individual values of n'/I_W were averaged for calculating the final result. In obtaining the individual values, first the beam was sent into the counter and a reading was made upon it (by using at least 75,000 counts) while simultaneously the background current of the ionization chamber was measured. Then the field was reversed and the beam was measured twice by using the ionization chamber while at the same time the background of the counter was determined. Then the field was reversed and measurements upon the beam with the counter and upon the background of the chamber, similar to the first ones, were taken. The average value of the counting rate was divided by the average value of the beam current (after these had been corrected for background) to give n'/I_W. In this way corrections for decay, which are unreliable with such an old source because of the possible presence of impurities, were usually avoided, though they were made when necessary (never greater than 0.2 percent). These measurements were started when the counting rate had decreased to 300 counts per second, some forty days after the experiment was started, and were continued for several days. At each of the five values of $H\rho$ a separate Geiger counter was used. The resolving time of each counter was measured three times: at the beginning, in the middle, and at the end of "weak source" measurements. The results of the resolving time measurements are published elsewhere.[11]

The largest source of experimental error in the collector current and "weak source" ionization current measurements was due to fluctuations in the background current. If the error caused by these fluctuations is assumed to be inversely proportional to the square root of the time duration of the reading,[17] it can be easily shown[1] that one obtains the greatest accuracy by dividing the available measuring time equally between the beam and background measurements. It can also be shown[1] that if all the individual values of the same quantity are to have the same relative accuracy, the time duration of each reading should be made inversely proportional to the square of the strength of the beam. (Therefore, there is little advantage to be gained in carrying on measurements on such quantities for more than one half-life.) These principles were followed throughout these measurements.

The first preliminary experiment was so rough that it is sufficient to say that it gave a result of the correct order of magnitude. The procedure of the second preliminary experiment is different from that of the final experiment in several respects. The foils were not placed in front of the collector, and therefore a numerical correction had to be made. Also only two counters were used, but each was used at all values of $H\rho$. As a weaker source was used and fewer observations were made, the results were not as accurate.

TABLE I. Results of second experiment.

$H\rho$	Charge of β-particle: Counter foil corrections used	Collector foil corrections used
2200	-1.62_7	—— $\times 10^{-10}$ coulomb
2400	-1.63_4	-1.58_2
2650	-1.67_7	-1.58_3
2900	-1.68_4	-1.60_4
3400	-1.69_3	-1.57_6
Unweighted average	-1.66_4	$-1.58_6 \times 10^{-10}$ coulomb
Or	-4.99	-4.75×10^{-10} e.s.u.

RESULTS

The results of the second preliminary experiment are given in Table I. While the foil corrections determined with the Faraday collector are the more reliable, values of the charge based upon both sets of corrections are given for comparison. It is to be noted that the values obtained with the counter foil corrections increase with $H\rho$, while those employing the collector foil corrections show no such dependence. The probable error in the average value is estimated to be less than 1.5 percent.

The results of the final experiment are shown in Table II and a summary of the experimental error of this experiment is given in Table III.

The first three items of Table III were found

[17] This assumption is based upon an analogy with the theory of counting (with a Geiger counter). If B counts are observed in a time T, the counting rate $N=B/T$. The mean error in B counts is $B^{\frac{1}{2}}$ and the mean error in N is $B^{\frac{1}{2}}/T=(N/T)^{\frac{1}{2}}$. Therefore, as N is constant, the error is inversely proportional to the square root of the time. This assumption is probably more valid in the case of the ionization current measurement, for the fluctuations in the background are mainly due to the alpha-particle contamination of the chamber than in the case of the collector current.

TABLE II. Results of final experiment.

$H\rho$	I_F (10^{-15} amp.)	I_S (10^{-12} amp.)	$I_F/I_S \times 10^3$ (pure number)	n'/I_W (reciprocal coulombs $\times 10^{15}$)	Charge $= \frac{I_F/I_S}{n'/I_W}$ 10^{-19} coulomb
2200	-9.35_8	-4.11_4	2.27_5	-1.42_6	-1.59_5
2400	-8.74_2	-4.64_4	1.88_2	-1.18_3	-1.59_2
2650	-8.78_8	-5.37_4	1.63_5	-1.01_3	-1.61_4
2900	-8.31_0	-5.59_0	1.48_7	-0.92_7	-1.60_4
3400	-7.01_2	-5.30_9	1.32_1	-0.79_5	-1.66_2
				Average	$-1.61_3 \times 10^{-19}$ coulomb
				Or	$-4.83_6 \times 10^{-10}$ e.s.u.

If the value at $H\rho$ 3400 gauss cm is excluded (see text) the average value is $-1.60_1 \times 10^{-19}$ coulomb or $-4.80_0 \times 10^{-10}$ e.s.u

TABLE III. Summary of experimental errors of final experiment.

Origin	Probable error at $H\rho$ 2200	2400	2650	2900	3400
Collector current	0.15%	0.07%	0.05%	0.18%	0.23%
"Strong source" ionization current	0.18%	0.11%	0.11%	0.11%	0.15%
"Weak source" measurements (n'/I_W)	0.34%	0.55%	0.23%	0.39%	0.30%
Error due to error in resolving time	0.15%	0.10%	0.07%	0.17%	0.16%
Inherent error of counter	1.2%	1.2%	1.2%	1.2%	1.2%
Total (square root of sum of squares)	1.3%	1.3%	1.2%	1.3%	1.3%

by application of the theory of error to the data. The fourth item was determined by the method described in another paper.[11] It is to be noted that the fifth item, the "inherent error" of the counter, is so much larger than the others that these can be nearly neglected and therefore the five values are essentially equally accurate. The probable error in the average value due to these items is found by dividing 1.3 percent by the square root of 5, giving 0.58 percent. These are not, however, the only experimental errors involved. Others to be included [see Eq. (2)] are: error in ratio of the condenser capacities 0.1 percent; error in calibration of small condenser 0.3 percent; and the error in the calibration of the potentiometer 0.1 percent. The total experimental error in the average value is 0.7 percent.

It is debatable whether the $H\rho$ 3400 value should be included because of the large discrepancy between it and the other values. If it is omitted, the average deviation between the remaining individual values is much smaller than one has a right to expect on the basis of Table III, while its inclusion leads to an average deviation of just the right size. It should be remarked, however, that the application of the theory of error to so few values is hardly justified. The discrepancy is probably largely due to the particular counter used for this value, which gave a lower value than the other counters when they were all used to measure the same beam. (This counter was No. 8 of Table I of the paper giving the resolving time data.[11]) If this value is omitted, the average becomes -1.601×10^{-19} coulomb or $-4.80_0 \times 10^{-10}$ e.s.u. with a probable error of 0.7 percent, which because of the reason just stated is to be considered as the final average of the present measurements.

In addition to these experimental errors, there were some systematic errors which are listed in Table IV. These have all been discussed previously.

DECAY OF RADIUM E

In the final experiment the decay of the source was followed until 50 days after the start. The half-lives used to correct the "strong source" ionization were found to predict the activity accurately except at the very end when a slight amount of radium D content became apparent. Because of this impurity these half-lives were 0.1 percent too large. The corrected values are shown in Table V. The probable error of each is about 0.2 percent, and they may be 0.2 percent too large because of a systematic error caused by imperfect saturation of the ionization chamber.

CONCLUSIONS AND DISCUSSION

(1) The charge of the β-particle is found to be $-4.80_0 \pm 0.03_5 \times 10^{-10}$ e.s.u., independent of the portion of the momentum spectrum from which the particles are selected. This value is in agreement within the uncertainty of the measurements with the charge of the electron of $-4.8025_1 \times 10^{-10}$ e.s.u.[18]

(2) The half-life of radium E is found to be 4.99_0 days with a probable error of 0.1 percent and is found to be independent of the portion of the momentum spectrum from which the particles are selected. This value is in fair agreement with that of 4.975 days found by Curtiss.[19]

(3) Geiger-Mueller counters can be used for absolute measurements with probable "inherent" errors of about one percent. This error was the largest single error in this work. Before any attempt is made to perform another experiment of this type in which counters are used the cause of this error should be investigated in the hope of building counters which agree with each other more accurately.

The electron multiplier suggests itself as a possible alternative to the Geiger counter in such an experiment. As the resolving time[20] is much smaller, it might be possible to make the counting measurements with the same strength of beam as is used for the collector measurements. Another advantage is that it requires no foils as it operates in a high vacuum. However, much development work must be done on this instrument before it can be used in such an experiment.

The ninety-degree type of β-ray spectrometer is much better suited to this work than the 180-degree type, which was used in the present experiment, for, according to Stephens,[21] the ninety-degree type brings the beam to a focus at a point outside the magnetic field. Therefore, the focal point can be made to be at the center of the detecting instruments (counter, collector, and ionization chamber) rather than at a point in front of their entrance slits. The source should be mounted at the bottom of the spectrometer rather than at the top so that active deposits could not fall into the spectrometer and contaminate it.

TABLE IV. Systematic error.*

Origin	Estimated upper limit	Sign
Imperfect efficiency of Faraday collector	0.5%	Negative
Scattering	—	Positive
Secondary electrons	1%	Positive
Imperfect saturation of ionization chamber	0.2%	Positive

* Positive and negative systematic errors are defined, respectively, as those which give too large and too small a magnitude of the charge of the β-particle.

TABLE V. Half-life of radium E.

$H\rho$	Half-life (days)
2200	4.97_5
2400	4.99_5
2650	4.99_5
2900	5.00
3400	4.98_5
Average	4.99_0

The method developed in the present work could be used for measuring the charge of the positive β-particle (positron), but there would be some difficulties not encountered in the present work. There would be an inherent error due to the annihilation gamma-rays. As it would be very difficult to prepare a source entirely free of negative particles, one would have to equip the apparatus with reliable shutters for measuring the background, while in the present experiment the background was measured by reversing the field, for the shutters which were included in the apparatus were not found reliable.

ACKNOWLEDGMENTS

The writer wishes to express his deep appreciation to Professor Rudolf Ladenburg, who suggested the problem and under whose direction the experiment was performed, for valuable advice and sympathetic encouragement; to Professor L. A. Turner for valuable discussions; to Dr. C. C. Van Voorhis for assistance in construction of some of the apparatus and in taking some of the measurements; and to Dr. Charles Rosenblum for assistance in preparing the sources.

[18] R. T. Birge, Rev. Mod. Phys. **13**, 233 (1941).
[19] L. F. Curtiss, Phys. Rev. **30**, 539 (1927).
[20] Z. Bray, Rev. Sci. Inst. **12**, 127 (1941); James S. Allen, Rev. Sci. Inst. **12**, 484 (1941).
[21] W. E. Stephens, Phys. Rev. **45**, 513 (1934).

Inelastic Scattering of Protons

ROBERT H. DICKE AND JOHN MARSHALL, JR.
University of Rochester, Rochester, New York

(Received December 17, 1942)

The proton energy lost in an inelastic collision with a nucleus reappears as an excitation energy of the nucleus. The measurement of the energy loss of inelastically scattered protons is a convenient method of determining the energies of nuclear excitation levels. Protons scattered at an angle of 135° by a thin scattering foil are detected by a proportional counter feeding a scaling circuit which is biased to count only the large pulses resulting from slowly moving protons. Aluminum stopping foils introduced between the scatterer and counter are used to slow down the scattered protons so that protons of a particular energy group move through the counter slowly and are counted. A plot of the number of counted protons against stopping foil thickness gives a curve in which peaks appear for different proton energy groups. Well-defined peaks corresponding to inelastically scattered protons are obtained for a number of substances and excitation energies are computed.

INTRODUCTION

IF a proton approaches a nucleus closely, any one of several things may happen. The proton may be scattered elastically so that the total kinetic energy after collision is the same as before. On the other hand, it may be scattered inelastically so that the nucleus is left in an excited state. Another possibility would be nuclear transformation induced by the proton. An example of this would be the (p, α) reaction.

Inelastic scattering can be thought of as a (p, p) reaction in which the proton enters the nucleus, and later a proton leaves it with a lower kinetic energy than that of the original proton, thus leaving the nucleus in an excited state. It has been shown that in general a (p, n) reaction is more likely to occur than a (p, p) reaction.[1] In the case of a (p, p) reaction, the proton must penetrate the Coulomb barrier in order to leave the nucleus. This is not the case for the neutron in a (p, n) reaction. Thus, if a (p, n) reaction is energetically possible, one would expect to observe very little inelastic scattering of protons. The substances most suitable for the observation of inelastic scattering then are those which have high (p, n) thresholds.

Heavy elements are, in general, unsuitable for inelastic scattering experiments because of the difficulty of penetration of the Coulomb barrier. In general, the substances most favorable for inelastic scattering are light elements with high (p, n) thresholds.

Wilkins and Kuerti,[2] Wilkins and Wrenshall,[3] and Wilkins,[4] using their photographic emulsion technique, observed the inelastic scattering of protons. From their work levels were found in Mg and Al. Their values agree fairly closely

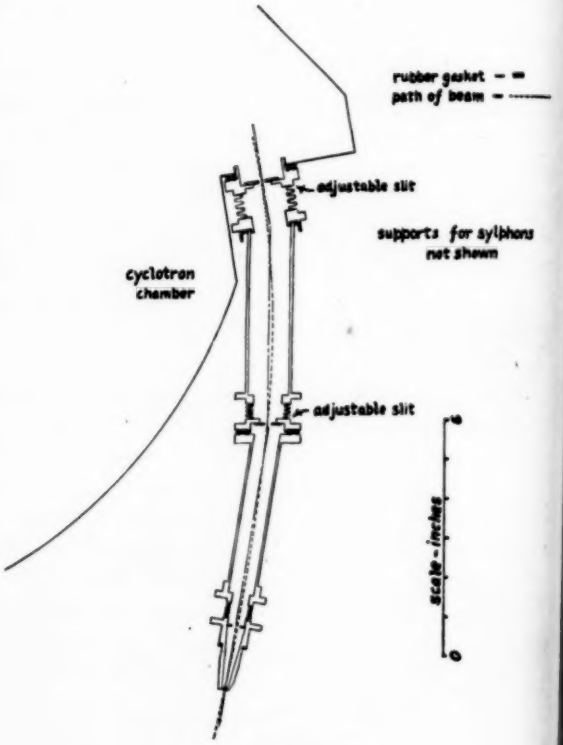

FIG. 1. Slit system.

[1] V. Weisskopf and D. Ewing, Phys. Rev. **57**, 472 (1940).

[2] T. R. Wilkins and G. Kuerti, Phys. Rev. **57**, 1081 (1940).

[3] T. R. Wilkins and G. Wrenshall, Phys. Rev. **58**, 758 (1940).

[4] T. R. Wilkins, Phys. Rev. **60**, 365 (1941).

with those given here. In the case of aluminum, there is agreement with a known γ-ray energy.

APPARATUS

The University of Rochester cyclotron gives a proton beam of approximately 6.9-Mev energy. The beam, however, is not completely homogeneous. To get a monochromatic beam of protons from the cyclotron, one may bring out the beam through a system of slits in the fringing field of the cyclotron magnet. With three slits it is possible to get as nearly monochromatic a beam as is desired by making the slits narrow enough. The system of slits used is shown in Fig. 1. The slit system is open to the cyclotron vacuum and the exit slit is covered by an aluminum window.

Figure 2 shows the scattering chamber, monitoring ionization chamber, and proportional counter used in these experiments. The foil is mounted in the center of the chamber which is evacuated to eliminate scattering from air around the foil. A small ionization chamber is mounted at the rear of the scattering chamber for the purpose of monitoring the beam. The window through which the scattered protons leave the chamber is mounted at an angle of 135° from the direction of the incident protons. It is composed of a thin aluminum foil waxed onto a supporting grid. After the scattered protons leave this window, they pass through an aluminum stopping foil and enter a proportional counter.

The proportional counter was filled to a pressure of 20 cm with commercial argon and operated a scale of 32 through a pulse amplifier. The scaling circuit could be adjusted to respond to pulses of various sizes.

There are, in general, two methods of range measurement. If the scaling circuit bias is adjusted so that all protons are counted but that the γ-ray background is not counted, we speak of the "plateau method." If the number of protons counted is plotted against absorber thickness, we obtain a step-like curve with a step at every proton energy group. If on the other hand, the bias is adjusted so that only the largest pulses are counted, we speak of the "peak method." Only very slowly moving protons can produce pulses which are large enough to be counted, and a plot of number of protons against number of absorbers gives a curve with peaks corresponding to the proton energy groups. This is illustrated in Fig. 3, which is a plot of number of recorded proton pulses against thickness of stopping foils for various scaling circuit biases.

A remote control system employing selsyn motors was used for changing the absorber foils. The absorber foils were cemented over holes around the edge of a large aluminum disk. This

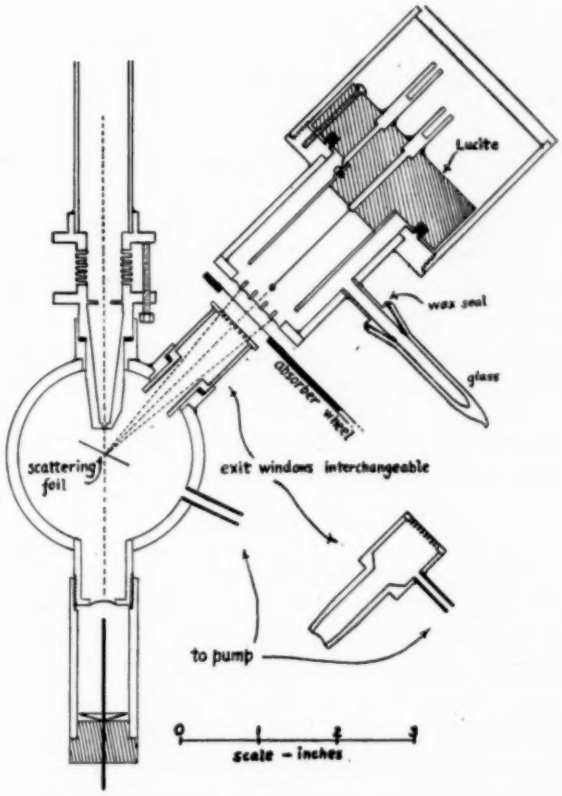

FIG. 2. Scattering chamber and counter.

disk was coaxial with a gear which was driven by a one-tooth pinion mounted on the selsyn motor shaft. Thus one revolution of the selsyn motor changed from one absorber foil to the next.

The absorber foils were calibrated by comparing their stopping power with that of air, by the use of the proportional counter as a detector. The foils were built up in multiple layers of approximately $\frac{1}{4}$ mil of aluminum foil. It was found that each of these $\frac{1}{4}$-mil absorbers was equivalent to 1.10 cm of air at 15°C and 760 mm of mercury. Proton energies were

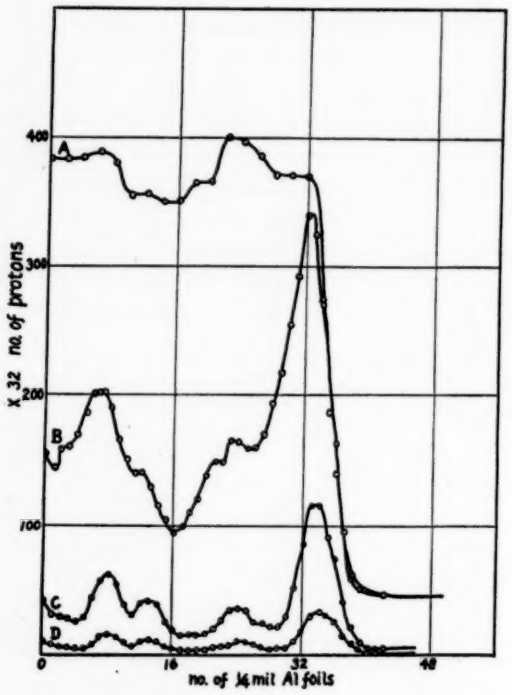

FIG. 3. Effect of scaling circuit bias on scattering curves of aluminum.

calculated from their ranges in aluminum and Livingston and Bethe's curves.[5]

RESULTS

Figure 4 is a plot of protons scattered by a Pt foil. As would be expected, there are no inelastic peaks observable. The background to the left of the elastic peak is probably due to coincidence between two small proton pulses giving the effect of a large one. The ordinate in this and the following curves if multiplied by 32 gives the total number of protons counted for any one point.

Aluminum

Figure 5 shows the scattering curve for a 0.35-mil Al foil. As can be seen, there are four peaks visible. The energy of the elastic peak was calculated from the known energy of the beam, correcting for the recoil of the nucleus. The beam energy was measured as 6.9 Mev by its range in air. Thus, the elastic peak for Al^{27} when protons are scattered at an angle of 135°, becomes 6.08 Mev.

[5] M. S. Livingston and H. A. Bethe, Rev. Mod. Phys. 9, 268 (1937).

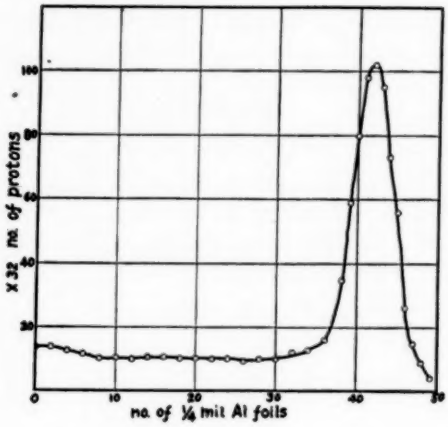

FIG. 4. Platinum scattering curve.

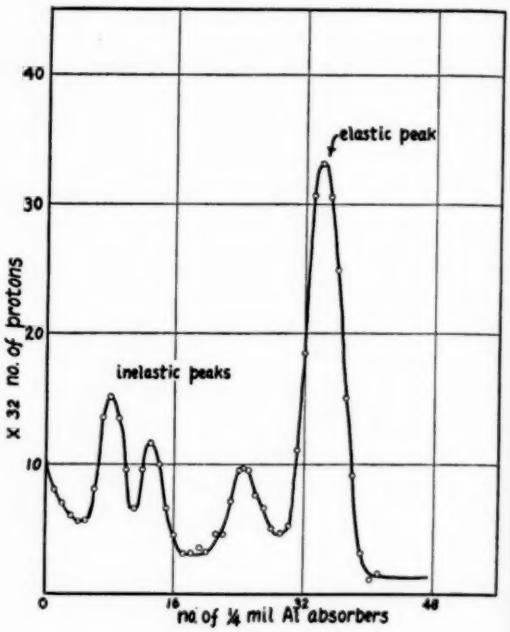

FIG. 5. Aluminum scattering curve.

TABLE I. Al^{27} scattering.

Run	Elastic peak energy Mev	Inelastic peaks I	II	III	IV
1	6.08	5.28	4.22	3.68	—
2	6.08	5.21	4.13	3.48	—
3	6.08	5.24	4.21	3.46	—
4	6.08	5.31	4.23	3.51	2.8
5	6.08	5.27	4.10	3.44	—
6	6.08	5.26	4.16	3.54	2.85
7	6.08	5.26	4.22	3.65	—
8	6.08	5.28	4.15	3.60	—
Average E	6.08	5.26	4.18	3.55	2.8
$6.08-E=\Delta$	0	0.82	1.90	2.53	3.3
Excitation energy Mev		0.87	2.03	2.70	3.5

Using the calculated value for the energy of the protons of the elastic peak, the air equivalence of our stopping foils, and Livingston and Bethe's range energy curves for air, we were able to compute the energies of the protons corresponding to the inelastic peaks. Table I shows a collection of the results of a number of scattering experiments. The first column contains the calculated values of the elastic peak. The other columns are the observed energies of the inelastic peaks. In two cases we are able to observe a fourth inelastic peak. The value for the energy of the fourth peak is rather questionable. From the observed energies of the elastic and inelastic peaks, it is possible to compute the nuclear excitation energies corresponding to these peaks. In this computation, correction was made for the difference in recoil energy of the nucleus in the case of elastic and inelastic scattering. The excitation energies for the nucleus are shown at the bottom of the table.

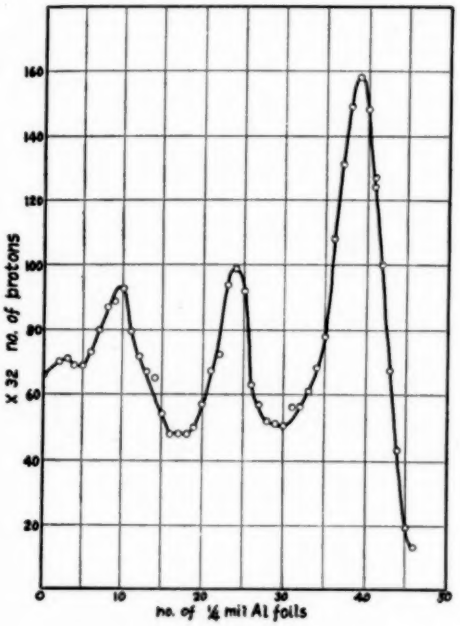

FIG. 6. Chromium scattering curve.

TABLE II. Cr^{52} scattering.

Run	Elastic peak energy Mev	Inelastic peaks I	II	III
1	6.46	5.15	3.70	—
2	6.46	5.21	3.74	2.9
Average	6.46	5.18	3.72	2.9
Δ	0	1.28	2.74	3.6
Excitation energy Mev		1.32	2.84	3.7

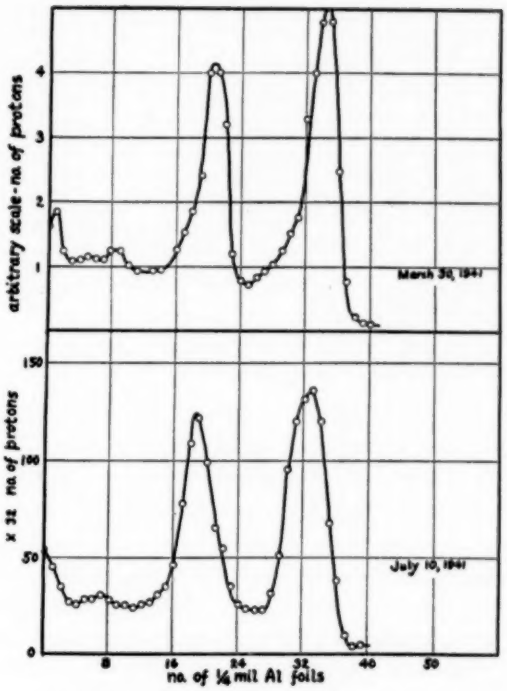

FIG. 7. Magnesium scattering curves.

TABLE III. Mg scattering.

Run	Elastic peak energy Mev	Inelastic peaks I	II	III
1	5.98	4.77	3.45	2.38
2	5.98	4.73	3.38	2.40
3	5.98	4.75	3.5	—
Average	5.98	4.75	3.44	2.39
Δ	0	1.23	2.54	3.59
Excitation energy Mev		1.32	2.74	3.88

Chromium

Figure 6 shows a scattering curve for Cr^{52}. As in the previous case, this curve shows both elastic and inelastic peaks. The foil was made by electroplating Cr on copper. The copper base was then dissolved away with concentrated nitric acid. We are very grateful to Dr. Flagg of the Chemistry Department for making these foils for us. The results of the Cr^{52} runs are shown in Table II.

Magnesium

Figure 7 shows a scattering curve for Mg. It is to be noted that the first inelastic peak is

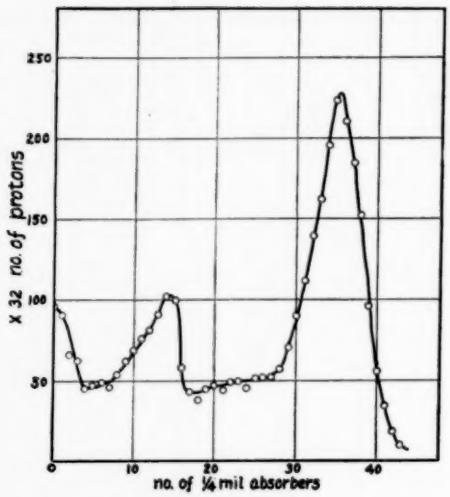

FIG. 8. Sulphur scattering curve.

almost as large as the elastic peak. There are two other observable peaks. The scattering foils used were 0.4 and 0.6 mil thick. They were obtained by rolling magnesium ribbon under oil. The results are shown in Table III. There is some doubt that all the excitation levels can be assigned to Mg^{24} since Mg^{25} and Mg^{26} have abundances of about 11 percent.

Sulphur

Figure 8 shows a scattering curve for S^{32}. Sulphur foils were prepared by rolling plastic sulphur between sheets of tantalum.

The foils obtained are quite small and a special technique was necessary to hold them in the beam. A pyroxylin film was laid down on water and the sulphur foil dropped on top before the film had hardened. This would break the film so that when it hardened it would adhere only to the edges of the foil. The film and enclosed foil were then removed on a wire frame which could be mounted in the scattering chamber. The results are given in Table IV.

A number of other elements were investigated, among them were Cu, Ni, Zn, A, Ag, N, and O. No conclusive evidence for inelastic peaks was obtained. In Zn there seemed to be faint evidence of inelastic peak structure, but this evidence was not considered good enough to warrant inclusion in these data. The reason for these negative results is probably found in the strong competition of other processes as (p, n) or (p, γ).

It would have been desirable to try a number of other elements. Among the desirable elements are Si, Na, Ne, P, and Cl. These should almost certainly yield results because of the high instability of the product nucleus of a (p, n) reaction in each case. They were not tried because of the difficulty of preparing good scattering samples.

TABLE IV. S^{32} scattering.

Run	Elastic peak energy Mev	Inelastic peaks I	Inelastic peaks III
1	6.2	4.35	2.57
2	6.2	4.32	2.57
Average	6.2	4.34	2.57
Δ	0	1.86	3.63
Excitation energy Mev		2.25	4.34

The authors wish to express their appreciation to the members of the University of Rochester Physics Department for helpful advice and criticism.

Gamma-Rays from As^{76}

C. E. MANDEVILLE
The Rice Institute, Houston, Texas
(Received December 16, 1942)

The recoil electron spectrum of the gamma-rays from As^{76} has been examined in a magnetic spectrograph. The spectrum was found to be composed of two electron groups corresponding to quantum energies of 0.83 ± 0.02 and 1.94 ± 0.04 Mev, the intensity ratio being 3.8 : 1. These results suggest excitation levels at 0.8 Mev and 2.8 Mev in the Se^{76} residual nucleus. No contributions to the spectrum of gamma-rays of energy greater than 1.94 Mev were observable.

INTRODUCTION

THE nuclear radiation of As^{76} has been the subject of a number of recent experiments,[1-5] and numerous conjectures have been made as to the energy levels of the Se^{76} residual nucleus resulting from beta-decay by As^{76}. A gamma-ray spectrograph[6] has been employed in examining the energies and relative intensities of the gamma-rays arising from the de-excitation of Se^{*76}.

PROCEDURE AND RESULTS

As_2O_3 of chemical purity 99.95 percent was activated by slow neutrons, the reaction being $As^{75}-n-\gamma$. As^{75} is the only stable isotope of arsenic. Of the known impurities in the chemically pure As_2O_3, none can form a radioactive isotope when irradiated by neutrons with a half-period which differs from that of As^{76} by less than a factor of two. The gamma-ray activity of the irradiated As_2O_3 was noted from time to time by means of an electroscope while the momentum distribution of the Compton recoils of the gamma-rays was being observed repeatedly in the gamma-ray spectrograph. The decay curve was followed for about 100 hours, and the activity was observed to decay with a half-life of 26.9 ± 0.3 hr. in agreement with previously determined values[1-5] running from 26 to 27 hr. The decay as observed in the electroscope is plotted in Fig. 1. Before being placed in the spectrograph, the As_2O_3 was compressed into small cylindrical pellets so as to obtain a considerable concentration of activity, the effective width of the source remaining small.

A typical curve of the momentum distribution of the Compton secondaries of the gamma-rays from As^{76} is given in Fig. 2. It is there apparent that the spectrum has two strong components. The end points of the electron groups correspond to gamma-ray energies of 0.83 ± 0.02 Mev and 1.94 ± 0.04 Mev, respectively. The ratio of the intensity of the gamma-ray at 0.83 Mev to that of the harder one is about 3.8 : 1. This momentum distribution was obtained at a number of different times over the 100-hr. period in which the gamma-ray activity was likewise being observed in the electroscope as previously mentioned. The shape of the curve was found to remain unchanged with time, suggesting the presence of only one half-life, in agreement with the decay curve of the electroscope. Moreover, ordinates corresponding to the same $H\rho$ value were observed to decrease in magnitude in accordance with a half-period of 27 ± 1.0 hr., associating the gamma-rays with the decay of As^{76} with certainty. A marked advantage of this method over the cloud-chamber technique when sources of sufficient strength are available is that a curve such as that of Fig. 2 may be completed in 3 or 4 hr. with high statistical accuracy whereas cloud-chamber methods require a much longer period.

DISCUSSION OF RESULTS

Harteck, Knauer, and Schaeffer[1] have reported gamma-rays at 1.50, 2.15, and 3.1 Mev using

[1] P. Harteck, F. Knauer, and W. Schaeffer, Zeits. f. Physik **109**, 153 (1938).
[2] F. Norling, Zeits. f. Physik **111**, 158 (1938).
[3] W. Schaeffer and P. Harteck, Zeits. f. Physik **113**, 287 (1939).
[4] A. C. G. Mitchell, L. M. Langer, and P. W. McDaniel, Phys. Rev. **57**, 1107 (1940).
[5] G. L. Weil, Phys. Rev. **62**, 229 (1942).
[6] C. E. Mandeville, Phys. Rev. **62**, 309 (1942).

the method of cloud-chamber pairs. Mitchell, Langer, and McDaniel[4] have reported a maximum gamma-ray energy of 2.05 Mev as a result of absorption experiments. It is, of course, not surprising that the intense gamma-ray at 0.83 Mev was not observed in the two foregoing experiments, since its energy is not sufficient to produce the rest masses of a positron-electron pair, and it is well known that absorption methods give only the value of the energy of the hardest gamma-ray present with any accuracy. No gamma-rays were observable in the neighborhood of 3 Mev. Statistical accuracy was very poor in that region, however, so that the possibility of the presence of radiation of low intensity at about 3 Mev is not excluded by this experiment. The quantum energy and intensity of the gamma-ray at 0.83 Mev, coupled with the results of previous experiments,[1-5] suggest immediately the level diagram for Se^{76} given in Fig. 3. γ_A and γ_B are there given the values reported in this experiment, and γ_C is suggested as corresponding to the 3-Mev radiation observed by Harteck, Knauer, and Schaeffer.[1]

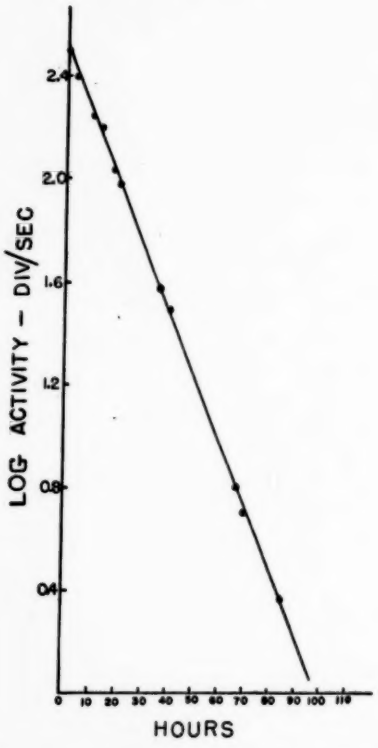

FIG. 1. Gamma-ray activity of As_2O_3 irradiated by slow neutrons. The half-life taken from the slope of this curve is 26.9±0.3 hr. The activity is therefore ascribed to As^{76} (T=27 hr.).

It is to be noted that the level arrangement of Fig. 3 agrees in a qualitative sense with the $\beta-\gamma$ and $\gamma-\gamma$ coincidence experiments of Norling[2] and of Mitchell, Langer, and McDaniel[4] in that γ_A is associated with the beta-ray spectrum of high maximum energy and two quanta are emitted per disintegration in cascade with the beta-ray spectrum of low maximum energy. The level diagram also eliminates the association of γ_C with a very soft beta-ray spectrum, in agreement with the findings of Schaeffer and Harteck.[3]

The maximum energies of the two beta-ray spectra have been tentatively assumed to be 1.0 and 3.0 Mev; these are means of the various observed and extrapolated values which have been previously reported. Any change in the assumed values would of course result in only a slight readjustment in the level diagram. The suggested arrangement of levels and the relative intensities of γ_A and γ_B are in approximate agreement with the value 3.5 : 1 given by Weil[5] for the ratio of the intensity of the beta-ray distribution of maximum energy about 3 Mev to the intensity of the less probable distribution of lower maximum energy.

ACKNOWLEDGMENTS

The author wishes to express appreciation for the preparation of the radioactive As^{76} by

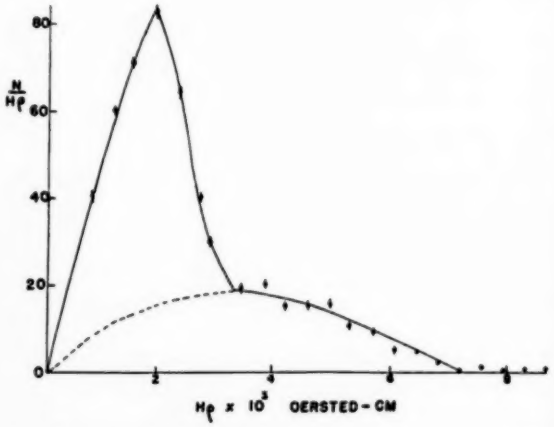

FIG. 2. Momentum distribution of the Compton recoils of the gamma-rays from As^{76}. The decay of the ordinates of this curve in the spectrograph was found to correspond to a half-life of 27±1.0 hr.

Professor A. L. Hughes and the cyclotron group of Washington University, St. Louis, Missouri.

Note added in proof: This experiment has been recently repeated. Cacodylic acid (Kahlbaum) in the form of an aqueous solution has been irradiated by slow neutrons, the Washington University cyclotron again being the neutron source. H_2S was passed into the solution, precipitating the activated As ions as a sulfide. $AsCl_3$ and HCl had been previously added.

The results were essentially the same, γ_A and γ_B again being present in about the same relative intensities. A better value of γ_B appears, however, to be 2.00 ± 0.04 Mev. Although the source was stronger and more highly concentrated, statistical uncertainty was still rather large in the neighborhood of 3 Mev, thus preventing any conclusive statement with regard to presence or absence of γ_C. Had γ_C been present with an intensity less than 20 percent of that of γ_B, it would have very probably escaped detection.

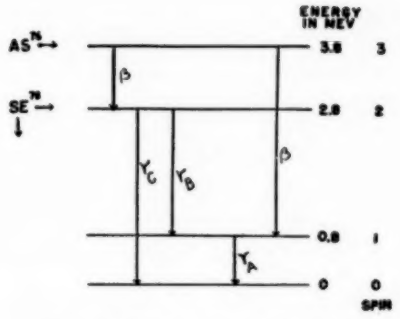

FIG. 3. Level scheme for Se^{76}.

PHYSICAL REVIEW VOLUME 63, NUMBERS 3 AND 4 FEBRUARY 1 AND 15, 1943

The Search for Element No. 87

F. R. HIRSH, JR.*
Cornell University, Ithaca, New York

(Received November 5, 1942)

An attempt to secure the element 87 $L\alpha_{1,2}$ x-ray lines in fluorescence spectra is made with negative results: no trace of the line sought for was found. The fluorescent material was $CsHSO_4$ derived from lepidolite, in which free thallium has been found. The writer suggests that the free thallium is derived from unstable element 87 atoms which had been present in the lepidolite molecule.

INTRODUCTION

THE status of the search for element 87 was fully discussed by the present writer in a previous paper.[1] Since then, there has been little further work done on the subject. Hulubei[2] has published x-ray spectrograms which reveal little or nothing. Moreover, the present writer's objections[1] to Hulubei's wave-length measurements still hold: the wave-lengths are far from the correct value; neither is the frequency separation of the "87" $L\alpha_{1,2}$ lines correct as given by Hulubei. As Hulubei admits,[3] they are "mésures très difficiles" and "raies très faibles."

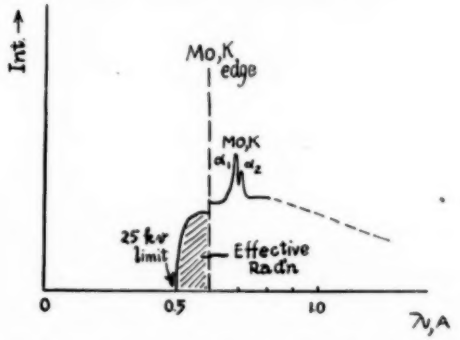

FIG. 1. Schematic spectral diagram showing effective portion of continuous spectrum emitted by molybdenum primary anticathode which might cause fluorescence of Mo portion of fluorescent target to effect registration of Mo K lines on plate.

One might possibly assume, then, that there is no evidence for the existence of element 87. There is, however, ample evidence for the existence of the unstable atom. J. A. Cranston,[4] in 1913, found that three atoms in 10^5 of $MsTh_2(89)$ emitted alpha-particles to form element 87 (see Fig. 4). He used the Geiger-Nuttall method. G. Guében,[5,6] of Liège, using the Geiger-Nuttall

* Now at the University of Southern California.

[1] F. R. Hirsh, Jr., Phys. Rev. **51**, 584 (1937).

[2] H. Hulubei, Comptes rendus **205**, 854 (1937).

[3] H. Hulubei, Comptes rendus **209**, 675 (1939).

[4] J. A. Cranston, Phil. Mag. **25**, 712 (1913).

[5] G. Guében, Ann. Soc. Sci. de Bruxelles **52**, 66 (1932).

[6] G. Guében, Ann. Soc. Sci. de Bruxelles **53**, 115 (1933).

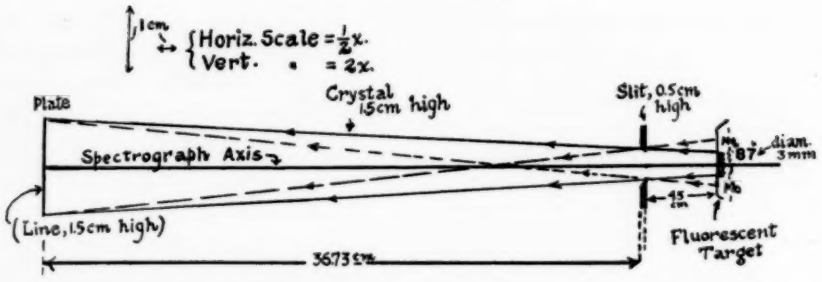

FIG. 2. Vertical section through spectrograph (note exaggerated scales) drawn from measured dimensions of spectrograph, and proving that both Mo K lines and element 87 $L\alpha_{1,2}$, produced by fluorescence, should register on photographic plate, since alignment is correct.

method, showed the existence of alpha-particles, estimated that one atom in 10^6 to 10^{10} atoms of $MsTh_2$ disintegrated to give alpha-particles and form an atom of element 87, instead of proceeding in the usual manner, with negative electron emission to form RaTh(90). He definitely showed that the alpha-particle activity had a half-life the same as that for the beta- and gamma-activity for $MsTh_2$. Thus the discovery of the unstable atom of element 87 is due to Cranston and Guében, with ample supporting evidence.

Paneth[7] has very recently reported the possible formation of element 87 by alpha-particle emission from Ac(89), forming radioactive AcK(87) of atomic weight 223. Meyer, Hess, and Paneth (see reference 7) found the alpha-activity, which was also found by Mlle. Perey. They estimate that one atom in one hundred of Ac(89) disintegrates by alpha-emission.

The present writer, however, at the instigation of Dr. T. G. Kennard of Claremont Colleges, California, who had an element 87 concentrate to be tested, decided to make a final search for the stable atom.

EXPERIMENTAL

In order to conserve the concentrate for further investigation, it was decided to attempt to excite the L x-radiations of element 87 by fluorescence. The writer has previously described the fluorescence x-ray tube[8] which was used. The Mo primary x-ray anticathode was operated at a potential of 25 kv, d.c. Since the Mo K radiation is excited at 20 kv, there should be a considerable beam of Mo K radiation leaving the primary x-ray anticathode and incident on the fluorescent target. The wave-length of the Mo $K\alpha_{1,2}$ lines is 0.707A; the L_{III} absorption edge of element 87, secured by interpolation from a Moseley graph, is located at 0.812A. Thus the Mo K radiation lies on the high absorption side of the L_{III} edge of element 87, and 87, $L\alpha$ should be strongly excited ($L\alpha$ comes from the transition $L_{III}M_V$).

The fluorescent target was made of Mo, with a three-mm hole in the center, into which the concentrate for element 87 was gently melted. The Mo-continuous radiation at 25 kv should excite the Mo K radiation, from the fluorescence target, as reference lines. The reference lines did not register on the photographic plate: this is not unreasonable, however, as very little of the continuous radiation is able to excite Mo K radiation (see Fig. 1). The shaded portion of the continuous spectrum alone can excite Mo K radiation by fluorescence. The short wave-length cut-off of the continuous spectrum is at 25 kv. Remembering the rule of 12.3 kv/A, we find the cut-off lies at $12.3/25 \approx 0.5$A. Mo K radiation is excited at 20 kv : $12.3/20 \approx 0.6$A. The Mo K radiation is at 0.7A approximately. Thus it will be seen that the Mo K reference lines should not be intense if they were registered. Lack of conditioning time for the x-ray tube made impossible the use of a higher potential for the primary anticathode. The axial alignment of the fluorescent target was excellent: this was done by rotating the glass insulating sleeve while the wax seal was hot. Figure 2, carefully constructed from the spectrograph and tube dimensions, shows that the photographic plate sees both top and bottom parts of the Mo part of the fluorescent

[7] F. Paneth, Nature **149**, 565 (1942).
[8] F. R. Hirsh, Jr. and F. K. Richtmyer, Phys. Rev. **44**, 955 (1933).

target, hence the Mo K reference lines should register if the fluorescence were intense enough. X-radiation was scattered by the fluorescence target, however, as evidenced by the presence of a central beam on the photographic plate (see Fig. 3). In this case:

$$h\nu = h\nu' + E\nu' + mc^2/2\,[(1-\beta^2)^{-\frac{1}{2}}-1] + MV^2/2,$$

where $h\nu$ is the original photon, $h\nu'$ the scattered photon, $E\nu'$ the recoil electron ejection energy, $mc^2/2\,[(1-\beta^2)^{-\frac{1}{2}}-1]$ the recoil electron kinetic energy, and $MV^2/2$ the energy of motion imparted to the atom.

Previously, under approximately the same operating conditions, an intense fluorescence plate had been secured in 10–20 hours. The plate used for testing the presence or absence of element 87 in the concentrate was exposed for 36 hours; the primary and fluorescence targets were cleaned hourly to minimize the absorption of tungsten deposits from the filament, which was run at an emission current of 15 ma, the primary anticathode was operated at 25-kv positive potential. No trace of element 87 $L\alpha_{1,2}$ lines was present on the photographic plate.

We conclude that element 87 was not present in the $CsHSO_4$ concentrate from lepidolite. Although this simple experiment shows that element 87, in the stable form, was not present in the lepidolite from which the $CsHSO_4$ was made, it does not prove it had not been present. In fact,

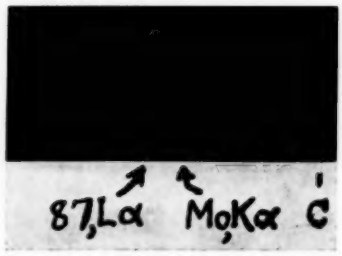

FIG. 3. Spectrogram showing registration of central (scattered) beam of x-radiation, and absence of element 87 lines. A quartz crystal was used: the Bragg angles for Mo, $K\alpha$ ($\lambda=0.707$A) and 87, $L\alpha$ ($\lambda=1.045$A) are 5° and 7°, respectively (approximately). (The plate faces in the direction from which the scattered x-rays came.)

Kennard and Rambo[9] have reported the presence of free Tl in this lepidolite molecule. The writer wishes to suggest that it is evidence that unstable element 87 had been present there. $MsTh_2(89)$ is derived by negative electron emission from

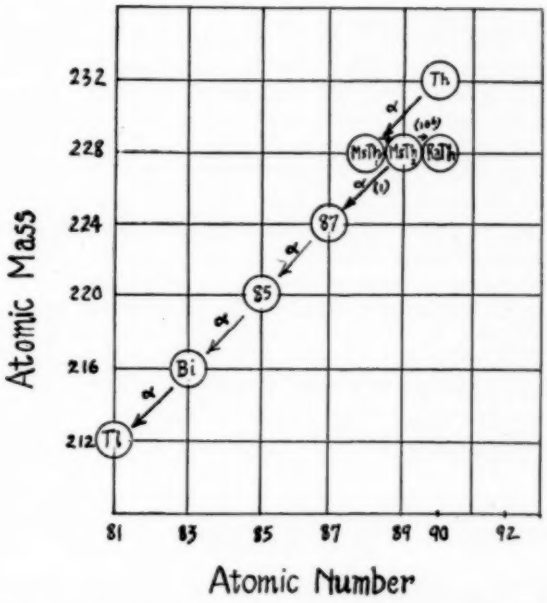

FIG. 4. Disintegration chart showing possible origin of Tl found in the lepidolite molecule. Atomic mass plotted against atomic number for the $MsTh_1-MsTh_2$ chain of disintegrations.

$MsTh_1(88)$, which in turn is derived by an alpha-emission from Th(90), (see Fig. 4). $MsTh_2(89)$ goes down by an alpha-emission to element 87; another alpha-emission produces element 85; two more alpha-emissions would produce Tl(81) of mass 212, and would account very nicely for the presence of Tl in the lepidolite molecule.

ACKNOWLEDGMENT

The writer especially wishes to thank Professors R. C. Gibbs and L. G. Parratt, at whose invitation this search was performed in the Cornell University Department of Physics, during the spring of 1941.

[9] T. G. Kennard and A. I. Rambo, Am. Mineral. **18**, 454 (1933).

Positive and Negative Point-to-Plane Corona in Pure and Impure Hydrogen, Nitrogen, and Argon

GERHARD L. WEISSLER
Department of Physics, University of California, Berkeley, California
(Received January 16, 1942)

To extend knowledge concerning the positive and negative point-to-plane corona, studies were made of the discharge in very pure H_2, N_2, and A. Neither pre-onset streamers nor burst pulses were observed in pure H_2 and N_2, in accordance with present theories of these effects. At high fields weak streamers developed which ultimately led to breakdown. Adding traces of O_2 to either H_2 or N_2 at once produced weak pre-onset streamers, and at higher concentrations produced burst pulses. Trichel pulses, which occur in properly triggered corona discharges in gases which form negative ions, are not observed in pure H_2 and N_2 but are immediately produced upon the addition of traces of O_2. For these gases the potentials for negative corona were observed to be lower than for the positive corona. In the case of argon, it was found that with positive point potential the first streamer formed was intense enough to cause spark breakdown, while with the point at a negative potential a heavy arc replaced the corona. Contamination of the argon with H_2 or N_2 introduced streamers for the positive corona which showed all the characteristics of those formed in air. This effect is attributed to the suppression of metastable atoms in the argon due to the presence of the impurity. For the negative corona small amounts of these gases (0.1 to 0.5 percent) prevented arcing and yielded a strong corona with glow discharge characteristics but no Trichel pulses. Addition of sufficient O_2 causes argon to act in all respects like air except that the onset potentials were much lower than in air. A clean-up of impurities in the negative corona in H_2 is shown to be due to formation and absorption of water vapor. The etching of negative points in the discharges in pure gases appears to be related to the sputtering process.

INTRODUCTION

THE application of newer techniques to the study of point-to-plane coronas in air has, as a result of recent studies,[1] revealed a series of mechanisms active in the individual cases of the discharge which depend on photo-ionization and space charge formation for their interpretation. In order to elucidate the mechanisms and to confirm the theories put forth, it seemed desirable to extend the studies to pure free electron gases of widely different photoelectric characteristics. This was especially important in view of the fact that one of the mechanisms, streamer formation, appears to be responsible for the sparking mechanism in uniform gaps above $pd=200$ (mm·cm) in air.

Investigations of the positive and negative point corona phenomena in the highly purified gases H_2, N_2, and A were undertaken. The results obtained indicated the value of studies with the admixture of certain impurities.

The results of W. H. Bennett[2] on the purification of H_2 by the negative corona and the attendant phenomenon of etching of points made it desirable to investigate these questions.

All measurements were made in Pyrex tubes, highly outgassed by being baked out, subjected to glow discharge in an induction furnace, and the pure gases then introduced into the tubes which were sealed off subsequent to filling. A cross-sectional diagram of a typical tube is shown in Fig. 1. Pt points, cylindrical in form with a hemispherical end carefully polished under the microscope with tin-oxide were used in the measurements. The platinum plates were 4 cm in diameter, with tungsten leads. The gap length ranged from 3.1 to 4.6 cm. The walls were shielded by evaporated thin gold films and all metal parts were heated to dull redness for approximately three hours with an induction furnace. Unless otherwise stated, all work was done at 760-mm Hg pressure and 22°C.

The tubes were filled with tank H_2, N_2, or A that had been passed over a conventional purifying train and liquid air, mercury being carefully excluded. In the case of N_2 a W filament in the sealed off tube was heated to incandescence for 20 hours to remove the last traces of O_2.

The d.c. high potential power supply was of the same type as the one employed by Sanders;[3]

[1] G. W. Trichel, Phys. Rev. **55**, 382 (1939); L. B. Loeb, and A. F. Kip, J. App. Phys. **10**, 3 (1939); L. B. Loeb, *Fundamental Processes of Electrical Discharge in Gases* (John Wiley & Sons, New York, 1939), p. 520.
[2] W. H. Bennett, Phys. Rev. **58**, 992 (1940).
[3] F. H. Sanders, Phys. Rev. **41**, 667 (1939), Fig. 1.

it was stabilized by an electronic stabilizer of the saturable core reactor type to better than one percent above 5000 volts. The discharge was observed visually by a telemicroscope (70×), and the electrical pulses were recorded by an oscilloscope[4] which was connected across a resistor between the plate electrode and ground.

POSITIVE CORONA

In order to analyze the behavior of the discharges in pure free electron gases and in contaminated gases it is necessary to recall some of its salient features as found in air.

The streamer[5] which characterizes the positive corona in air depends on the first Townsend coefficient, the field strength, and mainly the efficiency of photo-ionization in the gas. The positive ion space charge left behind by a streamer tends to choke off further streamer formation and gives rise to the laterally spread burst pulse corona. The crucial phenomenon, photo-ionization in the gas, occurs most efficiently in mixed gases or in gases where metastable states are abundantly produced.

Experimental Results in H_2

In H_2 with a gap of 3.1-cm corona onset occurred at 3500 volts, showing a very feeble localized light spot of 0.005 cm in diameter on the point. In air under the same geometrical conditions one observes a corona glow spread uniformly over the tip of the point. In the potential region of corona onset, streamers were not observed, and the discharge seemed to be a succession of electron avalanches which formed in the relatively localized region of highest field strength at the tip of the point. Photo-ionization in the gas seemed inadequate to spread the glow over the whole tip of the point. At corona onset no pulses of definite character could be detected with the oscilloscope. With a 4-stage amplifier an uninterrupted succession of small irregular kicks was observed which may be attributed to the avalanches approaching the point.

At 9000 to 10,000 volts the fields were such that weak streamers could form which increased in length and intensity with increasing fields and at higher potentials led to a spark.[6]

The addition of varying amounts of O_2 (less than 0.1 percent to 1 percent) to the H_2 immediately resulted in the formation of pre-corona onset streamers. These increased gradually in strength and number on raising the potential such that they could be seen visually as what is later in Table I termed a "streamer-corona." On further raising the potential the streamers finally led to a spark. Increasing the percentage of impurity again gave pre-onset and onset streamers which had a higher intensity than those for lower concentrations of O_2 in H_2. At potentials above corona onset further streamer formation was not observed, and the discharge degenerated into a burst pulse corona as described by Trichel and Kip. At still higher potentials breakdown streamers occurred. The potential range between the appearance of the burst pulse corona and the

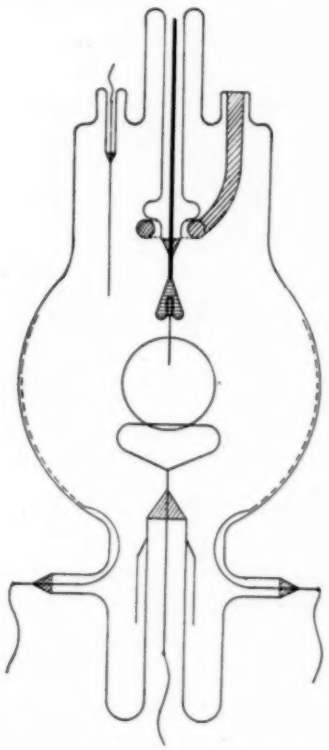

FIG. 1. Cross section of a typical discharge chamber, showing the point-to-plane gap which can be viewed through a plane window, the auxiliary W point in the upper left-hand corner, and the evaporated gold films which served shielding purposes.

[4] A. F. Kip, Phys. Rev. 55, 549 (1939), Fig. 1B.
[5] A. F. Kip, Phys. Rev. 55, 545 (1939).
[6] These streamers are later referred to as "breakdown streamers."

breakdown streamers is broadened with increasing amounts of O_2 impurities in H_2. Subsequent additions of O_2 led to an extension of the discharge area over the point. The currents in H_2 contaminated with O_2 were smaller than those in pure H_2 (Fig. 2).

For the interpretations of these results it seems profitable to recall that photo-ionization in the gas occurs most readily in mixed gases or in gases in which metastable states are abundantly produced. The intense photo-ionization in a mixed gas is due to the fact that one constituent has an ionization potential which is lower than the higher states of excitation of another constituent. In a pure gas such as H_2 one should expect very little photo-ionization. Since photo-ionization in the gas is the main mechanism to propagate a streamer from the high field region close to the point into the low field region several millimeters away it is not surprising to find that no streamers were observed at or before corona onset. The addition of 0.1 percent O_2 or more to H_2 realizes the state of a mixed gas, the efficiency of photo-ionization increases with increasing amounts of O_2, as is borne out by the fact that the intensity of streamers in successive mixtures also becomes greater. One percent O_2 in H_2 produced such intense streamers at corona onset that they were then able to leave a sufficiently large positive space charge behind such as to choke off further streamer formation by means of a considerable reduction in field intensity. The discharge then chose the way of least resistance and spread laterally over the point in the form of a burst pulse corona. To some extent this lateral extension of the glow is facilitated by the diffusion of negative ions which in turn produce triggering electrons for the formation of new avalanches the sum of which then constitutes a burst pulse.

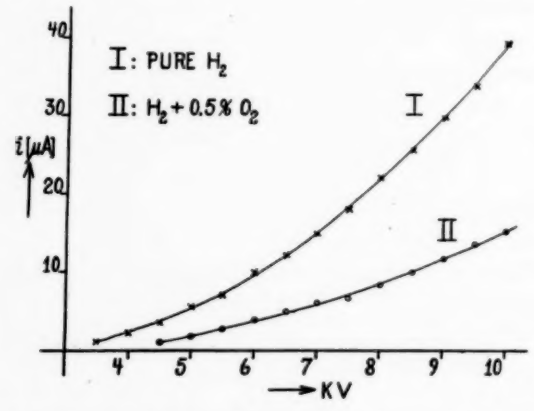

FIG. 2. Current-voltage characteristics for positive corona in pure and impure H_2, gap length 3.1 cm.

When the field is increased to the point where the positive ion space charge region is cleared in time to receive new initiating electrons from the burst pulse glow,[1] and it is increased such as to counterbalance the space charges, streamers will again appear. Under these conditions of higher fields the streamers will be sufficiently vigorous to cross the gap, form a cathode spot, and start an arc- or spark-breakdown.

It should be noted in Table I that the onset of an avalanche corona in pure H_2 occurs at 3500 volts, while the appearance of a streamer corona with 0.1 percent O_2 in H_2 requires 5000 volts. Subsequent additions of O_2 increased the efficiency of photo-ionization and therefore the ease of streamer and burst pulse formation, which lowered the threshold potential of corona onset.

The smaller currents in contaminated H_2 may be due to changes in Townsend coefficients and changes in ionic mobilities. A change in mobility would be more pronounced with O_2 in H_2 than in N_2 or A, owing to the great difference in ionic mobilities of O_2 and H_2. The ratio of mobilities in H_2 and O_2 is about five.

Experimental Results in N_2

In pure N_2 the conditions were not materially different from those in H_2: No pre-corona onset streamers were observed. Corona onset occurred at 4800 volts in form of a localized spot on the positive point. The oscillographic pattern was the same as in the case of H_2, namely, a sequence of irregular fluctuations of the electron avalanche type. Increasing the potential resulted in a brighter corona, which extended further toward the cathode in form of a continuous luminous channel, possibly due to the action of metastable atoms or active N_2. The potentials at which various phenomena appear is increased above those of H_2.

At 11,000 volts very faint streamers appeared, which give the well-known kicks in the oscilloscope superimposed upon the continuous corona ripple. In both N_2 and H_2 breakdown streamers could go across the gap at relatively low potentials without causing breakdown; but at

TABLE I. Essential data of the positive point-to-plane corona.

Gas	Pre-onset streamers	Corona			Current‡ μA	Onset of breakdown streamers	Breakdown potential approx.
		Onset potential	Visual character	Burst pulses			
H_2 pure†	none	3500 v	localized*	none	4	10,000 v	18,000 v
H_2+0.1% O_2	yes	5000 v	intermittent streamer-corona	none	—	8,000 v	—
H_2+0.5% O_2	yes	4500 v	streamer-corona	none	3	9,000 v	—
H_2+1% O_2	yes	4000 v	uniform**	small	3	15,000 v	18,000 v
N_2 pure†	none	4800 v	localized	none	1	11,000 v	20,000 v
N_2+0.2% O_2	incipient streamers	4500 v	streamer-corona	none	1	9,300 v	—
N_2+1% O_2	incipient streamers	4800 v	localized, for higher v uniform glow	yes	1	12,500 v	20,000 v
Room-air†	yes	5500 v	uniform	yes	—	15,000 v	—
A pure††	none	none	none	none	—	—	3,500 v
A+0.1% H_2	yes	3300 v	localized	none	0.5	—	—
A+0.5% H_2	yes	3500 v	localized	small	0.5	—	—
A+1% H_2	yes	3450 v	localized	small	0.5	—	—
A+0.3% N_2	none	none	none	none	—	3,500 v	3,500 v
A+0.5% N_2	yes	3600 v	streamer-corona	small	—	4,600 v	4,600 v
A+1% N_2	incipient streamers	3500 v	localized	small	0.5	6,500 v	6,500 v
A+0.1% O_2	yes	3800 v	streamer-corona	none	—	4,100 v	4,100 v
A+0.4% O_2	yes	4500 v	streamer corona	small	0.6	—	7,000 v
A+1% O_2	yes	4000 v	uniform	small	0.6	—	15,000 v

* Localized glow, due to electron avalanches approaching the point in the highest field region.
** Uniform glow, caused by the burst-pulse corona.
† Gap length 3.1 cm.
†† Gap length 4.6 cm.
‡ Current at a potential which is about 20 percent above the corona onset potential.

higher potentials the number of streamers increased considerably until in N_2 at 20,000 volts they became strong enough to initiate spark breakdown.

The effect of O_2 impurities in N_2 (less than 0.1 percent up to 1.5 percent) was studied. The sequence of streamer and burst pulse phenomena closely duplicated those in H_2. The visible corona also changed from a localized glow in pure N_2 to a uniformly spread glow with increased amounts of O_2. The magnitude of currents did not change materially by addition of O_2 to N_2.

Although metastable states and activated forms of atoms exist, their abundance seems to be too small to increase the probability of photoionization with respect to that of H_2 to any appreciable extent, since no streamers were formed in the region of corona onset. The first Townsend coefficient takes on appreciable values in N_2 at distinctly higher values of the field strength as compared to H_2, which accounts for the differences in starting potentials. The complete absence of pulse formation in the pre-onset and onset region of both pure H_2 and N_2 means that no Geiger counter regime exists in those gases and confirms the conclusion that Geiger counter action is determined by space charge action.[7]

Experimental Results in A

In argon a spark crossed a gap of 4.6 cm at approximately 3500 volts. Neither pulses of any kind nor visible corona occurred. Since both H_2 and N_2 are known to quench the metastable states of argon by collisions of the second kind, varying amounts of these two gases were tried in argon. When 0.3 percent N_2 was admitted, a very few strong streamers occurred at 3500 volts followed by a spark at the same potential. An increase of N_2 to 0.5 percent gave streamers in the corona onset region which disappeared above 4100 volts and a localized corona with occasional burst pulses was observed. A spark, preceded by a few strong breakdown streamers, broke down the gap of 4600 volts. Increasing the percentage of N_2 in argon to values above 0.5 shifted the breakdown potentials to higher values. Argon

[7] C. G. Montgomery, and D. D. Montgomery, J. Frank. Inst. **231**, 447 (1941).

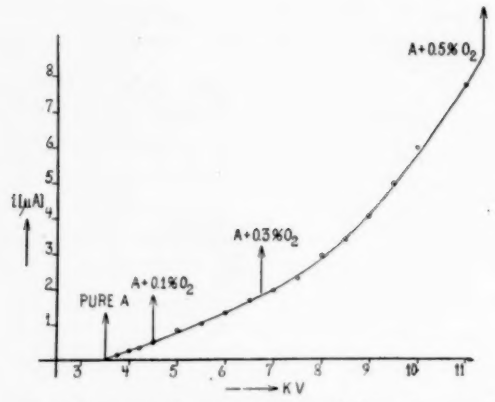

FIG. 3. Current-voltage characteristics for positive corona in pure and impure argon. The arrows indicate the upper limit of the current-voltage curve and the sparking threshold for a specific mixture of O_2 in A.

contaminated with H_2 showed essentially the same sequence of phenomena.

The addition of O_2 to argon again resulted in the formation of pre-corona onset and onset streamers without causing breakdown, while larger amounts of O_2 shifted the breakdown to higher potentials. The only difference was that above onset streamers still existed in the presence of a burst pulse corona (Fig. 3).

The current-voltage characteristics did not change materially for different amounts of N_2 or H_2 added to argon and were of the same type as those shown in Fig. 3 for O_2 in argon.

In argon the large production of metastable atoms distinctly enhances photoelectric ionization in the gas. In addition the first Townsend coefficient reaches effective values at very low values of the field strength, because electron impacts are highly elastic. For these reasons the first streamer was strong enough to cause a spark. The quenching of metastable states by H_2 and N_2 means a reduction of the efficiency of photo-ionization; as a consequence we were able to observe streamers which were stronger than commonly observed though not strong enough to cause an immediate breakdown. This is further supported by the fact that larger amounts of impurities destroy more of the metastable states, thus inhibiting formation of breakdown streamers at lower potentials and shifting breakdown to successively higher potentials.

Apparently the destructive effect of O_2 on metastable states is so great that streamers are so weakened at low potentials that they do not succeed in choking themselves off. With higher O_2 concentrations streamers were observed together with a burst pulse corona at higher potentials which indicates some choking of the streamers due to increased space charge formation. The presence of negative ions produced by O_2 appears to help spread the glow over the tip of the point at higher fields as distinguished from the case of H_2 and N_2 in argon.

Low Pressure Phenomena in H_2, N_2, and A

These gases were also studied at pressures of 300 and 100 mm Hg. The sequence of phenomena was the same as that at atmospheric pressure except that corresponding onset potentials were lowered as the pressure was lowered and that the visual appearance of the corona tended to become more diffuse (Fig. 8).

It is interesting to note that despite the greater diffusion at lower pressures, streamers can still form and propagate. This differs from streamer formation in sparking in a plane parallel gap in air[8] and must be ascribed to the high fields around the point which makes streamer formation still possible when it cannot take place in a plane parallel gap. The current-voltage characteristics were such that the slope of the curves increased with decreasing pressure due to the higher mobilities at lower pressures (Fig. 4) as observed by J. Zeleny[9] in gases of less purity.

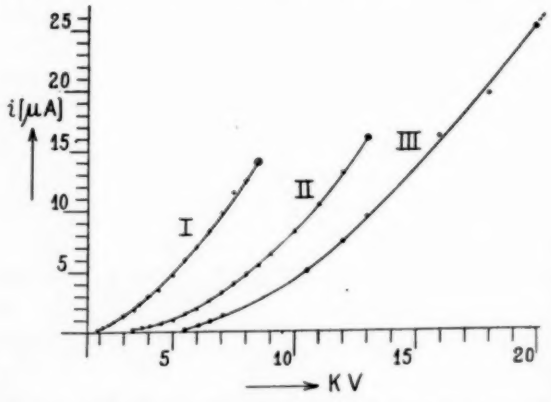

FIG. 4. Current-voltage characteristics for positive corona in pure N_2 at 3 pressures. I: $p=100$ mm Hg, II: $p=300$ mm Hg, III: $p=760$ mm Hg. The end points of curves *I* and *II* indicate spark breakdown, curve *III* ends at approximately 23 kv with a spark gap length 4 cm.

[8] L. B. Loeb, *Mechanism of the Electric Spark* (Stanford University Press, 1941).

[9] J. Zeleny, Phys. Rev. **25**, 304 (1907); J. Zeleny, J. Frank. Inst. **232**, 23 (1941).

NEGATIVE CORONA

The intermittent relaxation oscillator-like character of the negative corona has been ascribed to the formation of negative ion space charges[10] due to electron attachment to O_2 molecules.[11] In the very complex sequence of ionization phenomena in the concentrated field region owing to the differences in mobilities of positive and negative ions the negative ion space charge cloud acts to choke off the discharge until it is dissipated several millimeters into the gap. Thus we should expect to find the regular Trichel pulses appearing in all gases forming negative ions, the pulses becoming regular if the necessary triggering electrons[12] can be provided, either by field emission from rough points, fine dust specks,[13] thermionic emission, or photoelectrons. In the absence of electron attachment we should not expect to observe discharges interrupted by space charges since the high electron mobilities would preclude the formation of negative space charges.

For the same conditions as for the positive point the following experimental results were obtained.

Experimental Results in H_2

In pure H_2 negative corona onset occurred at 2600 volts, which is notably lower than the onset for the positive corona. The discharge began as a continuous discharge with no Trichel pulses or other discontinuities and appeared to be spread at onset uniformly over the tip of the point. This form of discharge was exceedingly unstable and sooner or later contracted to a concentrated point discharge in the region of highest field strength. The change was accompanied by a change in current by a factor of 10^3, it occurred more rapidly at lower pressures and more rapidly if the potential was raised slightly above the onset value. At 2800 volts the discharge appeared in the concentrated form within a few seconds, showing no indications of the Trichel mechanism and had all the characteristics of a glow discharge with Crookes' and Faraday's dark spaces, negative glow, and positive column. The onset of this discharge only is registered in Table II. At lower pressures or higher potentials the Crookes' dark space became distinctly visible. In the region from onset of the high current corona to breakdown two interesting facts were observed:

1. The concentrated discharge above onset tended to move continually over the surface of the point.
2. The form of the corona changed frequently and unsystematically from the concentrated glow to one which was uniformly spread over the tip of the point *without* change in current.

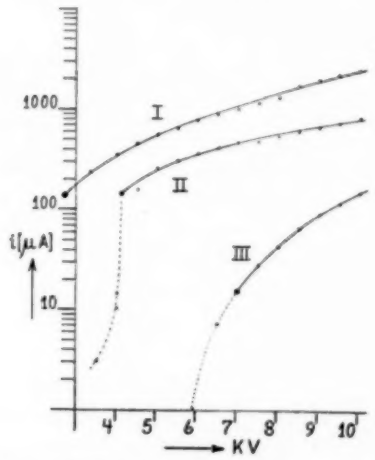

FIG. 5. Current-voltage characteristics for negative corona in pure and impure H_2. I: pure H_2, III: H_2+0.7 percent O_2, II: after clean-up run on auxiliary W electrode as discussed in the paragraph on clean-up corona. Lower end of the fully drawn curves marks onset of steady corona, dotted lines mark intermittent corona. Gap length 3.1 cm.

While the localized glow if it was not changing positions did not reveal any pulses, the uniform glow at the higher currents showed a succession of irregular inductive pulses of no definite character in the oscilloscope. On microscopic examination of a point run on a negative corona in form of a uniform glow with high currents, it was found that the whole tip over which the glow was visible was pitted with innumerable holes.

The introduction of the smallest amounts of O_2 immediately produced Trichel pulses, the onset of corona was 4200 volts, the currents were lowered to approximately one-half of their value in pure H_2 (Fig. 5). On increasing the amount of O_2 the onset of the steady corona was preceded by a region of interrupted Trichel pulses which

[10] G. W. Trichel, Phys. Rev. **54**, 1078 (1938).
[11] N. E. Bradbury, Phys. Rev. **44**, 883 (1933).
[12] L. B. Loeb, A. F. Kip, G. Hudson, and W. H. Bennett, Phys. Rev. **60**, 714 (1941).
[13] H. Paetow Zeits. f. Physik **111**, 770 (1939).

TABLE II. Essential data on the negative point-to-plane corona.

Gas	Localized corona: Onset potential	Localized corona: Onset current μA	Localized corona: Visual character	Trichel pulses	Breakdown potential approx.	Peculiarities
H_2† pure	2800 v	140	unsteady glow*	none	—	alternation uniform+localized glow
H_2+0.1% O_2	4200 v	70	unsteady glow	yes	—	same as above
H_2+0.6% O_2	5800 v	2	unsteady glow	yes	—	same as above
N_2† pure	3700 v	90	steady glow**	none	14,000 v	
N_2+0.1% O_2	4300 v	50	steady glow	yes	—	
N_2+1% O_2	5500 v	0.1	intermittent***	yes	—	5,000 to 7,000 v intermittent corona
Room-air	8000 v	0.1	intermittent	yes	—	8,000 to 11,000 v intermittent corona
A†† pure	—	—	—	—	3,500 v	no corona
A+0.3% N_2	2500 v	200	steady glow	none	4,100 v	
A+1% N_2	3900 v	250	steady glow	none	—	
A+0.1% H_2	3200 v	400	unsteady glow	none	4,100 v	
A+1% H_2	3300 v	300	unsteady glow	none	—	
A+0.1% O_2	3000 v	1	steady glow	yes	—	
A+0.4% O_2	3000 v	0.1	intermittent	yes	24,000 v	3,000 to 6,000 v intermittent corona
A+1% O_2	3300 v	0.1	steady glow	yes	—	

* See experimental data in H_2.
** See experimental data in N_2.
*** Due to lack of triggering electrons.
† Gap length 3.1 cm.
†† Gap length 4.6 cm.

began at 5800 volts for 0.6 percent O_2 and was caused by a lack of triggering electrons.[12] The steady corona began at 7500 volts. With increasing potential the frequency of the Trichel pulses at onset increased. Larger amounts of O_2 required higher breakdown potentials and caused lower currents.

The difference in onset potentials for the positive and negative corona in pure H_2 is very distinct from those in air. In air the efficiency of photo-ionization is such that the discharge mechanism operates through electrons generated in the gas by photo-ionization in preference to the liberation of electrons from the cathode by positive ion bombardment. Since photo-ionization also determines streamer formation from positive points, we can explain the nearly identical onset potentials for both positive and negative corona in air by the fact that one mechanism is dominating in both cases. In the case of pure H_2 with inefficient photo-ionization in the gas the mechanism for maintaining the discharge from the positive point is different from that maintaining the negative corona as will be discussed more in detail in the paragraph on Positive and Negative Currents. Consequently the onset potentials for both signs of corona differ considerably.

Because negative ions are not formed in pure H_2 no Trichel pulses were observed.

The two above-mentioned facts on the behavior of the high current corona between onset and breakdown can be explained in the following way: In the event of insufficient photo-ionization secondary electron liberation would occur from the negative point by positive ion bombardment. The work function of the point and its conditioning would greatly influence electron emission, and the discharge would be sensitive to such alterations. Extreme variations of work function from 6 volt to 4 volt have been observed[14] between O_2-coated Pt surfaces and H_2-coated Pt surfaces. The continuous bombardment of Pt by positive ions effectively alters the work function even in a given gas. This instability of the surface would explain the movements of the concentrated discharge over the surface, and, together with the microscopically observed pitting, it is suggested that the discharge form of a uniform glow with high currents is caused by the action of one or more simultaneous localized spots, constantly changing their positions on the tip where every change was accompanied by an inductive kick in the oscilloscope. These changes as judged from

[14] C. W. Oatley, Proc. Phys. Soc. **51**, 318 (1939).

the approximate frequency of the pulses occurred so rapidly, of the order of several thousand for the time of persistence of vision, that the observations gave the illusion of a uniform glow. The validity of this viewpoint also seemed to be indicated by the fact that the current did not change during those transitions, being much too high for a Trichel mechanism, and that the uniform glow faintly showed a cathode glow, Faraday dark space, and positive column which extended laterally over the whole tip.

The interpretation of the very first mentioned transition of a low current uniform glow to the concentrated discharge with increased current, which was a continuous phenomenon, must lie in the conditioning of some spot in the high field region by positive ion bombardment leading to the formation of an adequate cathode spot.

Experimental Results in N_2

The sequence of phenomena in pure N_2 is essentially the same as in pure H_2. The onset potential of the localized corona was 3700 volts, which is higher than in H_2 but still lower than the onset of the positive corona in N_2. A schedule of the potentials at which various phenomena occur is given in Table II. As in H_2 the discharge began as a uniform glow at 3600 volts (not mentioned in Table II), it contracted in time visibly to the concentrated discharge with resultant increase in current by a factor of 10^3. The gradual transition of the discharge could be observed visually and the current increase accompanying this visual change noted. The localized corona differed from the case of H_2 only in remaining steadily at one position instead of moving over the surface.

The effects of small amounts of O_2 ranging from 0.1 percent to 1.5 percent introduced into pure N_2 were also studied. The smallest percentage of O_2 resulted immediately in Trichel pulses. Their choking action caused the currents to drop

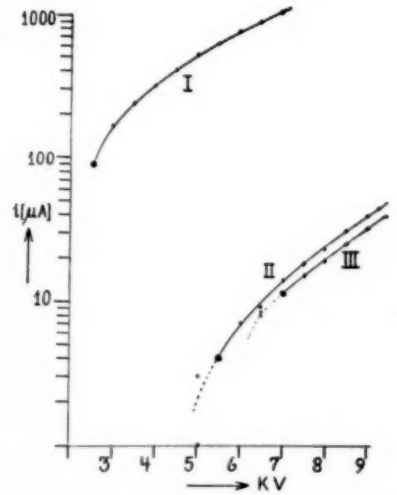

FIG. 6. Current voltage characteristics for negative corona in pure and impure N_2. I: pure N_2, II: N_2+0.8 percent O_2, III: after clean-up run, refers to the paragraph on clean-up corona. Gap length 3.1 cm.

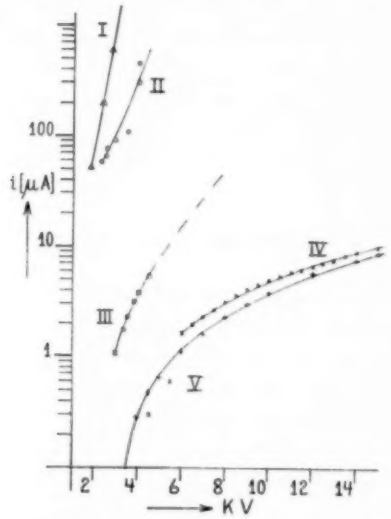

FIG. 7. Current-voltage characteristics for negative corona in pure and impure A. I: pure A, II: A+<0.1 percent O_2, III: A+0.1 percent O_2, IV: A+0.5 percent O_2, V: A+1.5 percent O_2. The low potential end of the curves marks the "offset" potential of the steady discharge. Gap length 4.6 cm.

to approximately one-half of the magnitude in the pure gas (Fig. 6). The behavior in general was similar to that in H_2.

It is obvious that in the conditioning of the point surface there must be two mechanisms that work: One occurs in both H_2 and N_2 and appears to be a conditioning of the rested[15] point by positive ion bombardment giving increased electron emission. The other appears in H_2 only and results in a de-activation of the point by strong H_2-ion bombardment.

The lower onset in H_2 as compared to N_2 is to be expected from the difference in value of the first Townsend coefficient in the two gases.

[15] The initial uniform glow which transformed to the concentrated high current form did not appear on a surface after a discharge had been freshly interrupted. It apparently took a rest period of a few seconds to reform the gaseous film causing the uniform glow at low currents.

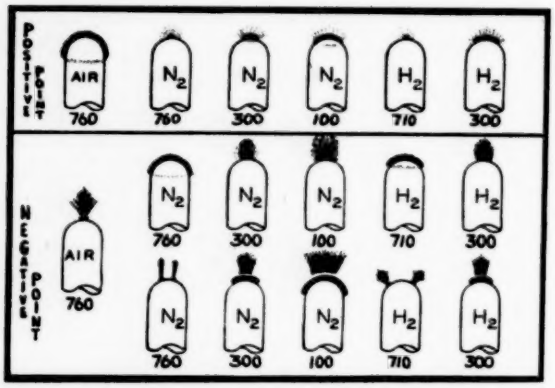

FIG. 8. Visual forms of corona discharges under indicated conditions in the onset region. Pressures in mm Hg. The forms in the second row show the uniformly spread discharge at low currents which contracts sooner or later to the concentrated forms of discharge with high currents which can be seen in the last row.

Experimental Results in A

For the same reasons as were mentioned in the discussions of the positive corona in argon we found that no matter whether the gap distance was 3.1 or 4.6 cm an arc discharge set in at approximately 3500 volts. It was continuous across the gap and no current fluctuations or pulses were observed. The current was of the order of magnitude of 10^3 microamperes. Once the arc had kindled, it persisted even with decreased potentials to a definite "offset" potential. The current voltage characteristics from onset to offset are shown in Fig. 7. Increasing the gap length had the effect of prolonging the time necessary for the arc to build up. This lag was of the order of seconds for a 3.1-cm gap and tens of seconds for a 4.6-cm gap. It must be pointed out that these results can only be achieved in argon of the highest purity as shown by the effects produced by traces of added gases.

The addition of 0.3 percent of N_2 to argon did not result in an arc immediately, but corona onset occurred at 2500 volts: Once started it continued to operate on reducing the potential to an offset at 1300 volts. On increasing the potential a few hundred volts above onset, a continuous transition to an arc was observed. Admitting larger quantities of N_2 merely shifted the arcing potential to higher values above corona onset. This may be ascribed to the quenching action of the metastable states by N_2.

Essentially the same succession of phenomena occurred on addition of H_2 to argon. There is one notable difference with this mixture which is the erratic movement of the corona glow from one spot on the tip of the point to another in rapid succession. This can also be seen oscillographically in the production of irregular inductive pulses. These indicate brief interruptions of the current but are definitely not due to a Trichel mechanism, since the currents were orders of magnitude larger than those connected with Trichel pulses. This motion of the discharge is again characteristic of the Pt point in the presence of H_2 as already stated. It does not occur with N_2 in argon. Increasing the amount of impurity of either H_2 or N_2 in argon decreases the slope of the current-voltage characteristics.

Admission of varying small amounts of O_2 (less than 0.1 percent to 1 percent) immediately initiated regular Trichel pulses, and the breakdown was at once raised to 10,000 volts, or more if the O_2-content exceeded 0.3 percent. Adding 1 percent of O_2 altered the appearance of the corona at onset, apparently through the nearly complete destruction of metastable states. In place of the regular Trichel pulses found with small amounts of O_2 present, due to the triggering electrons from the few metastables still existing, the larger amounts of O_2 caused the fluctuating corona observed by Hudson[12] on smoothly polished points to appear, when no triggering electrons from metastables were present. The currents in argon in the presence of O_2 were reduced below those in the presence of H_2 or N_2 in argon by a factor of approximately 10^{-3} as a result of the action of the negative space charges inhibiting the free flow of electrons and ions (Fig. 7).

As already mentioned above, in gases with efficient photo-ionization we find the same onset potentials for both signs of corona, because in both cases we find that electron generation in the gas is the primary mechanism for the maintenance of the discharge. Pure argon confirms this even stronger than air with its spark breakdown without preceding corona for the positive point at 3500 volts and its arc breakdown also without preceding corona for the negative point at 3500 volts.

The phenomenon of an offset markedly lower than the onset potential is characteristic of all

negative corona phenomena. In H_2, N_2, and air the difference in potentials amounts to a few hundred volts for a 3-cm gap, while in argon it extends over a range of more than a thousand volts, probably due to the action of metastable states.

Low Pressure Phenomena for Pure H_2, N_2, and A

In the case of the negative corona a decrease in pressure resulted in the same sequence of phenomena as at atmospheric pressure. The corresponding potentials were decreased, as was to be expected, and the visual form was spread out (Fig. 8), emphasizing its glow discharge-like characteristics. The current-voltage curves again showed a steeper slope[9] for lower pressures due to increased mobilities (Fig. 9).

POSITIVE AND NEGATIVE CORONA CURRENTS

In pure gases transparent to photons it will in general be expected that near onset the negative corona currents would be several orders of magnitude greater than the positive corona currents for the reason that with a negative point the high field is concentrated about the cathode. Hence the necessary secondary ionization due to any one of three agencies, photo-ionization in the gas, photoelectric effect at the cathode, secondary electron emission by positive ion bombardment, is active in a high field region and ion multiplication is effectively ensured. In the case of the positive point the main source of electrons available for maintaining the discharge is the photoelectric effect at the distant plate. The low fields at the plate yield practically no electrons by positive ion bombardment and photoelectric emission from the plate is small. Hence, in the case of the positive point in H_2 or N_2, both of which fulfill the condition of being transparent to photons, secondary electron emission is small, and the observed currents at onset are small. For the negative point in H_2 and N_2 the positive ions are accelerated in the high field region toward the point without interruption by negative space charges and hit the point surface with energies 10 to 100 times higher than the energies with which they would strike the negative plate during a positive point corona; therefore, it is assumed that the second Townsend coefficient takes on relatively large values, thus yielding high currents (Figs. 4 and 9, also shown by current values in Tables I and II).

CLEAN-UP CORONA

Clean-up effects on H_2 contaminated with O_2 had been noted earlier. Bennett[2] ascribed them to the formation of an oxide of tungsten. The points used in our work were chiefly Pt but for test purposes an auxiliary W point was mounted in the chamber.

1. In the point-to-plane gap used in these measurements the point was of cylindrical shape with a hemispherical cap 0.05 cm in diameter, while in Bennett's work points of much smaller radius of curvature were employed, which naturally could not be shaped as accurately as the larger points.

2. The auxiliary W point was used so that the carefully shaped Pt point was not changed in form by the cleansing discharge, a procedure which was omitted by Bennett. Only under such carefully controlled condition can the observed current-voltage characteristic be completely ascribed to a change in the gas composition. For it follows both theoretically and from Bennett's observations that the Trichel mechanism which was used to detect electron attaching impurities

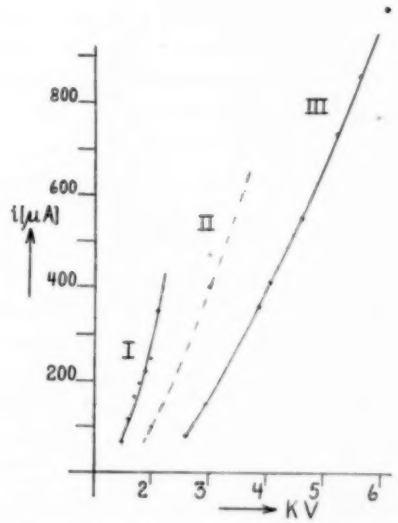

FIG. 9. Current-voltage characteristics for negative corona in pure N_2. The low potential end of the curves indicates "offset;" the high potential end does not indicate breakdown. Gap length 4 cm. I: $p = 100$ mm Hg, II: $p = 300$ mm Hg, III: $p = 760$ mm Hg.

is not active on fine points. At the same time a severe etching of the fine points of Bennett was observed in the clean-up run. Thus it could not be determined whether the disappearance of the Trichel pulses was due to clean-up or to etching.

The procedure in this study was as follows: The chamber was carefully cleaned and filled with the pure gas, either N_2 or H_2. The phenomena occurring from corona-onset to spark breakdown were then observed in the main gap on the Pt point to serve as a check on previous results and as a control for purity. Then a small amount, around 0.4 percent, of O_2 was introduced into the chamber and the phenomena were recorded over the same potential interval as before. After this the clean-up discharge was run from the auxiliary W point for 8 to 12 hours at a high negative current. At the end of the run the condition of the gas was examined by a repetition of the test procedure with the clean Pt point.

Admitting traces of O_2 of less than 0.1 percent into pure H_2, one obtained in the test run the characteristic phenomena with positive and negative points detailed above. After the cleansing run with a W point no pre-onset streamers were observed for the positive corona and no Trichel pulses for the negative corona. Clean-up had obviously occurred and seemed to be complete.

If the impurities exceed 0.1 percent in H_2, the negative corona currents before clean-up fell to very low values due to Trichel pulse formation and the positive corona revealed streamers. Cleaning the gas with the discharge on the auxiliary W point restored in a large measure the purity of the gas; the currents, however, never reached the initial values in the pure gas, and incipient streamers were noted in the positive corona. It was clear that some clean-up had occurred, but with large amounts of O_2 it was never complete (Fig. 5). Use of a Pt point to produce the clean-up did not materially change the results of the clean-up compared with the W point, which seemed to indicate that the formation of tungsten oxide was not the primary mechanism for the clean-up action. This was substantiated by repeating experiments in N_2 which was contaminated by O_2. Under these conditions no clean-up was detected (Fig. 6). Therefore, clean-up in H_2 may be ascribed primarily to the formation of water. If the concentration of O_2 is low, the water formed by the discharge will be completely adsorbed by the baked-out and very hygroscopic walls of the Pyrex chamber. Above 0.1 percent of O_2 the amount of water vapor generated was too great to be completely adsorbed. Hence, one may ascribe the residual pulse formation to the remaining water vapor.

ETCHING OF THE POINT ELECTRODE

The occurrence of etching in pure nonreactive or inert gases about a negative point, as noted by Bennett, seemed peculiar owing to the high pressures used in these experiments and owing to the fact that Hudson[12] found pitting always associated with oxidation. While the phenomenon of sputtering occurs at the cathode of many discharge tubes, the sputtering becomes important only with higher cathode falls and low pressures. It is clearly a function of the energy of the incoming ions. In our experiments the positive ions strike the cathode with an energy not much in excess of one electron volt.

An attempt was made to correlate the degree of etching with some properties of the metals, and point electrodes of W, Pt, Cu, Al, and Pb were tested on the negative corona in gases H_2 and N_2 under standardized conditions (12-hour run, constant current of 1250 μa corresponding to a current density of about 1 amp./cm^2, gap length 3.1 cm). The points were carefully polished with tin-oxide and examined under the microscope. Etching occurred in all cases except Al and manifested itself in a symmetrical crater-like pit with a depression below the level of the point surface surrounded by a heaping up of metal at the sides. This heaping up may be due to the fact that a considerable fraction of the sputtered particles were reflected back and redeposited in the neighborhood of the region of impact owing to the high pressure of the gas molecules present. The amount of displaced material could be estimated roughly and appeared to be greater in N_2 than in H_2. No discoloration or other indications of chemical activity were observed. No simple correlation between any properties of the metals and the number of displaced atoms could be made. Etching in Al did not result in a crater-like pit, instead the whole surface of the tip of the point was roughened by a large number of fine

holes which were caused by a discharge constantly changing its position of the point because of alterations of the oxide-coated surface film by the impact of positive ions.

The introduction of impurities made the investigations difficult because it immediately reduced the currents by a factor of more than one hundred, thus making the time of observation prohibitively long. There was no doubt, however, that etching also occurred in these cases.

While not many data as to the mechanism are at hand, the character of the process is sufficiently like the sputtering phenomenon in glow discharges to make one feel that one is here dealing with a type of sputtering occurring at relatively low positive ion energies, but in distinction to sputtering caused by positive ions of high energies in low pressure glow discharges, this sputtering occurs with low ion energies at high current densities.

ACKNOWLEDGMENTS

The writer wishes to express his appreciation to Professor Leonard B. Loeb, who suggested the problem, guided its progress, and helped in the interpretation of the observed data. The writer is also indebted to the Research Corporation of New York, under whose Research Fellowship Grant at the University of California the main part of this work has been completed.

PHYSICAL REVIEW VOLUME 63, NUMBERS 3 AND 4 FEBRUARY 1 AND 15, 1943

The Specific Primary Ionization of Cosmic Rays in Helium

WAYNE E. HAZEN
University of California, Berkeley, California

(Received November 17, 1942)

Values for the specific primary ionization of 46 cosmic rays in helium have been determined from cloud-chamber photographs. A magnetic field allowed separation into two groups: 21 electrons with energies near the energy for minimum ionization had a mean ionization of 7.33 ± 0.12 per cm, and 26 mesotrons with energies greater than the energy for minimum ionization had a mean ionization of 7.23 ± 0.12 per cm. The expected value for the latter figure, taking into account a logarithmic rise of ionization with energy, is 8.80 ions/cm. The experimental value for the minimum specific primary ionization in helium (corrected for the ionization in the vapor) is 6.5 ± 0.1 at N.T.P. Three protons were observed in the $H\rho$ range in which they can easily be identified; in this $H\rho$ range three particles constituted approximately one percent of the radiation.

THE primary ionization of electrons from radioactive sources has been determined by Williams and Terroux[1] in hydrogen and oxygen and by Skramstad and Loughridge[2] in nitrogen and neon. C. T. R. Wilson[3] counted the primary ions along the tracks of electrons with energies between ten and thirty kev. Theory predicts a logarithmic increase in ionization with energy when the kinetic energy is large compared to the rest energy. Kunze[4] failed to detect any rise in ionization in measurements on ten cosmic-ray particles with energies around 10^9 ev. Since it is now known that most of the particles with this energy are mesotrons, the ionization should correspond to that of electrons with $H\rho=10^9m/300\mu$, where μ and m are the masses of the mesotron and the electron, respectively. When this correction is made, Kunze's value of 19 ions/cm in normal air agrees with the minimum ionization found for electrons. C. T. R. Wilson[3] also counted primary ions in nine straight tracks of unknown energy which presumably were cosmic-ray mesotrons and obtained a value of 20 ions/cm. In the present experiment the primary ionization of both cosmic-ray electrons and mesotrons was measured.

[1] E. J. Williams and F. R. Terroux, Proc. Roy. Soc. **A126**, 289 (1930).
[2] H. K. Skramstad and D. L. Loughridge, Phys. Rev. **50**, 677 (1936).
[3] C. T. R. Wilson, Proc. Roy. Soc. **A104**, 192 (1923).
[4] P. Kunze, Zeits. f. Physik **83**, 1 (1933).

APPARATUS

The cloud chamber used in obtaining the photographs was 30 cm in diameter and 30 cm deep with a magnetic field of about 1000 oersteds from two Helmholtz coils. Illumination was provided by four 6000-lumen medium bi-post street lamps which were operated at about 70 volts for one second. Four sets of four-inch condensing lenses were adjusted to give slightly convergent beams of light which entered the cloud-chamber cylinder near the rear and passed out of the cylinder near the front, making an angle of 50° with the axis. Photographs were taken on Agfa Ultraspeed 35-mm film with a stereoscopic camera equipped with 5-cm lenses and a curtain type shutter. The lenses were focused for different distances (54 and 59 cm) in order to make use of a large portion of the cloud-chamber volume. With lens apertures of f : 8 the depth of focus of each lens was about 5 cm. The program of operations involved in taking photographs was controlled by a cam system driven by an induction motor, the speed of which was essentially 1800 r.p.m. A pulse of x-radiation could be sent into the chamber at any desired time during the program in order to see if the chamber was still sensitive. The pulse came from a Coolidge type tube during the application of a 15,000-volt a.c. pulse to the target.

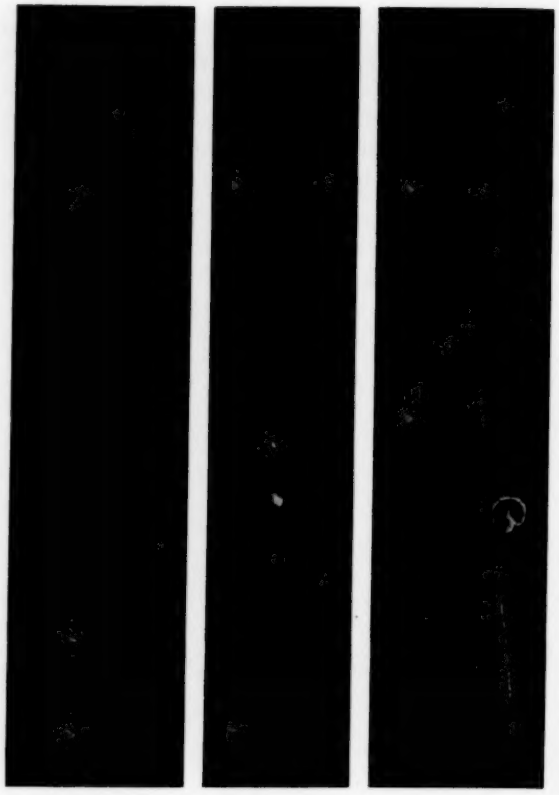

FIG. 1. Post expansion tracks of cosmic rays. There are two electron tracks in the left picture, a mesotron in the middle picture, and a proton and two electrons in the right picture. A pre-expansion diffuse track also appears in the right picture. The index marks represent 5 cm in the cloud chamber.

PROCEDURE

The chamber was filled with helium gas and the saturated vapor from a 1:3 water-ethanol liquid mixture, to a total pressure of 1.2 atmos. Such a gas mixture gives about seven primary ions per centimeter of cosmic-ray path at the expanded pressure and since the magnification was about one-tenth, one obtains about seven droplet images per millimeter on the film. The mean image diameter was 0.003 cm so that the correction factor for overlapping of images is 1.1. In using the cloud chamber to determine ionization one must consider the efficiency of ions as condensation nuclei at the time the track in question was formed. In measuring primary ionization only post-expansion tracks can be used because a large cloud chamber cannot conveniently be expanded quickly enough to produce a truly sharp track. Expansions are therefore made at random and sharp tracks in good focus sometimes occur. The frequency of occurrence depends on the usable sensitive time of the chamber, which in turn may depend on the velocity of fall of the drops or on the actual sensitive time of the chamber. In the case of the present experiment, the maximum sensitive time for condensation on about 50 percent of the positive ions was 0.3 sec. The dependence of condensation efficiency on expansion ratio has been determined by Bagley[5] and by Nielsen[6] and the dependence of sensitive time on expansion ratio by the author.[7] From such information the fraction of the sensitive time during which the condensation efficiency on ions remains greater than say 90 percent can be found. This fraction is approximately one-third

[5] G. D. Bagley, Phys. Rev. **56**, 851 (1939).
[6] C. E. Nielsen, Ph.D. thesis, University of California (1941).
[7] W. E. Hazen, Rev. Sci. Inst. **13**, 247 (1942).

and the usable sensitive time, when we allow ten percent for uncertainty, was therefore 0.1 sec. in the present experiment. The sensitive time was checked after every few expansions and the chamber was adjusted to keep the sensitive time greater than 0.3 sec.

Since the drops required 0.15 sec. or more to grow to photographable size, under the conditions existing in this experiment, the camera shutter was tripped 0.25 sec. after the expansion. At the end of 0.25 sec. a water-alcohol drop in helium falls two cm/sec. and as a result the image moves 0.2 cm/sec. A shutter speed of 1/150 sec. therefore allows an image motion of only 0.0013 cm (less than one-half the image diameter) and the resulting elongation is scarcely noticeable. With this shutter speed good photographic images were obtained with lens apertures of f:9; larger apertures increase the image size and hence lower the resolution. Tracks of particles that passed through the cloud chamber immediately after the expansion were not appreciably distorted by their fall of 3 mm which occurred before the photograph was taken.

The position and angle of the tracks were determined by reprojection through the camera onto a screen which was adjusted so that the two images coincided. This method allowed the determination of track lengths to within a few percent. The apparent curvature of the images of straight lines that did not pass through the camera axis was found to be negligible (40-m radius of curvature). Reproductions of some of the photographs are shown in Fig. 1.

TABLE I. Figures used in estimating mean primary ionization per cm for a group of cosmic rays with $H\rho > 10^6$. Blackett gives the spectrum in terms of energy E. Since the values for E were obtained from $E = 300H\rho$ and since there are significant departures from this simple relation for mesotrons in the lower energy range, Blackett's values of E were changed to $H\rho$ by dividing by 300.

$H\rho$ group	Fraction of sea level radiation	Fraction of particles with $H\rho > 10^6$	Mean ionization	Products of columns one and two
$1-3\times10^6$	0.142	0.213	7.7	1.64
$0.3-1\times10^7$	0.276	0.414	8.5	3.52
$1-3\times10^7$	0.173	0.260	9.3	2.42
$0.3-1\times10^8$	0.051	0.077	10.3	0.80
$>10^8$	0.024	0.036	11.7	0.42
	Expected mean ionization			$=8.80$

RESULTS

Out of 180 photographs, 46 tracks of high velocity particles were obtained which were in sharp focus for at least several centimeters. These 46 tracks fall into two distinct groups; one group consists of 21 electrons in the $H\rho$ range from 2.5×10^5 to 3×10^4, the other of 25 particles with $H\rho \geq 10^6$. The electron group extends over an energy band which is roughly centered on the minimum and is sufficiently narrow to allow consideration of the ionization of all the particles as a group.

The weighted mean for the specific primary ionization of the 21 electrons is 7.33 ions/cm with a probable error of the mean of 1.6 percent or a mean error of 11 percent for one observation. The mean statistical error $1/\sqrt{n}$ for the individual observations averages 13 percent; the main error in the observations is therefore statistical. The weighted mean for the 25 particles with $H\rho \geq 10^6$ is 7.23 ions/cm with a probable error of the mean of 1.7 percent or a mean error of 12.7 percent for one observation. Again the mean statistical error for individual observations averages 13.4 percent and the main error is therefore statistical.

The close agreement between the specific ionization for the electrons, which are known to have velocities near that for minimum ionization, and the specific ionization for the group of particles with $H\rho \geq 10^6$, indicates either that nearly all of the latter particles had an $H\rho$ less than 6×10^6 or that the primary ionization does not increase as rapidly with velocity as the theory predicts. The energy spectrum for particles with $H\rho$ greater than 10^6, as determined by Blackett,[8] is given in Table I together with the ionization[9] predicted by assuming a minimum

[8] E. J. Williams, Proc. Roy. Soc. **A172**, 206 (1939).

[9] The value for the ionization ($\bar{I}$) to be multiplied with the fractional number of particles in a given energy band can be approximated as follows for the higher energies. The fractional number of particles df with energy between E and $E+dE$ is essentially $df = cdE/E^2$, where c = constant. The ionization I of particles beyond the minimum is given approximately by $I = k \log E/E_0$, where k and E_0 are constants. Then $\bar{I} = \int_1^2 I df / \int_1^2 df$ and if all the quantities are expressed in terms of E

$$\log \bar{E}/E_0 = \frac{E_2 \log E_1/E_0 - E_1 \log E_2/E_0}{E_2 - E_1} + 1,$$

where $k \log \bar{E}/E_0 = \bar{I}$. For $E_2 = nE_1$

$$\bar{E} = eE_1/n^{1/(n-1)}$$ (e is the base of natural logarithms)

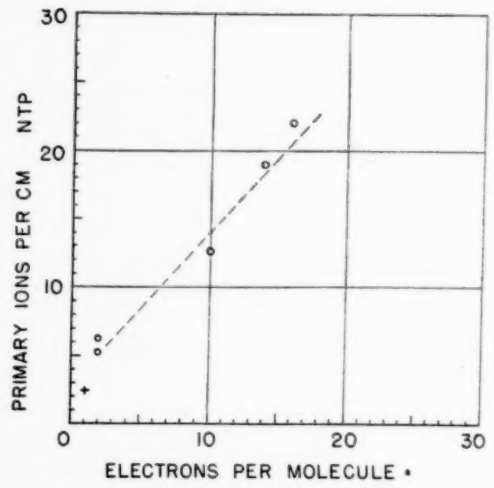

FIG. 2. Experimental values for the minimum primary ionization per centimeter in H_2, He, Ne, N_2, and O_2 are indicated by the circles (the upper circle at abscissa 2 is for He). The calculated value for atomic hydrogen is indicated by the cross. The straight line was used merely to estimate values for other molecules.

ionization of 7.3 and by assuming that the proportional increase in ionization with $H\rho$ is the same as that for atomic hydrogen.[10] Since the logarithmic rise obtained experimentally by Corson and Brode[11] for the probable ionization in nitrogen is about the same as the calculated value for atomic hydrogen, the second assumption just noted seems amply justified. By weighting each ionization with the corresponding fractional number of particles in that part of the spectrum, and by summing the resulting products, one obtains 8.80 ions/cm as the expected value for the mean ionization. This result is 22 percent larger than the observed value of 7.23 ions/cm, whereas the probable error of the mean is only 1.7 percent. Fermi[12] has shown that polarization of the medium reduces the ionization, but the effect is negligible in air for energies less than 10^{10} ev. There are so few particles with energy greater than 10^{10} ev that even if one assumes no increase whatsoever for the ionization in this range, the mean ionization should still be 8.70 ions/cm.

The above values are for the ionization in the helium, alcohol, and water atmosphere existing in the cloud chamber at a total pressure of 1.03 atmos. and a temperature of 22°C. The ionization in the alcohol and water vapor can be estimated from their partial pressures and their electron densities. If one plots the values for the ionization in H_2, Ne, N_2, and O_2 obtained by previous experiments[1,2] as a function of the number of electrons per molecule the ionization of other elements can be estimated from the resulting curve (Fig. 2). Thus for C_2H_5OH the value for I is 33 or 42 ions/cm depending on whether one chooses to extrapolate to $n=26$ electrons per molecule or to add values of I for C_2, $3H_2$, $\frac{1}{2}O_2$. The latter method seems more reasonable and was adopted. The partial pressures of H_2O and C_2H_5OH in equilibrium with a 1:3 liquid mixture were obtained from Gautier and Ruark.[13] The final value for He at N.T.P. is 6.5 ions/cm.

Three of the observed tracks had ionization and momentum consistent with protonic mass. Two of these were diffuse and appreciably curved in the magnetic field; the third (Fig. 1) was straight on each side of a bend produced by a close nuclear encounter but a delta-ray aided in the identification. These three particles constituted approximately one percent of the radiation in the $H\rho$ band from 10^6 to 3×10^6.

The magnet used in the investigation was designed and assembled by William Fretter. A detailed description will probably appear elsewhere at some later date. In concluding, the author wishes to express his appreciation to Professor R. B. Brode for the suggestion of the problem and for advice in carrying out the research.

and for $n=3$, $\bar{E}=1.6E_1$ or for $n=\infty$, $\bar{E}=eE_1$. The particles must be considered in several energy bands because the energy spectrum does not follow the $1/E^2$ distribution closely: the spectrum has a maximum at $E=10^9$ and falls off less rapidly, than $1/E^2$ for higher energies.

[10] E. J. Williams, Proc. Roy. Soc. **A139**, 163 (1933).

[11] R. B. Brode, Rev. Mod. Phys. **11**, 222 (1939).

[12] E. Fermi, Phys. Rev. **57**, 485 (1940).

[13] T. N. Gautier and A. E. Ruark, Phys. Rev. **57**, 1040 (1940).

PHYSICAL REVIEW VOLUME 63, NUMBERS 3 AND 4 FEBRUARY 1 AND 15, 1943

The Specular Reflection of Plane Wave Pulses in Media of Continuously Variable Refractive Properties

M. E. Rose*
Bartol Research Foundation of the Franklin Institute, Swarthmore, Pennsylvania
(Received December 3, 1942)

The specular reflection of plane waves is treated by the wave theory method. For the case in which the velocity of wave propagation and the radiation impedance vary sufficiently slowly that multiple reflection may be neglected the reflection coefficient is first obtained for monochromatic waves incident on a set of n plane parallel plates with otherwise arbitrary properties. The method may also be used to obtain the reflection coefficient in the case of large reflectivity but the results are exceedingly cumbersome for a large number of plates. The result for monochromatic waves is used to obtain the reflection coefficient for a plane wave pulse of arbitrary shape and duration. It is shown that the reflected wave train consists of a series of pulses of exactly the same form as the incident pulse with the amplitude of each reduced by the value of the appropriate Fresnel reflection coefficient. The interference effects are also represented. The sufficient condition for reproduction of the form of the incident pulse in the reflected wave is that the reflection coefficient for monochromatic waves be expressible as a sum of terms each of which is periodic in the frequency. In contrast to previous statements in the literature, periodicity of the coefficient itself is unnecessary. The results for the n plate problem are generalized for both monochromatic waves and pulses for the case of stratified media having reflective properties which vary continuously in any manner. The special case of rectangularly shaped pulses is analyzed and application is made to the reflection in sea water and in the atmosphere.

I. INTRODUCTION

IT is a well-known fact that the propagation of wave disturbances is characterized by reflection wherever there is a change in the physical properties of the medium. In the case that these changes are discontinuities localized at simple surfaces it is a very simple matter to determine the fraction of the incident energy which is reflected. Thus, the reflection coefficient for monochromatic plane waves incident obliquely on a plane parallel plate of homogeneous material separating two media with refractive indices differing from each other and from that of the plate is to be found in most standard texts.[1,2] The same problem has been solved for the case of plane wave pulses of arbitrary shape by Muskat who showed that the reflected train of waves will consist of a series of pulses of the same shape as the incident one but, of course, with diminished amplitude.[2] The problem of reflection of plane waves, whether monochromatic or not, in a medium of continuously varying refractive index (and/or density) does not appear to exist in the literature.

Some examples for which the treatment of this problem would be of interest may be mentioned. Thus, for the propagation of sound signals (or electromagnetic signals) through the atmosphere the properties of the medium on which the reflection depends are, in general, continuously variable. A similar situation applies in the case of the propagation of sound in sea water where the acoustic velocity depends on hydrostatic pressure, salinity, and temperature and hence changes continuously with depth. In the two cases cited the reflected intensity is, in general, partly due to convection currents which are usually present but in order to understand the role of each mechanism of reflection it is advantageous to consider each separately. We therefore leave out of consideration any movement of the medium. In the following we shall first consider the reflection of monochromatic plane waves in a medium of arbitrarily varying reflective properties. We may then proceed to the treatment of plane wave pulses of arbitrary shape and duration.[3]

* Now at Princeton University.

[1] For example, Rayleigh, *Theory of Sound* (Macmillan and Company, New York, 1929) second edition, vol. 2, p. 86.

[2] M. Muskat, J. App. Phys. 9, 275 (1938). Each pulse in the reflected train corresponds to an odd number of internal reflections in the plate and the amplitude of each individual multiply-reflected pulse contains the well-known Fresnel reflection coefficient raised to an appropriate power. Although the pulses retain their form this would be recognizable in the reflected wave pattern only if there is no overlapping, that is, if the time for traversing the plate twice along the directions of the incident and reflected waves is less than the duration of the initial pulse.

[3] It is perhaps worthy of mention that Rayleigh, in his book (reference 1) on page 86 gives the following reference which is here quoted verbatim: "It is interesting and

II. REFLECTION OF MONOCHROMATIC PLANE WAVES

Although the following analysis is equally applicable to sound waves in fluid media, transverse polarized waves in general elastic media and to polarized electromagnetic waves, we shall adopt the language of acoustics. The appropriate modifications in terminology for application to the other types of waves will be readily apparent and needs no further comment at this time.

Concerning the medium in which the plane waves are propagated we make the following assumptions:

(a) The medium is stationary, that is, there are no convection currents, nor thermal currents, etc.

(b) The medium is isotropic. This is obviously the case in those media for which the present problem is pertinent.

(c) The medium is stratified. That is, all physical properties upon which reflection depends (velocity and radiation impedance mainly) are constant over a set of parallel planes and vary only in the direction normal to these planes.

(d) The medium is non-dissipative. This assumption is particularly well justified in the acoustic case or for the longer electromagnetic radiations.

(e) The medium is non-dispersive. This assumption is, of course, of particular importance for the more general case of reflection of pulses considered in Section III below.

In accordance with assumption (c) the velocity of sound c, and the density and compressibility of the medium as well, depends on only one variable x. In the planes in which the velocity, etc., are constant we use a rectangular coordinate system y, z and we choose the y axis in the plane of incidence. The problem is then two-dimensional and z is a non-essential coordinate. Without loss of generality we may suppose that there exists a region of uniform properties in which the incident wave travels. The reflecting medium may then extend from $x=0$ to $x=a$ and we suppose that for $x>a$ the medium is again uniform and non-reflecting. As will be evident, the case in which a discontinuity in reflective properties occurs at any point is readily obtained from the analysis to be given.

The wave equation for the velocity potential may then be set up with the physical constants which enter it being regarded as arbitrary functions of x. In order to solve this equation for the most general case we adopt the following procedure.[4] The reflecting region between $x=0$ and $x=a$ is divided into n subregions by $n+1$ planes at $x=x_\nu$, $\nu=0, 1\cdots n$. In each subregion or lamina, whose thickness is $\delta_\nu=x_\nu-x_{\nu-1}$, the velocity c (also the density ρ) have arbitrary but constant values. We thus consider the case of reflection from n plane parallel plates of homogeneous material. Since this problem possesses some intrinsic interest we may treat the general case in which the plate thicknesses δ_ν are not necessarily equal. This generalization is, of course, unnecessary for the transition to the case of continuous media which will be made later.

We denote the region of the νth plate by the subscript ν. The homogeneous medium in which the wave is incident ($x<0$) is then denoted by the subscript 0 and the homogeneous medium for $x>a$ by the subscript $n+1$. Then if ϕ_ν is the velocity potential in the νth region ($x_{\nu-1}\leqslant x\leqslant x_\nu$) and c_ν is the corresponding velocity, the wave equation is

$$\frac{\partial^2\phi_\nu}{\partial x^2}+\frac{\partial^2\phi_\nu}{\partial y^2}=\frac{1}{c_\nu^2}\frac{\partial^2\phi_\nu}{\partial t^2}=-k_\nu^2\phi_\nu, \qquad (1)$$

where we have used the time dependence $e^{-i\omega t}$

encouraging to note Laplace's remark in a correspondence with T. Young. The great analyst writes (1817) 'Je persiste à croire que le problème de la propagation des ondes, lorsquèlles traversent différens milieux, n'a jamais été résolu, et qu'il surpasse peut-être les forces actuelles de l'analyse.' (Young's *Works*, vol. I, p. 374)." On the other hand, quoting from Rayleigh, page 78 of the same reference: "The problem of vibrations of a variable medium is probably quite beyond the grasp of our present mathematics"!

[4] An alternative method for the solution of the wave equation with arbitrarily given functions $c(x)$, etc., would be the approximate W.K.B. procedure, see for example G. Wentzel, Zeits. f. Physik **38**, 518 (1926). Here one assumes that the relative change in velocity, etc., in a distance of one wave-length λ is small; i.e., $\lambda d\log c/dx\ll 1$, etc. Although this assumption is justified in most cases of interest and the correct order of magnitude of the reflection coefficient is obtained, the W.K.B. method neglects interference effects, which are in general important. The method used here, on the other hand, is exact and automatically takes the interference effects into account in a proper manner.

for monochromatic waves, and

$$k_\nu=\omega/c_\nu. \quad (\omega=2\pi\times\text{frequency}). \tag{2}$$

In each region the velocity potential will consist of two terms corresponding to a wave traveling in the direction of increasing x (incident wave), and a reflected wave traveling toward decreasing x. Denoting the angle between the direction of propagation and the positive x axis by ϑ_ν and ϑ_ν' for these two waves, respectively, we have aside from the time factor

$$\phi_\nu=B_\nu \exp\left[ik_\nu(x\cos\vartheta_\nu+y\sin\vartheta_\nu)\right] + B_\nu' \exp\left[ik_\nu(x\cos\vartheta_\nu'+y\sin\vartheta_\nu')\right], \tag{3}$$

where B_ν and B_ν' are amplitude constants which, in general, are complex. For $x>a$ we have no further reflection; therefore

$$B_{n+1}'=0. \tag{4}$$

Since we are interested in obtaining the reflection coefficient (for the amplitudes) which is given by the ratio

$$r=B_0'/B_0, \tag{5}$$

we may, without loss of generality, take $B_0=1$. Then $r=B_0'$, and the fraction of the incident energy flux which is reflected is

$$R=|r|^2=|B_0'|^2. \tag{6}$$

There remains $2n+2$ unknown constants, B_0', B_1, B_1', $\cdots$, B_n, B_n' and B_{n+1} which are to be determined by the boundary conditions:

(a) Continuity of the normal component of velocity $\partial\phi/\partial x$ and

(b) Continuity of the pressure $\rho\partial\phi/\partial t$ or of $\rho\phi$, at each of the $n+1$ boundaries. These conditions are $2n+2$ in number and are therefore just sufficient to determine all the constants, and in particular B_0'.

In order that the boundary conditions which are to be applied at $x=x_\nu$ be fulfilled at all points of the boundary it is evident that the exponents

$$k_\nu(x_\nu\cos\vartheta_\nu+y\sin\vartheta_\nu),$$
$$k_{\nu+1}(x_\nu\cos\vartheta_{\nu+1}+y\sin\vartheta_{\nu+1}),$$
$$k_\nu(x_\nu\cos\vartheta_\nu'+y\sin\vartheta_\nu'),$$
$$k_{\nu+1}(x_\nu\cos\vartheta_{\nu+1}'+y\sin\vartheta_{\nu+1}'),$$

be the same for all y. Hence

$$k_\nu\sin\vartheta_\nu=k_\nu\sin\vartheta_\nu'=k_{\nu+1}\sin\vartheta_{\nu+1} =k_{\nu+1}\sin\vartheta_{\nu+1}', \tag{7}$$

or

$$\sin\vartheta_\nu=\sin\vartheta_\nu', \quad \vartheta_\nu=\pi-\vartheta_\nu', \tag{7a}$$

and

$$\sin\vartheta_\nu/\sin\vartheta_{\nu+1}=k_{\nu+1}/k_\nu=c_\nu/c_{\nu+1}. \tag{7b}$$

Equation (7a) gives the specular law of reflection and (7b) gives the usual Snell law for refraction. The latter relationship, of course, defines the path of a ray in the medium for each angle of incidence.

We may now drop the common factors in (3) and apply the boundary conditions to

$$B_\nu\exp(ik_\nu x\cos\vartheta_\nu)+B_\nu'\exp(-ik_\nu x\cos\vartheta_\nu).$$

Applying these conditions at x_ν and introducing

$$\beta_\nu=\rho_\nu B_\nu, \quad \beta_\nu'=\rho_\nu B_\nu',$$
$$\alpha_{\nu+1}=\frac{\rho_\nu k_{\nu+1}\cos\vartheta_{\nu+1}}{\rho_{\nu+1}k_\nu\cos\vartheta_\nu}, \quad \xi_\nu=k_\nu x_\nu\cos\vartheta_\nu,$$
$$\eta_{\nu+1}=k_{\nu+1}x_\nu\cos\vartheta_{\nu+1}, \tag{8}$$

we find

$$\beta_\nu\exp(i\xi_\nu)+\beta_\nu'\exp(-i\xi_\nu) =\beta_{\nu+1}\exp(i\eta_{\nu+1})+\beta_{\nu+1}'\exp(-i\eta_{\nu+1}), \tag{9a}$$

$$\beta_\nu\exp(i\xi_\nu)-\beta_\nu'\exp(-i\xi_\nu) =\alpha_{\nu+1}[\beta_{\nu+1}\exp(i\eta_{\nu+1}) -\beta_{\nu+1}'\exp(-i\eta_{\nu+1})], \tag{9b}$$

$$\nu=0, 1\cdots n.$$

These equations constitute recurrence formulae in the β's whose definition is completed by the auxiliary conditions

$$\beta_0=\rho_0, \quad \beta_{n+1}'=0. \tag{9c}$$

The reflection coefficient is now given by

$$r=\beta_0'/\beta_0=\beta_0'/\rho_0. \tag{10}$$

The recurrence formulae may be placed in more convenient form by solving (9a) and (9b) for β_ν and β_ν'. We find

$$\beta_\nu=\tfrac{1}{2}\exp(-i\xi_\nu)[(1+\alpha_{\nu+1})\exp(i\eta_{\nu+1})\beta_{\nu+1} +(1-\alpha_{\nu+1})\exp(-i\eta_{\nu+1})\beta_{\nu+1}'], \tag{11a}$$

$$\beta_\nu'=\tfrac{1}{2}\exp(i\xi_\nu)[(1-\alpha_{\nu+1})\exp(i\eta_{\nu+1})\beta_{\nu+1} +(1+\alpha_{\nu+1})\exp(-i\eta_{\nu+1})\beta_{\nu+1}']. \tag{11b}$$

Although these equations may be solved for any β_ν' or β_ν in terms of $\beta_0=\rho_0$ by a straightforward iterated process of substitution, it seems impossible to obtain a general formula for arbitrary α and an arbitrary number of laminae. Thus, the above equations may be used for the problem of a finite number of plates although the result for a large number of plates is extremely cumbersome; but it is evident that for the case of a continuously varying α, where the number of plates must be taken to be very large, it is necessary to make some simplification in order to obtain a practical solution. We now make the simplifying assumption, which will be generally well fulfilled, that all the α_ν are very nearly equal to unity. This means that the relative change of α [cf. Eq. (8)], is small compared to α itself. Thus we write

$$\alpha_\nu=1+\epsilon_\nu \quad \text{and} \quad \epsilon_\nu \ll 1. \tag{12}$$

The physical meaning of this approximation will be made clear in the following.

It is to be noted that the magnitude of the reflection coefficient, aside from interference effects, is determined by α (or better $\alpha-1=\epsilon$), which contains the velocity and density (and the angle of incidence as well). The velocity and angle of incidence are also contained in the exponents ξ and η but these exponential factors control the interference phenomena only. With the approximation (12) it is easy to see that the reflection coefficient β_0'/β_0 will be of order ϵ and all the other ratios β_ν'/β_ν will also be of order ϵ. Therefore we write (11a) and (11b) in the form

$$\beta_\nu=\beta_{\nu+1}\exp(is_\nu), \tag{12a}$$

$$\beta_\nu'=\beta_{\nu+1}'\exp(-is_\nu)-\gamma_\nu, \tag{12b}$$

where

$$s_\nu=\eta_{\nu+1}-\xi_\nu, \tag{12c}$$

and

$$\gamma_\nu=\tfrac{1}{2}\epsilon_{\nu+1}\beta_{\nu+1}\exp[i(\xi_\nu+\eta_{\nu+1})]. \tag{12d}$$

From (12a) we find[5]

$$\beta_\nu=\beta_0\exp[-i(s_0+s_1+\cdots+s_{\nu-1})], \tag{13a}$$

so that

$$\gamma_\nu=\tfrac{1}{2}\epsilon_{\nu+1}\beta_0\exp[-i(s_0+s_1+\cdots+s_\nu)+i(\xi_\nu+\eta_{\nu+1})]. \tag{13b}$$

From (12b) we find

$$\beta_0'=-\gamma_0-\gamma_1\exp(-is_0)-\gamma_2\exp[-i(s_0+s_1)]-\cdots-\gamma_\nu\exp[-i(s_0+s_1+\cdots+s_{\nu-1})]+\beta_{\nu+1}'\exp[-i(s_0+s_1+\cdots+s_\nu)].$$

Setting $\nu=n$ and using (9c) and (13b) we have for the reflection coefficient:

$$r=-\tfrac{1}{2}[\epsilon_1\exp[2i(\eta_1-s_0)]+\epsilon_2\exp[2i(\eta_2-s_0-s_1)]+\cdots+\epsilon_{n+1}\exp(2i(\eta_{n+1}-s_0-s_1\cdots-s_n))]. \tag{14}$$

This result can be put in more convenient form if we note that the exponent in the term with $\epsilon_{\nu+1}$ as a factor is

$$2\chi_\nu=2(\eta_{\nu+1}-s_0-s_1-\cdots-s_\nu)=2(\eta_{\nu+1}-\sum_1^{\nu+1}\eta_i+\sum_0^{\nu}\xi_i).$$

Since $\xi_0=0$ [$x_0=0$, see Eq. (8)], we can write

$$\chi_\nu=\sum_1^{\nu}(\xi_i-\eta_i)=\sum_1^{\nu}k_i\delta_i\cos\vartheta_i; \quad \chi_0=0. \tag{15}$$

The final result for the reflection coefficient for n plates in the case that the density and compressibility (and therefore the velocity) change slowly is

$$r=-\tfrac{1}{2}\sum_1^{n+1}\epsilon_\nu\exp(2i\chi_{\nu-1}), \tag{16}$$

where χ_ν is given by (15) and ϵ_ν is given by (8) and (12). That is,

$$1+\epsilon_{\nu+1}=\frac{\rho_\nu c_\nu}{\rho_{\nu+1}c_{\nu+1}}\frac{\cos\vartheta_{\nu+1}}{\cos\vartheta_\nu}=\frac{\rho_\nu\tan\vartheta_\nu}{\rho_{\nu+1}\tan\vartheta_{\nu+1}} \tag{17}$$

by (7b).

This result for the reflection coefficient may be readily understood. Let us consider the case in which the first $\nu-1$ plates have identical properties and the remaining plates are also identical but differ in their reflecting properties from the first group of plates. Thus, a discontinuity occurs only at the interface of the $(\nu-1)$st and the νth plates and the reflection takes place only at this

[5] This approximation would not be sufficient for the determination of the transmitted intensity $\sim|\beta_{n+1}|^2$. For this it is necessary to consider the correction terms of order ϵ^2. This may be seen directly from a development of the recurrence relations and it is to be expected from the conservation of energy flux since the reflected energy is of order ϵ^2 as compared to the incident energy, [see Eq. (16) below].

interface. The reflection coefficient is then

$$r_\nu=\frac{Z_{\nu-1}-Z_\nu}{Z_{\nu-1}+Z_\nu}, \tag{16a}$$

where $Z_{\nu-1}$, Z_ν are the radiation impedances for the media to the left and right of the reflecting plane. For oblique incidence the impedance is given by[6]

$$Z_\nu=\rho_\nu c_\nu \sec \vartheta_\nu. \tag{16b}$$

For our case in which the impedance changes slowly we have

$$Z_{\nu-1}+Z_\nu\approx 2Z_{\nu-1}\approx 2Z_\nu.$$

Hence, using (17), we have

$$r_\nu\approx\tfrac{1}{2}\left(1-\frac{Z_\nu}{Z_{\nu-1}}\right)=-\tfrac{1}{2}\epsilon_\nu, \tag{16c}$$

as in (16). Thus, aside from the interference effects contained in the exponential factors of (16) the result given for the reflection coefficient is simply the sum of the reflected amplitudes arising at each of the $n+1$ interfaces with the proper Fresnel coefficient, $-\frac{1}{2}\epsilon_\nu$. That the factor $\exp(2i\chi_{\nu-1})$ correctly represents the effect of interference may easily be seen when it is noted that $2\chi_{\nu-1}$ represents the change in phase of a wave reflected at the νth interface between plates $\nu-1$ and ν. The factor 2 arises, of course, from the fact that the reflected wave is observed in the medium of incidence (medium 0) after propagation to and from the reflecting plane and the ray trajectories to and from this plane are symmetrical and give the same phase change.

The significance of the approximation made above [Eq. (12)] is now obvious. It is assumed that the impedance changes so slowly that multiple reflections contribute a negligible amount to the amplitude of the reflected wave. The terms corresponding to multiple reflection will be of order ϵ^3, $\epsilon^5\cdots$ corresponding to three, five, etc., reflections. The terms of order ϵ^3 must evidently involve a triple summation since the three reflections may occur at any set of three planes.[7]

[6] See, for example, J. C. Slater, *Microwave Transmission* (McGraw-Hill, New York), pp. 103–105. For the electromagnetic case there considered we have the following correlations in notation: $\rho=\mu$, magnetic permeability, $c=1/(\epsilon\mu)^{\frac{1}{2}}$, ϵ is the dielectric constant (cf. below).

[7] This is subject, of course, to the condition that the second plane lies between the first one and the medium 0 and the third lies between the second and the medium $n+1$.

The terminology may now be generalized so as to include reflection of other types of radiation:

(1) For the reflection of transverse waves polarized normal to the plane of incidence, $1/\rho$ is the rigidity modulus and r is the ratio of displacement amplitudes in the reflected and incident waves.

(2) For the reflection of electromagnetic waves polarized normal to the plane of incidence, ρ is the dielectric constant, and for polarization in the plane of incidence ρ is the magnetic permeability. In each case r is the ratio of magnetic or electric field vectors for the reflected and incident waves.

In concluding our treatment of the reflection of monochromatic waves from n plates we consider the problem of non-reflecting systems. Such considerations are then applicable to the elimination of reflection of light from glass or other materials by interference of the waves reflected from a set of plates, or the elimination of reflection of longer electromagnetic waves in transmission lines. For these purposes it is advantageous to select the properties of the reflecting system so that the waves reflected from adjacent plates (for instance) are exactly out of phase. Thus, for the n plates, the thickness and refractive index of each plate may be chosen so that a phase change of $\pi/2$ takes place in traversing the plate once in the propagation direction, (quarter wave-length plates). For short waves it is convenient to use larger thicknesses and in this case the phase change may be made equal to $\pi/2$ plus any integral multiple of π (integral multiple of half wave-lengths). This additional thickness does not change the interference effect and therefore gives the same reflection. Then for each plate

$$q_\nu\equiv k_\nu\delta_\nu\cos\vartheta_\nu=\frac{\pi}{2}+m\pi, \quad m=0,1\cdots, \tag{18}$$

which may be fulfilled for a particular angle of incidence.

In this case it is possible to solve the recurrence relations (11) in a rigorous manner. We introduce

$$F_\nu=\exp(i\xi_\nu)\beta_\nu, \quad F_\nu'=\exp(-i\xi_\nu)\beta_\nu', \tag{19}$$

so that (11a) and (11b) become

$$F_\nu=\tfrac{1}{2}[(1+\alpha_{\nu+1})\exp(-iq_{\nu+1})F_{\nu+1} +(1-\alpha_{\nu+1})\exp(iq_{\nu+1})F'_{\nu+1}]$$
$$=(-)^m\frac{i}{2}[(1+\alpha_{\nu+1})F_{\nu+1}-(1-\alpha_{\nu+1})F'_{\nu+1}], \quad (20a)$$

$$F_\nu'=\tfrac{1}{2}[(1-\alpha_{\nu+1})\exp(-iq_{\nu+1})F_{\nu+1} +(1+\alpha_{\nu+1})\exp(iq_{\nu+1})F'_{\nu+1}]$$
$$=(-)^m\frac{i}{2}[(1-\alpha_{\nu+1})F_{\nu+1}-(1+\alpha_{\nu+1})F'_{\nu+1}], \quad (20b)$$

where we have used (18). The solution of these recurrence formulae gives for the reflection coefficient:

(1) The number of plates n is even:

$$r=\frac{\alpha_2\alpha_4\cdots\alpha_n-\alpha_1\alpha_3\cdots\alpha_{n+1}}{\alpha_2\alpha_4\cdots\alpha_n+\alpha_1\alpha_3\cdots\alpha_{n+1}}. \quad (21a)$$

In terms of the impedances of each plate [cf. Eq. (16b)] this becomes

$$r=\frac{Z_0(Z_2Z_4\cdots Z_n)^2-Z_{n+1}(Z_1Z_3\cdots Z_{n-1})^2}{Z_0(Z_2Z_4\cdots Z_n)^2+Z_{n+1}(Z_1Z_3\cdots Z_{n-1})^2}. \quad (21b)$$

(2) The number of plates n is odd:

$$r=\frac{\alpha_2\alpha_4\cdots\alpha_{n+1}-\alpha_1\alpha_3\cdots\alpha_n}{\alpha_2\alpha_4\cdots\alpha_{n+1}+\alpha_1\alpha_3\cdots\alpha_n}$$
$$=\frac{(Z_1Z_3\cdots Z_n)^2-Z_0Z_{n+1}(Z_2Z_4\cdots Z_{n-1})^2}{(Z_1Z_3\cdots Z_n)^2+Z_0Z_{n+1}(Z_2Z_4\cdots Z_{n-1})^2}. \quad (22)$$

Both (21a) and (22) reduce to the proper limiting value in the case of small ϵ_ν [cf. Eq. (16)]:

$$r=-\tfrac{1}{2}(\epsilon_1-\epsilon_2+\epsilon_3-\cdots(-)^n\epsilon_{n+1}).$$

It is obvious that there are many ways in which the impedances may be adjusted so as to give no reflection. One convenient way is to choose:

(1) for n even

$$\alpha_1=\alpha_2, \quad \alpha_3=\alpha_4\cdots\alpha_{n-1}=\alpha_n$$

or,

$$Z_1^2=Z_0Z_2, \quad Z_3^2=Z_2Z_4\cdots Z_{n-1}^2=Z_nZ_{n-2}; \quad (23a)$$

(2) for n odd

$$\alpha_1=\alpha_2, \quad \alpha_3=\alpha_4\cdots\alpha_n=\alpha_{n+1}$$

or,

$$Z_1^2=Z_0Z_2, \quad Z_3^2=Z_2Z_4\cdots Z_n^2=Z_{n-1}Z_{n+1}. \quad (23b)$$

Thus, the impedance of each plate is the geometric mean of the impedances of the neighboring plates. In the case that n is odd it is seen that the reflection coefficient is zero. In this way the reflection from each pair of adjacent interfaces (at x_0x_1, x_2x_3, $\cdots$, $x_{n-1}x_n$) vanishes by interference. In the case that n is even, the values of the impedances given by (23a) gives a reflection coefficient [from Eq. (21b)]

$$r=\frac{Z_n-Z_{n+1}}{Z_n+Z_{n+1}}. \quad (24)$$

This result is also obvious since there are an odd number of interfaces and the choice of impedances has been made so that the reflection from all but the last interface vanishes (in pairs) by interference. To obtain no reflection in this case it is only necessary to match the impedances Z_n and Z_{n+1} so that no reflection takes place at the last interface.

III. REFLECTION OF PLANE WAVE PULSES. CASE OF N PLATES

In his treatment of the reflection of a plane wave pulse from a single plate Muskat[2] has shown that if the reflection coefficient for the monochromatic case is exactly periodic in the frequency, the reflection from the plate of a pulse will consist of a series of wave trains of exactly the same form as the incident pulse. The reflection coefficient for two or more plates is not, in general, periodic in the frequency as is evident from the result (16) of the previous section. Nevertheless, it can be shown that the theorem demonstrated by Muskat still holds in our case. The periodicity condition is therefore sufficient but not necessary.

The treatment of the reflection of the plane pulse for the case of n plates proceeds in just the same manner as for the case of a single plate. The incident pulse has an amplitude Φ_i given by

$$\Phi_i=f(\zeta); \quad 0\leqslant\zeta\leqslant b,$$
$$\Phi_i=0; \quad \zeta>b \text{ and } \zeta<0, \quad (25)$$

where

$$\zeta=t+s_i/c_0. \quad (25a)$$

Here s_i is the distance in the medium 0 measured along the wave normal, the time t is measured from the moment of incidence and s_i is measured from the point of incidence. The form of the

pulse $f(\zeta)$ is entirely arbitrary as is the duration of the pulse b.

The pulse may be regarded as a superposition of monochromatic plane waves given by the Fourier integral

$$\Phi_i(\zeta)=\frac{1}{2\pi}\int_{-\infty}^{\infty}d\omega\int_0^b f(\omega)e^{i\omega(u-\zeta)}du. \quad (26)$$

Since each component plane wave of frequency ω is reflected with an amplitude $r(\omega)$ times the corresponding incident amplitude, the reflected pulse is given by

$$\Phi_r(\zeta')=\frac{1}{2\pi}\int_{-\infty}^{\infty}r(\omega)d\omega\int_0^b f(u)e^{i\omega(u-\zeta')}du, \quad (27)$$

where $\zeta'=t-s_r/c_0$ and s_r defines the phase planes in the reflected wave system. Inserting the reflection coefficient $r(\omega)$ from (16) we have

$$\Phi_r(\zeta')=-\frac{1}{4\pi}\sum_1^{n+1}\epsilon_\nu\int_0^b duf(u)\int_{-\infty}^{\infty}d\omega \times\exp\left[i\omega(u-\zeta'+2p_{\nu-1})\right], \quad (28)$$

wherein the order of integration has been interchanged. In (28) we have introduced

$$p_{\nu-1}=\sum_1^{\nu-1}\frac{\delta_i}{c_i}\cos\vartheta_i \quad (28a)$$

[cf. Eq. (15)].

The integral

$$\frac{1}{2\pi}\int_{-\infty}^{\infty}d\omega e^{i\omega x}\equiv D(x),$$

which occurs in (28) has the following properties: $D(x)=0$ except for $x=0$ where D has a singularity of such strength that

$$\int_{-\infty}^{\infty}D(x)dx=\int_{-0}^{+0}D(x)dx=1. \quad (29)$$

From (29) it follows that

$$\int_{-0}^{+0}f(x)D(x)dx=f(0) \quad (29a)$$

provided $f(0)$ is non-singular. The limits of integration in (29) and (29a) need only include the singular point. Now the reflected pulse may be written

$$\Phi_r=-\tfrac{1}{2}\sum_1^{n+1}\epsilon_\nu\int_0^b duf(u)D(u-\zeta'+2p_{\nu-1})$$

$$=-\tfrac{1}{2}\sum_1^{n+1}\epsilon_\nu f(\zeta'-2p_{\nu-1}), \quad (30)$$

where $f=0$ unless $0\leqslant\zeta'-2p_{\nu-1}\leqslant b$. Equation (30) shows that the reflected pulse is given by a series of pulses each corresponding to the reflection of the incident pulse at one of the $n+1$ interfaces. Each component of this train of reflected pulses has an amplitude equal to the incident value multiplied by the Fresnel coefficient $-\frac{1}{2}\epsilon_\nu$. The interference is represented by the change in the argument (phase) of f and this change $2p_{\nu-1}$ is, as was explained before, just the expected phase change (divided by ω) for reflection at the νth interface. Thus, the reflected pulse consists of a series of wave trains identical in form with the incident pulse, aside from overlapping. The duration of each pulse in the reflected train is b and at $s_r=0$ the νth pulse starts at $t=2p_{\nu-1}$. Overlapping occurs whenever

$$b>\Delta t_\nu=2(p_\nu-p_{\nu-1})=\frac{2\delta_\nu}{c_\nu}\cos\vartheta_\nu. \quad (31)$$

Otherwise the pulses are separated by a time interval $\Delta t_\nu-b$. It is obvious that for the case of continuously varying velocity and impedance, overlapping must occur and the form of the incident pulse will not be recognizable in the reflected wave pattern.

The present results may be compared with the case of a single plate.[2] It may be noted that the assumption of small reflection (no multiple reflection) corresponds in Muskat's procedure to neglecting all terms in the Fourier series expansion of the monochromatic reflection coefficient beyond the second [cf. Eq. (7) of reference 2]. The first term of this expansion (frequency independent) corresponds to direct reflection at the first interface so that the wave does not enter the medium proper. The second term corresponds to a single reflection at the far side of the plate. It is easily verified that Muskat's result for the reflected amplitude [Eq. (12) of reference 2] reduces to the first two terms of (30) in the limiting case of small reflection.

IV. REFLECTION OF PLANE WAVES IN CONTINUOUS MEDIA

The transition to the case of a medium with continuously varying velocity and impedance is readily made. For this we have only to consider the Fresnel reflection coefficient and the phase change $2p_{\nu-1}\omega$. For the former we have

$$\epsilon_{\nu+1}=\frac{\rho_\nu \tan\vartheta_\nu-\rho_{\nu+1}\tan\vartheta_{\nu+1}}{\rho_{\nu+1}\tan\vartheta_{\nu+1}}.$$

In the limit of continuous variation this becomes (with $\delta_\nu\to dx$)

$$\epsilon_{\nu+1}\to\epsilon(x)=-dx\frac{d}{dx}\log\rho\tan\vartheta. \tag{32}$$

For the phase change we have

$$p_{\nu-1}\to\varphi(x)=\int_0^x\frac{dx}{c}\cos\vartheta. \tag{33}$$

For monochromatic waves the reflection coefficient now becomes

$$r=\tfrac{1}{2}\int_0^a dx\left(\frac{d}{dx}\log\rho\tan\theta\right)e^{2i\varphi(x)}, \tag{34}$$

where a is the thickness of the reflecting medium; i.e.,

$$a=\sum_1^n\delta_i. \tag{34a}$$

For plane wave pulses the reflected wave is from (30)

$$\Phi_r(\zeta')=\tfrac{1}{2}\int_0^a dx\left(\frac{d}{dx}\log\rho\tan\vartheta\right)\times f(\zeta'-2\varphi(x)). \tag{35}$$

It may be noted that while the departure of the radiation impedance from homogeneity is essential for the magnitude of the reflection this inhomogeneity is not essential in the interference factor $\varphi(x)$. In fact, to take the variation in velocity into account in evaluating φ would lead to correction terms of higher order in the parameter of smallness (ϵ). Therefore, in view of the approximation of small reflection already made it is consistent and necessary to evaluate φ for a homogeneous medium. Then the reflected wave (35) becomes

$$\Phi_r=\tfrac{1}{2}\int_0^a dx\left(\frac{d}{dx}\log\rho\tan\vartheta\right)\times f\left(\zeta'-\frac{2x}{c_0}\cos\vartheta_0\right). \tag{36}$$

This constitutes our final result. The reflection then depends only on the radiation impedance. It is evident that when the variation in impedance is given and the form and duration of the initial pulse is known it is a fairly simple matter to obtain the reflected wave pattern from (36).

A particularly interesting example to which these results may be readily applied is that of the rectangular pulse. Then for arguments between 0 and b the pulse f is constant, and since this constant enters only as a scale factor it may be taken equal to unity. Then

$$\Phi_r=\tfrac{1}{2}\int_{x_1}^{x_2}dx\frac{d}{dx}\log\rho\tan\vartheta=\tfrac{1}{2}\log\frac{\rho_2\tan\vartheta_2}{\rho_1\tan\vartheta_1}, \tag{37}$$

where x_1 and x_2 are the values of x for which the argument of f in (36) has the values b and 0, respectively; ρ_2, ϑ_2 and ρ_1, ϑ_1 are the values of ρ and ϑ at x_2 and x_1, respectively. Since we may take $s_r=0$, $\zeta'=t\geq 0$ and $x_2\geqslant x_1\geqslant 0$. For other values of s_r we need only make a shift of time scale to obtain the reflection pattern from that at $s_r=0$. In order to evaluate the limits x_1 and x_2 as functions of the time it is necessary to distinguish between two cases. Introducing τ according to

$$\tau=\frac{2a}{c_0}\cos\vartheta_0 \tag{38}$$

we must consider separately the cases $b>\tau$ and $b<\tau$.

In case (1), $b>\tau$, the duration of the pulse is greater than the propagation time τ. Then it is seen that the limits are:

$$\begin{aligned}
&\text{for } 0<t<\tau, && x_1=0, && x_2=\tfrac{1}{2}c_0t\sec\vartheta_0;\\
&\tau<t<b, && x_1=0, && x_2=a;\\
&b<t<b+\tau, && x_1=\tfrac{1}{2}c_0(t-b)\sec\vartheta_0, && x_2=a.
\end{aligned} \tag{39a}$$

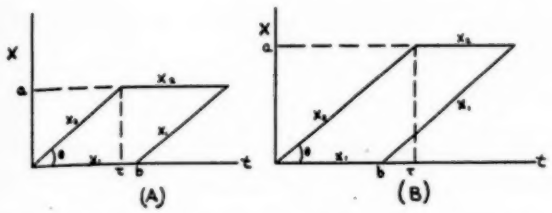

FIG. 1. Limits x_1 and x_2 [Eq. (39)] plotted against t.

In case (2) $b<\tau$ we find

$$\begin{aligned}
&\text{for } 0<t<b, && x_1=0, \quad x_2=\tfrac{1}{2}c_0 t \sec\vartheta_0;\\
&\quad b<t<\tau, && x_1=\tfrac{1}{2}c_0(t-b)\sec\vartheta_0,\\
& && x_2=\tfrac{1}{2}c_0 t\sec\vartheta_0;\\
&\quad \tau<t<b+\tau, && x_1=\tfrac{1}{2}c_0(t-b)\sec\vartheta_0, \quad x_2=a.
\end{aligned} \tag{39b}$$

If the limits x_1 and x_2 are plotted against t in the same diagram the figure obtained is a parallelogram as shown in Figs. 1A and 1B, which correspond to cases (1) and (2), respectively. In Fig. 1 the pulse duration b is considered to be the same in each case but for case (2) the reflecting layer is thicker. Similarly, for a fixed reflecting layer, case (1) corresponds to a pulse of longer duration than does case (2). In either case the parallelograms have the same base b and the same angle θ. Finally, the duration of the reflected train is always $\tau+b$.

The meaning of the foregoing is evident. At any time t the reflected wave is made up of contributions due to reflections at points extending at first from 0 to x_2, where x_2 is the maximum depth to which the wave may penetrate in order that after reflection it reaches a detector at $x=0$, at time t. As t increases x_2 obviously increases until it reaches the maximum value of a. Eventually x_1 departs from 0 because for larger values of t reflection from the layer at $x=0$ reaches the detector too soon. This must always occur for $t=b$, the duration of the pulse. The only difference between cases (1) and (2) is that in the former case the reflection from the deepest point $x_2=a$ is attained before x_1 departs from 0, while in the latter case the opposite is true. Therefore there is a time interval $\tau<t<b$ in case (1) during which the entire reflecting medium is operative in contributing to the intensity at the detector at a given time.

From the results obtained in (39a) and (39b) the reflected wave is obtained at once from (37):

Case (1)

$$\begin{aligned}
&\text{for } 0<t<\tau, && \Phi_r=\tfrac{1}{2}\log\frac{\rho_2\tan\vartheta_2}{\rho_0\tan\vartheta_0};\\
&\quad \tau<t<b, && \Phi_r=\tfrac{1}{2}\log\frac{\rho_a\tan\vartheta_a}{\rho_0\tan\vartheta_0}\\
& && \quad =\text{constant};\\
&\quad b<t<b+\tau, && \Phi_r=\tfrac{1}{2}\log\frac{\rho_2\tan\vartheta_2}{\rho_1\tan\vartheta_1}.
\end{aligned} \tag{40a}$$

Case (2)

$$\begin{aligned}
&\text{for } 0<t<b, && \Phi_r=\tfrac{1}{2}\log\frac{\rho_2\tan\vartheta_2}{\rho_0\tan\vartheta_0};\\
&\quad b<t<\tau, && \Phi_r=\tfrac{1}{2}\log\frac{\rho_2\tan\vartheta_2}{\rho_1\tan\vartheta_1};\\
&\quad \tau<t<b+\tau, && \Phi_r=\tfrac{1}{2}\log\frac{\rho_a\tan\vartheta_a}{\rho_1\tan\vartheta_1},
\end{aligned} \tag{40b}$$

where $\rho_1\tan\vartheta_1$ and $\rho_2\tan\vartheta_2$ are evaluated at

$$x_1=\tfrac{1}{2}c_0(t-b)\sec\vartheta_0, \quad x_2=\tfrac{1}{2}c_0 t\sec\vartheta_0. \tag{40c}$$

It is apparent that the reflected amplitude vanishes at the beginning and at the end of the time interval during which the reflected pulses reach the detector, ($x_1=x_2$ at $t=0$ and at $t=b+\tau$). Hence the absolute value of the amplitude or the intensity must reach a maximum during this time interval. If the impedance is a monotonic function of depth this maximum will occur during the second time interval $\tau<t<b$ in case (1). In case (2) the reflected amplitude must reach a maximum in the second interval ($b<t<\tau$) since from $t=0$ to b, Φ_r must increase while during the interval τ to $b+\tau$, Φ_r must decrease. The maximum in this case will not be as great as in case (1) however. When the impedance does not vary monotonically it is not possible to predict the time interval within which the maximum occurs but in any case this maximum cannot exceed the value

$$(\Phi_r)_{\max}=\tfrac{1}{2}\log\frac{(\rho\tan\vartheta)_{\max}}{(\rho\tan\vartheta)_{\min}}. \tag{41}$$

It is of interest to consider a numerical example in order to obtain a quantitative idea of the amount of reflection taking place in various media. For purposes of simplicity we consider the case of normal incidence which will suffice to give an order of magnitude estimate for the re-

flection. For normal incidence the impedance is simply ρc and in the above formula the factor $\tan\vartheta$ is omitted. The reflected wave is then given by

$$\Phi_r=\tfrac{1}{2}\log(\rho_{x_2}/\rho_{x_1}). \tag{42}$$

Consider the case of reflection in sea water in which the density is a function of depth alone. The temperature and salinity of sea water are fairly constant for small depths (up to about 500 meters at certain latitudes and at certain seasons). The temperature and salinity then decrease comparatively rapidly over a distance of order 1000 meters and then remain roughly constant, with the temperature approaching a value in the neighborhood of 4°C. Since the relative change of salinity is not very great (from about 0.036 to 0.035 from the surface to 3000 meters depth) we may consider only the temperature variation. Then the maximum reflected amplitude is given by

$$(\Phi_r)_{\max}=\tfrac{1}{2}\log(\rho_{\max}/\rho_{\min}), \tag{43}$$

where $\rho_{\max}$ is the density at great depths and $\rho_{\min}$ is the surface density. For a surface temperature of 15°C and a salinity content of 0.036 the surface density is 1.0255 g/cm³. For a temperature of 5°C and the same salinity the density at great depths is 1.0286 g/cm³.[8] Hence

$$(\Phi_r)_{\max}=\tfrac{1}{2}\log\frac{1.0286}{1.0255}=0.0015.$$

Therefore at most the reflected energy flux is 2×10^{-4} percent of the incident flux. We may conclude that unless much greater variations of density may occur, reflection in sea water is extremely small and provides a relatively unimportant mechanism of absorption.

A much more important case of reflection occurs in the atmosphere where relatively greater density variations take place. As a rough approximation we may take the barometric formula for the variation of density with height x above the surface of the earth.

$$\rho=\rho_0\varepsilon^{-\mu x}, \tag{44}$$

where $1/\mu=8000$ meters. Considering again the case of normal incidence we have for the reflected wave a formula of the type

$$\Phi_r=\tfrac{1}{2}\mu(x_1-x_2). \tag{45}$$

Since the reflecting layer will be, in general, sufficiently large to make the propagation time longer than the pulse duration, we must use the results found above for case (2). In this case the maximum reflection occurs for $b<t<\tau$ where x_2-x_1 attains a (constant) maximum value. Then

$$\Phi_r=-\tfrac{1}{4}\mu c_0 b. \tag{45a}$$

For a pulse duration measured in seconds, and with $c_0=330$ meters per sec. we find

$$\Phi_r=-10^{-2}b. \tag{45b}$$

Thus for 1-sec. pulses, 1 percent of the energy flux is reflected.

The ratio of reflected energy to incident energy is

$$\frac{E_r}{E_i}=\frac{1}{b}\int_0^{b+\tau}\Phi_r^2dt=\frac{\mu^2c_0^2}{16}(\tfrac{1}{4}\tau^2+\tfrac{1}{2}b\tau-\tfrac{1}{3}b^2) \tag{46}$$

from (45) and (39b), and when we use (38) for $\vartheta_0=0$. Since $\tau>b$ we may write

$$E_r/E_i\approx\mu^2c_0^2\tau^2/64=\tfrac{1}{16}(\mu a)^2. \tag{46a}$$

Equation (46) is valid only if $\mu a\ll1$. For $a=2000$ meters (which implies a pulse duration $b<12$ sec.), $E_r/E_i\approx1/256\approx0.4$ percent. Since we have used the barometric formula which underestimates the variation of density with elevation, the reflection should be somewhat more intense than is here indicated.

We may note that the reflection of monochromatic waves in the isothermal atmosphere, the density being given by (44), is also quite small. From (34) we find (since the sound velocity is constant and therefore ϑ is constant),

$$r=-\frac{i}{4}\frac{\mu}{k_0}\sec\vartheta_0. \tag{47}$$

For a frequency of 1000 sec.$^{-1}$, $|r|=1.6\times10^{-6}$ sec ϑ_0. This small reflection is essentially due to the slow rate of variation of the density. The distance $1/\mu$, in which the density changes appreciably, is much larger than any other length involved in the problem.

[8] *International Critical Tables* (McGraw-Hill, New York), first edition, vol. III, p. 100.

PHYSICAL REVIEW VOLUME 63, NUMBERS 3 AND 4 FEBRUARY 1 AND 15, 1943

Ionization and Dissociation by Electron Impact: The Methyl and Ethyl Radicals*

JOHN A. HIPPLE AND D. P. STEVENSON†
Westinghouse Research Laboratories, East Pittsburgh, Pennsylvania

(Received December 5, 1942)

The lead tetra-alkyls, $Pb(CH_3)_4$ and $Pb(C_2H_5)_4$, were decomposed to yield free methyl and ethyl radicals in a specially designed furnace built into the ionization chamber of a 180° mass spectrometer tube. From the initial breaks of the ionization efficiency curves of the ions, CH_3^+ and $C_2H_5^+$, we have found the ionization potentials of the methyl and ethyl radicals to be $I_{vert}(CH_3) = 10.0_0 \pm 0.1$ ev and $I_{vert}(C_2H_5) = 8.6_0 \pm 0.1$ ev. These values are in excellent agreement with those found by indirect calculations from other electron impact data on hydrocarbons. Some of the implications of these results are briefly discussed.

INTRODUCTION

BESIDES their importance to the formulation of the theory of the thermal decomposition of hydrocarbons,[1] the energies of the methyl and ethyl free radicals have considerable theoretical significance. The calculation of the relative energies of CH_4, CH_3+H, CH_2+2H, $CH+3H$, and $C+4H$ is a very suitable test of any quantum mechanical theory of valence.[2] Thus accurate values of these energies are desirable for checking the calculations or for the evaluation of parameters in the theoretical equations. A knowledge of the ionization potentials of the various radicals is important for the same reasons.

In the recent past a considerable body of information has been built up pertaining to the ionization and dissociation of various hydrocarbons by electron impact. In order to interpret these data in an unambiguous fashion and to check those interpretations which have been made, the energetic quantities mentioned above were needed.

Several years ago Fraser and Jewitt[3] reported values for the ionization potentials of the methyl and ethyl radicals, determined by the molecular beam technique. Their well conceived experiments suggested to us the desirability of repeating this work with the mass spectrometer as a detector of the ionization. The repetition seemed particularly desirable, inasmuch as a great deal of the more recently obtained data were very difficult to reconcile with the ionization potentials reported by Fraser and Jewitt.

EXPERIMENTAL

The mass spectrometer used in this research is to be described by one of the authors (J. A. H.) in a separate publication, hence only pertinent details will be reported here.

The electrons are obtained from an oxide-coated platinum cathode, their accelerating potential being controlled by means of a wire wound drum potentiometer. The accelerating voltage is read with an accuracy of ±0.1 percent on a calibrated voltmeter. A separate pumping

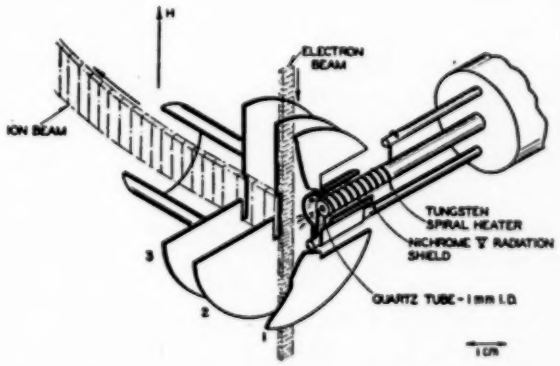

FIG. 1. The furnace and ion source assemblage. The lead alkyls were admitted to the tube through the quartz tube —the end of which is heated by the tungsten spiral. Emerging from the quartz tube, some of the molecules and free radicals are ionized by the electron beam. The ions are drawn to 2 by a small field between 1 and 2; passing through 2, they are accelerated through the slit in 3 by a difference of potential of about 500 volts between 2 and 3, entering the analyzer region where the magnetic field (H) sorts out the ions of different masses (180°-analyzer).

* Presented at the Physical Society Meeting at State College, Pennsylvania, June, 1942.

† Westinghouse Research Fellow. Present address—Shell Development Company, Emeryville, California.

[1] F. O. Rice and K. K. Rice, *The Aliphatic Free Radicals* (Johns Hopkins Press, Baltimore, 1935).

[2] H. H. Voge, J. Chem. Phys. **4**, 584 (1936). The most elaborate quantal calculation.

[3] R. G. J. Fraser and T. N. Jewitt, Phys. Rev. **50**, 1091 (1936); Proc. Roy. Soc. **A160**, 563 (1937).

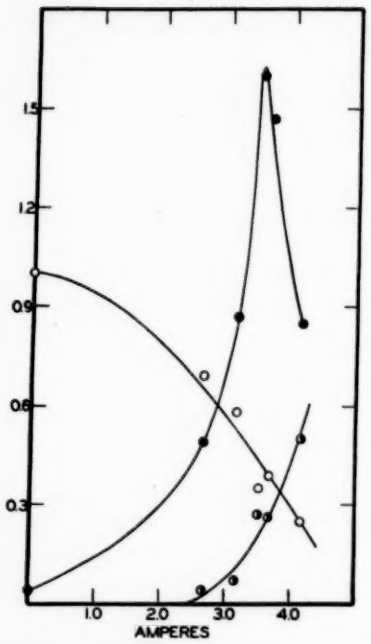

FIG. 2. The effect of furnace temperature on the relative abundance of the ions $Pb(CH_3)^+$ (open circles), CH_3^+ (closed circles) and CH_4^+ (half closed circles) in the spectrum obtained from $Pb(CH_3)_4$.

lead to the arm of the tube, containing the cathode chamber, assures the complete removal of any pyrolysis products formed on the filament itself and on the adjacent parts of the tube heated by radiation from the filament. Argon admitted simultaneously with the substance being studied serves to calibrate the electron accelerating voltage scale.

An isometric view of the ion source and the furnace in which the lead alkyls were thermally dissociated is shown in Fig. 1. The furnace consists of a quartz capillary tube (I.D.$\sim$1 mm) closely wound with 20-mil tungsten wire for the last 1.5 cm of its length. The wound zone is surrounded by a nichrome *V* radiation shield. This radiation shield, welded to one of the tungsten heater leads (80 mil) is connected to the high voltage electrode 1. The heater current is controlled by a variac, isolated from the high voltage electrodes by means of an insulating transformer. We have no means of measuring the temperature in the present arrangement, but five amperes bring the furnace to incipient red heat ($\sim$500°C). The end of the quartz tube is about 5 mm from the electron beam, which is indicated in the figure.

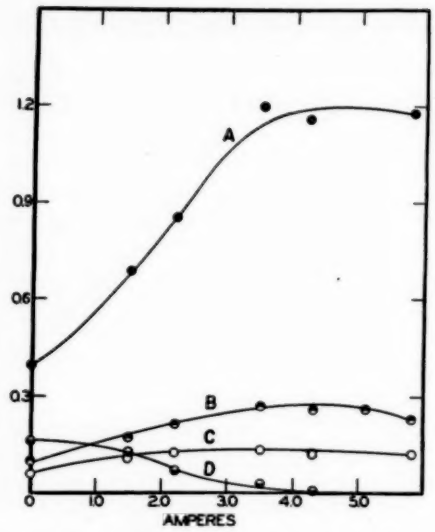

FIG. 3. The variation of the relative abundance of the ions $C_2H_4^+$ (*A*), $C_2H_5^+$ (*B*), $Pb(C_2H_5)_3^+$ (*C*), and $C_2H_6^+$ (*D*) in the spectrum of $Pb(C_2H_5)_4$ with furnace temperature.

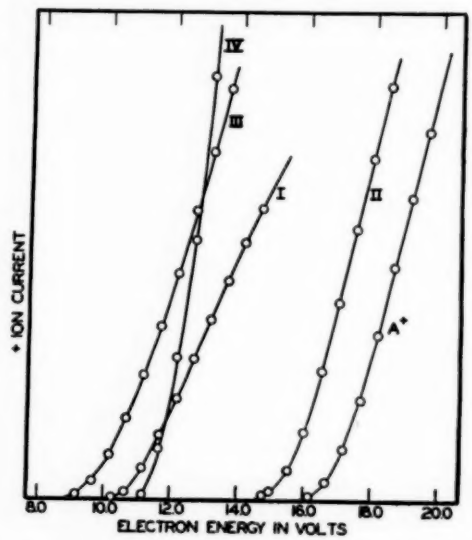

FIG. 4. Ionization efficiency curves: *I* and *II* are CH_3^+, *III*, $C_2H_5^+$, and *IV*, $C_2H_4^+$. See text, Table I.

The lead alkyls were admitted at low pressure to the lead connecting to the furnace by means of a fine capillary leak, the pressure in back of the leak being adjusted by fixing the temperature of the liquid ($Pb(CH_3)_4 \sim -10°C \cdot Pb(C_2H_5)_4 \sim +30°C$). The argon was admitted simultaneously through a parallel leak. The vapor (and argon) flow through the quartz furnace into the path of the electron beam where the ionization takes place. The products of the thermal dissoci-

ation in the furnace can then be studied with the mass spectrometer.

The specially purified samples of the lead alkyls were kindly supplied to us by the Ethyl Gasoline Corporation. In Fig. 2 the relative currents of the positive ions $Pb(CH_3)_3^+$, CH_4^+, and CH_3^+ produced from $Pb(CH_3)_4$ with 20-volt electrons are shown as a function of the heating current. The $Pb(CH_3)_3^+$ is used as an indicator of the completeness of the thermal decomposition because the parent ion is absent. The striking feature of these curves is the sharp resonance found for the production of the methyl radicals as a function of the temperature. It should be noted that, as the temperature is increased beyond that shown in the figure, the CH_3^+ current passes through a minimum and then increases at the same rate as the CH_4^+ current; this indicates that in the higher temperature range the CH_3^+ observed is the product of the dissociation of methane by electron impact. In addition to the ions mentioned above, there is a very large current at mass 28, increasing with temperature, which can be attributed to ethylene with confidence.

At first it was hoped that a sufficient number of free radicals would be formed by dissociation of the lead compounds on a filament close to the electron beam. The failure to observe any free radical formation by this technique with either tungsten or platinum filaments was explained by the sharp maximum for the CH_3^+ current as obtained with the final arrangement.

As may be seen from Fig. 3, the behavior of lead tetraethyl is similar to that of lead tetramethyl except for the lack of a pronounced resonance maximum in the current of the radical ion.

From the observations reported in the preceding paragraphs and the fact that the pressure of the lead alkyls in the furnace was very low (about 10^{-5} mm) it is clear that these compounds decompose on a hot quartz or tungsten surface to give primarily stable hydrocarbons, e.g., methane, ethylene, ethane, etc., at all temperatures. At first sight this result may seem to contradict the results of Paneth type experiments on the preparation and properties of free radicals.[1] The latter experiments are carried out at much higher pressures and the decompositions are probably homogeneous thermal gas reactions. Our results are those of purely heterogeneous dissociation of the lead alkyls, and may well depend on the past history of the quartz or tungsten surfaces involved.

RESULTS

I. The Methyl Radical

Curves *I* and *II* of Fig. 4 are the ionization efficiency curves for mass 15 (CH_3^+) obtained with 3.5 and 5.5 amperes through the furnace. Comparison with the curves of Fig. 2 indicates the following assignment of reactions to these ionization efficiency curves:

$$I.\ CH_3 \rightarrow CH_3^+ + \epsilon^- \qquad A_I(CH_3^+) = 10.0_0 \pm 0.1 \text{ ev}^4$$
$$II.\ CH_4 \rightarrow CH_3^+ + H + \epsilon^- \qquad A_{II}(CH_3^+) = 14.4_4 \pm 0.1 \text{ ev.}$$

The numerical values of the appearance potentials are based on the value $I^z(A) = 15.69$ ev for the ionization potential of argon.[5] This value is dependent on the old value of the conversion factor relating cm^{-1} to ev. If the new value,[6] 1 ev = 8066 cm^{-1}, is accepted $I^z(A) = 15.76$ ev and the appearance potentials should be increased 0.07 ev. Since the dissociation energies which we deduce from electron impact data involve differences between appearance potentials, the error in the absolute voltage scale cancels. The appearance potentials were taken from the initial breaks of the curves.[7] The appearance potential A_I is to be associated with the vertical ionization potential of the methyl

[4] The uncertainties indicated for the appearance potentials in this paper are meant to show the reproducibility and the accuracy of differences. The range of voltages within which the absolute values of the appearance potentials lie is probably about twice as great as the indicated uncertainty, e.g., $A_I(CH_3^+) = 10.0 \pm 0.2$ ev on an absolute scale.

[5] R. F. Bacher and S. Goudsmit, *Atomic Energy States* (McGraw-Hill, New York, 1932).

[6] G. Herzberg, *Molecular Spectra I* (Prentice-Hall, New York, 1939).

[7] D. P. Stevenson and J. A. Hipple, J. Am. Chem. Soc. **64**, 1588 (1942).

TABLE I. Summary of results.

Source	Furnace current	Fig. 4	Ion	$A(X^+)$	Reaction
$Pb(CH_3)_4$	3.5 amp.	I	CH_3^+	$10.0_0 \pm 0.1$ ev	$CH_3 \rightarrow CH_3^+ + \epsilon^-$
$Pb(CH_3)_4$	5.5 amp.	II	CH_3^+	$14.4_4 \pm 0.1$	$CH_4 \rightarrow CH_3^+ + H + \epsilon^-$
$Pb(C_2H_5)_4$	4.0 amp.	III	$C_2H_5^+$	$8.6_0 \pm 0.1$	$C_2H_5 \rightarrow C_2H_5^+ + \epsilon^-$
$Pb(C_2H_5)_4$	4.0 amp.	IV	$C_2H_4^+$	$10.8_4 \pm 0.1$	$C_2H_4 \rightarrow C_2H_4^+ + \epsilon^-$

radical. A_{II} agrees exactly with the value reported by Smith[8] for the appearance potential of CH_3^+ in the mass spectrum of methane.

Provided there is no activation energy for the formation of a bond between a methyl ion and a hydrogen atom, the difference, $A_{II} - A_I = 4.4_4 \pm 0.2$ ev, is equal to the strength of the first carbon-hydrogen bond of methane. This value of $D(CH_3 - H)$ is in much better agreement with the recent indirect estimate,[9] $4.3_8 \pm 0.2$ ev,[9] than the estimated uncertainty would lead us to expect.

The reason that the value reported by Fraser and Jewitt[2] for the ionization potential of the methyl radical, $I(CH_3) = 11.2 \pm 0.8$ ev, is so much higher than our value probably lies in the inability of their molecular beam technique to distinguish between the various thermal dissociation products of the lead tetramethyl. As there was no evidence to the contrary, they assumed the predominate product of the thermal decomposition to be the methyl radical. We found that under all conditions the yield of ethylene far exceeded that of methyl radicals, even at the very low pressure of lead tetramethyl we employed, as has been discussed above. Thus their ionization efficiency curve was probably a composite one representing the sum of ionization efficiency curves for the various ions arising from ionization and dissociation of ethylene, methane and the methyl radical.

Some rough measurements on the relative abundances of the lead-methyl ions, made with the furnace cold, showed the trimethyl lead ion to be about fifty times as abundant as the tetramethyl lead ion for 15-volt electrons. For this reason the ionization potential assigned to lead tetramethyl by Fraser and Jewitt should probably be associated with the appearance potential of $Pb(CH_3)_3^+$ in the $Pb(CH_3)_4$ spectrum. This absence of the parent ion from the mass spectrum has also been noted for tertiary butyl chloride.[10]

II. The Ethyl Radical

The furnace temperature was not as critical for the formation of ethyl radicals as for methyl radicals. Curves *III* and *IV* of Fig. 4 were taken with 4 amperes through the furnace. From their initial breaks we deduce

$$III.\ C_2H_5 \rightarrow C_2H_5^+ + \epsilon^- \quad A_{III}(C_2H_5^+) = 8.6_0 \pm 0.1 \text{ ev}$$
$$IV.\ C_2H_4 \rightarrow C_2H_4^+ + \epsilon^- \quad A_{IV}(C_2H_4^+) = 10.8_4 \pm 0.1 \text{ ev}.$$

Thus we have 8.6_0 ev for the vertical ionization potential of the ethyl radical. Equation *IV* was assigned to the appearance potential of $C_2H_4^+$ on the basis of the agreement of the value, $A_{IV}(C_2H_4^+) = 10.8_4$ ev, with that reported by Kusch, Hustrulid and Tate[11] for the appearance potential of this ion in the spectrum of ethylene.

Since Fig. 3 indicates that the $C_2H_4^+$ ion far exceeds the $C_2H_5^+$ ion in the spectrum obtained from the decomposition products of $Pb(C_2H_5)_4$, it is likely that Fraser and Jewitt were actually measuring the ionization potential of ethylene by their molecular beam technique rather than that of the ethyl radical. This is the most reasonable explanation of their value, 10.6 ± 0.8 ev.

As is the case with lead tetramethyl, the abundance of the parent ion in the $Pb(C_2H_5)_4$ spectrum

[8] L. G. Smith, Phys. Rev. **51**, 263 (1937).
[9] D. P. Stevenson, J. Chem. Phys. **10**, 291 (1942).
[10] D. P. Stevenson and J. A. Hipple, J. Am. Chem. Soc. **64**, 2766 (1942).
[11] P. Kusch, A. Hustrulid, and J. T. Tate, Phys. Rev. **52**, 843 (1937).

is almost unmeasurably small. Thus the value given by Fraser and Jewitt for the ionization potential of $Pb(C_2H_5)_4$ should probably be associated with the appearance potential of $Pb(C_2H_5)_3^+$.

From data on the appearance potentials of the ethyl ion in the spectra of ethane and *n*-butane, we deduce $8.6_8 \pm 0.2$ ev[7] for $I_{vert}(C_2H_5)$. The direct and indirect determinations are in excellent agreement.

The results described in this section, and the conditions under which they were obtained are summarized in Table I.

DISCUSSION

The indirect method[9] of determining dissociation energies, $D(\ )$, from electron impact data involves taking differences between appearance potentials of similar processes. Formally we have

$$R-R' \rightarrow R^+ + R' + \epsilon^-; \quad A_1(R^+) \geq \Delta E_1, \tag{1}$$

$$R-H \rightarrow R^+ + H + \epsilon^-; \quad A_2(R^+) \geq \Delta E_2, \tag{2}$$

$$R'-R+2H \rightarrow (R'-H)+(R-H); \quad \Delta E_3, \tag{3}$$

$$R'-H = R'+H; \quad D(R'-H) = \Delta E_1 - \Delta E_2 - \Delta E_3 \leqq A_1 - A_2 - \Delta E_3, \tag{4}$$

where the ΔE's are the minimum energies for the various processes. The equality sign in Eq. (4) for $D(R'-H)$ holds for two conditions: (1) The equalities $A_1 = \Delta E_1$ and $A_2 = \Delta E_2$, or (2) the appearance potentials A_1 and A_2 exceed ΔE_1 and ΔE_2 by the same amount.

The direct method of determining $D(\ )$'s from electron impact data is based on the equations

$$(R'-H) \rightarrow R'^+ + H + \epsilon^-; \quad A_5(R'^+) \geq \Delta E_5, \tag{5}$$

$$R' \rightarrow R'^+ + \epsilon^-; \quad A_6(R'^+) \geq I^s(R'), \tag{6}$$

$$(R'-H) = R'+H; \quad D(R'-H) = \Delta E_5 - I^s(R') \leqq A_5 - A_6. \tag{7}$$

Because process (6) involves the removal of a non-bonding electron from a radical R′ it seems reasonable to assume the equality of A_6 and I^s. Thus the direct method should give an upper limit for $D(R'-H)$. If R of Eq. (2) and R′ of (5) are similar, e.g., aliphatic radicals, one would expect A_2 and A_5 to deviate from ΔE_2 and ΔE_5 by the same amount. Under these conditions the only way $D(R'-H)$ calculated by Eq. (4) can agree with that calculated by Eq. (7) is for equality signs to hold for Eqs. (1), (2), and (5) and thus for (4) and (7). The excellent agreement found to obtain between the direct and indirect estimates of $D(CH_3-H)$ and $D(C_2H_5-H)$, indicated above, offers strong evidence for the absence of an activation energy in such reactions as

$$R^+ + H \rightarrow RH^+, \tag{8}$$

$$R^+ + CH_3 \rightarrow RCH_3^+, \tag{9}$$

where R^+ is an aliphatic radical ion.

The datum of Cummings and Bleakney[12] on the appearance potential of CH_3^+ in the methyl alcohol provides another check on the direct method of calculation.

$$CH_4 + H_2O = CH_3OH + H \qquad \Delta E^0 = 5.65 \text{ ev}, \tag{10}$$

$$CH_3OH \rightarrow CH_3^+ + OH + \epsilon^- \quad A(CH_3^+) = 14.0 \pm 0.4 \text{ ev}, \tag{11}$$

$$H + OH = H_2O \qquad \Delta E^0 = -5.17 \text{ ev}, \tag{12}$$

$$CH_3 \rightarrow CH_3^+ + \epsilon^- \qquad A(CH_3^+) = 10.0_0 \pm 0.1 \text{ ev}, \tag{13}$$

$$CH_4 = CH_3 + H; \quad D(CH_3-H) = 5.65 + 14.0 - 5.17 - 10.0 = 4.4_8 \pm 0.4 \text{ ev}. \tag{14}$$

[12] C. S. Cummings and W. Bleakney, Phys. Rev. **58**, 787 (1940).

Hipple's[13] datum on $A(CH_3^+)$ in the ethane spectrum does not lead to quite as good agreement.

$$2CH_4 = C_2H_6 + 2H \qquad \Delta E^0 = 5.18, \tag{15}$$

$$C_2H_6 \rightarrow CH_3^+ + CH_3 + \epsilon^- \qquad A(CH_3^+) = 14.2 \pm 0.4, \tag{16}$$

$$CH_3 \rightarrow CH_3^+ + \epsilon^- \qquad A(CH_3^+) = 10.0_0 \pm 0.1, \tag{13}$$

$$CH_4 = CH_3 + H \qquad 2D(CH_3-H) = 5.18 + 14.2 - 10.0 \tag{17}$$

$$D(CH_3-H) = 4.6_9 \pm 0.3 \text{ ev}.$$

The deviation of this value of $D(CH_3-H)$ from that which we accept, namely, $4.4_0 \pm 0.1$,[14] is almost large enough to be real. If the deviation is real, one must assign an activation energy of ~ 0.3 ev to the reaction $CH_3^+ + CH_3 \rightarrow C_2H_6^+$, but no activation energies to the reactions, $CH_3 + H \rightarrow CH_4^+$, $CH_3^+ + OH \rightarrow CH_3OH^+$, $C_2H_5^+ + CH_3 \rightarrow C_3H_8^+$, etc. It seems more likely that the value of $A(CH_3^+)$ in the ethane spectrum is in error by 0.2 to 0.3 ev.[15]

Data acquired by one of the authors on butene-1, on the other hand, clearly indicate that reactions involving the vinyl and allyl radical ions adding to H, CH_3, or C_2H_5 to form the corresponding olefinic ions require an activation energy of ~ 0.4 ev. The addition of a vinyl radical to an ethyl ion, however, seems to require no activation energy.

In a recent paper[7] it was pointed out that for exactly similar processes in various molecules, simple ionization for instance, the differences between the initial breaks of the ionization efficiency curves are equal to the differences between the intercepts of the extrapolated linear portions of the ionization efficiency curves. To state this in another manner, for such processes as $M \rightarrow M^+ + \epsilon^-$, the difference $V_L^- - V_B^- = 1.06_5 \pm 0.060$ ev where V_L^- is the linear intercept and V_B^- the initial break of the ionization efficiency curve. For eleven reactions of the type $R-R' \rightarrow R^+ + R' + \epsilon^-$, $V_L^- - V_B^- = 1.54 \pm 0.09$ ev. If the linear intercepts are used, the combination of the appearance potential of $C_2H_5^+$ in the ethane spectrum with $D(C_2H_5-H)$ leads to 9.1_7 ev for $I^e(C_2H_5)$, while the initial break gives 8.6_8. Both methods yield 8.6 ev when applied to the ionization efficiency curve of $C_2H_5^+$ in the ethyl radical spectrum. The fact that the value of $I^e(C_2H_5)$ deduced from the initial break of the ionization efficiency curve of $C_2H_5^+$ in the ethane spectrum agrees with the directly measured value offers further substantiation of our conclusion that the linear intercepts are not applicable to the determination of appearance potentials.[16]

It is interesting to note that the decrease in the vertical ionization potential brought about by the substitution of CH_3 for H in the methyl radical, 10.0 to 8.6 ev is parallel to the difference previously found between methane[8] and ethane,[7] ethylene[11] and propylene,[10] chlorine atom and methyl chloride,[17] and other similar pairs. Price[17] has discussed the reasons for these decreases.

In conclusion, we should like to express our sincere thanks to Dr. H. A. Beatty and his colleagues at the Ethyl Gasoline Corporation Research Laboratories for their generous cooperation in supplying us with the specially purified samples of the lead tetramethyl and lead tetraethyl.

[13] J. A. Hipple, Phys. Rev. **53**, 530 (1938).

[14] This value $D(CH_3-H) = 4.4_0 \pm 0.1$ seems to be a good representation of the indirect value, 4.3_8 ev (reference 9), the direct value from $I^e(CH_3)$ and $A(CH_3^+)$ in the methane spectrum 4.4_4, and the value recently deduced by Kistiakowsky and co-workers (J. Chem. Phys. **10**, 305 (1942)) from kinetic data, 4.3_8 ev. Similarly we take $D(C_2H_5-H) = 4.2_0 \pm 0.1$ from the indirect value, 4.1_6,[9] the direct value, 4.2_4, and the kinetic value 4.2_2. We have modified the values quoted by Kistiakowsky and co-workers to account for the difference between that which they took for $D(H-Br)$ and that given by Herzberg (reference 6).

[15] It should be noted that on the basis of the conclusions reached in the preceding paragraphs it is no longer possible to reconcile the electron impact values of $D(CH_3-H)$ with the estimate made by Burton (J. Chem. Phys. **6**, 818 (1938)) from photochemical data. See reference 9.

[16] D. P. Stevenson and J. A. Hipple, Phys. Rev. **62**, 237 (1942).

[17] W. C. Price, J. Chem. Phys. **4**, 539 (1936).

PHYSICAL REVIEW VOLUME 63, NUMBERS 3 AND 4 FEBRUARY 1 AND 15, 1943

Theory of the Magnetron. III

LÉON BRILLOUIN
Brown University, Providence, Rhode Island
(Received October 22, 1942)

The general theory of the magnetron tubes, as developed in a former paper, showed that the magnetron should sustain oscillations in an outer circuit, when the frequency was nearly $\sqrt{2}$ times the Larmor's frequency ω_H. The present paper contains a more detailed study of the behavior of a magnetron with one cylindrical anode, when the radius a of the filament and b of the anode are both taken into account. It is shown that the magnetron is able to sustain oscillations on the frequency

$$\omega=\omega_H(2+2a^4/b^4)^{\frac{1}{2}}$$

which lies between $\sqrt{2}\omega_H$ and $2\omega_H$, according to the dimensions of the electrodes. The agreement of this theory with some interesting results obtained by Blewett and Ramo is shown, and the limiting case of the plane magnetron is briefly discussed.

1. INTRODUCTION. PROPER OSCILLATIONS OF AN ELECTRON CLOUD IN A MAGNETIC FIELD

THE aim of the present paper is to give a more precise and accurate discussion of some results obtained in a former paper[1] and to show their agreement with a similar theory developed by Blewett and Ramo[2] and with the very interesting experimental proofs brought forth by these authors.

All the known effects, as the apparent change in dielectric power, and the possibility of sustaining oscillations depend on the fact that the rotating electron cloud has a proper frequency of oscillations (provided the radius of the filament can be neglected) given by

$$\omega=\sqrt{2}\omega_H, \tag{1}$$

where ω_H = Larmor frequency, as noticed in the previous paper. It can be shown by a very direct calculation how such oscillations of cylindrical symmetry will take place in the electron cloud. Equations have been obtained [see Eq. (12) of reference 1] for motions of this type

$$\dot{\eta}=C/r^2, \quad \ddot{r}/r=(e/m)2\pi\rho+\dot{\eta}^2-\omega_H^2, \tag{2}$$

where $\dot{\eta}$ is the angular velocity with respect to an axis rotating with Larmor angular velocity. Critical conditions, as observed in a magnetron, correspond to

$$C=0, \quad \dot{\eta}=0, \quad \rho_0=(m/2\pi e)\omega_H^2. \tag{3}$$

Let us now assume small oscillations of cylindrical symmetry to be excited in this cloud. An electron, originally located, at the instant t, at a distance r_0 will be displaced to

$$r=r_0(1+\xi) \text{ in which } \xi \text{ is small.} \tag{4}$$

This means an expansion of the whole cloud, the density of which becomes

$$\rho=\rho_0(1-2\xi) \tag{5}$$

so that the total electric charge ρr^2 remains constant. Introducing (4) and (5) in the equation of motion (2) one obtains

$$\ddot{r}/r=\ddot{\xi}/(1+\xi)=\omega_H^2(1-2\xi)-\omega_H^2$$

or

$$\ddot{\xi}=-2\omega_H^2\xi, \tag{6}$$

which yields very directly the proper frequency (1) of these cylindrical oscillations. It is now easy to understand how a medium possessing such a proper frequency of oscillations will show an abnormal behavior of its dielectric power,

$$\epsilon=1-(2\omega_H^2/\omega^2) \text{ e.s.u.} \tag{7}$$

as was proved both theoretically and experimentally by Blewett and Ramo.

Turning back to the problem of the magnetron and assuming these elementary calculations to yield a first approximation we come to the following conclusion: A magnetron, with a

[1] L. Brillouin, "Theory of the magnetron. I," Phys. Rev. **60**, 385 (1941) and Elec. Commun. **20**, 112 (1941).
[2] J. P. Blewett and S. Ramo, J. App. Phys. **12**, 856 (1941).

filament of radius a and an anode of radius b should behave like a cylindrical condenser filled with a medium of dielectric power ϵ [Eq. (7)]. Its capacity would then amount to

$$C=\frac{\epsilon}{2\log(b/a)} \tag{8}$$

per unit of length of the filament. This yields an impedance, at the frequency ω

$$Z=-\frac{i}{C\omega}=-i\frac{2\log(b/a)}{\omega\epsilon}=i\frac{2\omega\log(b/a)}{2\omega_H^2-\omega^2}. \tag{9}$$

Z would be positive for $\omega<\sqrt{2}\omega_H$ and negative for $\omega>\sqrt{2}\omega_H$, so that the magnetron would behave like a self-inductance below its frequency of resonance $\sqrt{2}\omega_H$, and like a capacity above this proper frequency.

Such a treatment is, however, just a crude first approximation; a more accurate discussion shows that the internal frequencies of oscillation are not constant throughout the electron cloud, but vary from $2\omega_H$ near the filament to $\sqrt{2}\omega_H$ at a distance. This will result in a modification of formula (9) as shall be shown in the next sections, where the problem of the positive or negative internal resistance will be discussed simultaneously.

2. INTERNAL IMPEDANCE OF A MAGNETRON

The theory developed in "Magnetron. I" for a one-anode magnetron is correct so far as Eq. (57) is concerned, but some approximations made in the deduction of Eq. (58) proved to be unreliable, and the calculations have to start again from that point.

It should be first noticed that all potentials $V(r)$ are with reference to the filament, taken as zero potential point. The current I per unit of length of the filament has been defined by a formula (38) and is thus taken as positive if running from the filament to the anode. This is the opposite of the usual assumption in electricity, where a current running from a point at potential zero to a point at a positive potential $V(b)$ should be counted as a negative current.[3] We shall now revert to these usual definitions and change the sign of the currents, writing

$$I_a=-J_a e^{i\omega t}$$

$$\int_{t_0}^{t} I_a dt=i(J_a/\omega)e^{i\omega t}[1-e^{-i\omega\tau}] \qquad t=t_0+\tau \tag{10}$$

instead of formula (54) in "Magnetron. I." As already noticed in Section 7 [Eq. (60)] of the earlier paper it is necessary, for physical and mathematical reasons, to add in Eq. (49) a small damping term s. This will result in the following small change in formula (57):

$$\frac{\partial V_a}{\partial r}=\frac{m}{e}\omega^2 r_a=J_a e^{i\omega t}\frac{2i\omega}{\omega^2(r)-\omega^2+is\omega}\frac{1-e^{-i\omega\tau}}{r}. \tag{11}$$

This formula gives the alternative potential $V_e(r)$ at a distance r; it contains the transit time τ from the filament ($r=a$) to r. The damping coefficient s is assumed to be very small, and its absolute value will play a very small role

The assumption is that the direct current I_e flowing through the magnetron is small enough not to perturb appreciably the potential distribution $V(r)$ inside the tube. The average potential should thus be the one obtained under critical conditions

$$V_e(r)=-\frac{m}{2e}\omega_H^2 r^2\left(1-\frac{a^2}{r^2}\right)^2 \tag{12}$$

as shown in "Magnetron. I," Eq. (51), while the space charge density is

$$\rho_e(r)=\frac{m\omega_H^2}{2\pi e}\left(1+\frac{a^4}{r^4}\right) \tag{13}$$

and the proper frequency, Eq. (52),

$$\omega^2(r)=2\omega_H^2\left(1+\frac{a^4}{r^4}\right). \tag{14}$$

The value of $\omega(r)$ thus decreases from $2\omega_H$ near the filament down to $\sqrt{2}\omega_H$ at a distance. We furthermore need the relation between transit time τ and distance r, which we obtain from Eq. (43), corrected for the change in the sign of the current:

$$\frac{2}{r}I_e\tau=-E(r)=\frac{\partial V_e}{\partial r}=-\frac{m}{e}\omega_H^2 r\left(1-\frac{a^4}{r^4}\right).$$

[3] The same correction was also applied in "Magnetron. II," Phys. Rev. **62**, 166 (1942), p. 175, before Eq. (77).

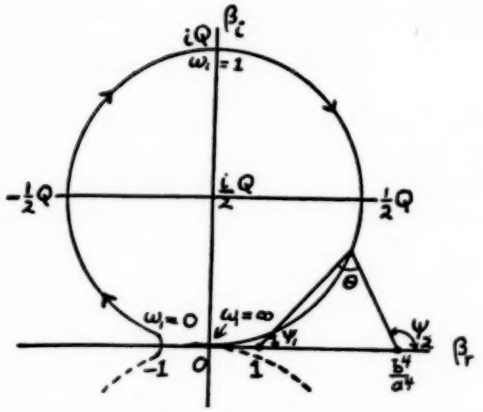

FIG. 1. Curve described by β in the imaginary plane, when ω increases.

Hence

$$\tau=-\frac{m\omega_H^2}{2I_e e}r^2\left(1-\frac{a^4}{r^4}\right)=\frac{r^2}{2\omega_H L^2}\left(1-\frac{a^4}{r^4}\right), \quad (15)$$

where L is the characteristic length defined in "Magnetron. I," Eq. (33).

$$L^2=-eI_e/m\omega_H{}^3.$$

This enables us to give a more precise statement of our assumptions: It is assumed that the direct current I_e is small enough to make L smaller than the radius of the filament:

$$L\ll a, \quad \xi_0=\omega a^2/2\omega_H L^2\gg 1. \quad (16)$$

Expressions (14) and (15) for ω^2 and τ must be used in formula (11) from which we obtain the potential $V_a(r)$:

$$V_a(r)=2i\omega J_a e^{i\omega t}$$
$$\times\int_a^r\left(\frac{1-e^{-i\xi}}{2\omega_H{}^2-\omega^2+is\omega+2\omega_H{}^2(a^4/r^4)}\right)\frac{dr}{r} \quad (17)$$

with

$$\xi(r)=\omega\tau(r)=\xi_0\left(\frac{r^2}{a^2}-\frac{a^2}{r^2}\right).$$

The problem is now to perform the integration, and to obtain the potential $V_a(b)$ on the anode, from which we deduce the internal impedance of the magnetron:

$$Z=\frac{V_a(b)}{J_a e^{i\omega t}}=2i\omega\int_a^b(\cdots)\frac{dr}{r}. \quad (18)$$

It is convenient to use a new variable ζ and to put

$$\zeta=r^2/a^2$$

$$\beta=\frac{-2\omega_H{}^2}{2\omega_H{}^2-\omega^2+is\omega}=2\omega_H{}^2\frac{\omega^2-2\omega_H{}^2+is\omega}{(2\omega_H{}^2-\omega^2)^2+s^2\omega^2}, \quad (19)$$

which yields

$$Z=\frac{i\omega}{2\omega_H{}^2-\omega^2+is\omega}$$
$$\times\int_{1-}^{\zeta-b^2/a^2}\frac{1-\exp\left[-i\xi_0(\zeta-1/\zeta)\right]}{\zeta^2-\beta}\zeta d\zeta. \quad (20)$$

This is the integral to discuss, and it should be stated that no approximations have been used, but for (15). These equations differ from those of "Magnetron. I," only for the introduction of the damping term s. The physical necessity for this damping term was already emphasized in "Magnetron. I," but one more word of explanation should be added: There is no damping term for a magnetron of infinite length, which does not emit any radiation (no more than an infinite solenoid or a toroidal one) but for a magnetron of finite length, damping is unavoidable, as any motion of the electrons inside the magnetron will result in electromagnetic fields emitted from both ends, and radiative dissipation of energy. There is also a possibility for energy dissipation inside the magnetron itself resulting from the non-linear terms which have been neglected in the equations.

3. INTEGRATION AND DISCUSSION

It is essential to discuss the variation of β and $\beta^{\frac{1}{2}}$ as functions of the frequency ω. The last expression must be of importance in the calculation of the integral (20), which has two poles

$$\zeta_P=\pm\beta^{\frac{1}{2}}, \quad \zeta_P{}^2=\beta. \quad (21)$$

This condition has a clear physical meaning, as it corresponds to the resonance on one of the internal frequencies of the electron cloud. If we neglect, for one moment, the damping term s (supposed to be very small) then condition (21) means

$$\omega^2=\omega^2(r)=2\omega_H{}^2(1+a^4/r^4) \quad (21a)$$

which indicates resonance on the layer at dis-

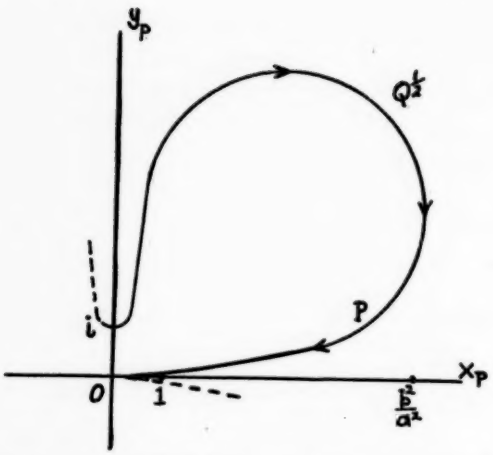

FIG. 2. Curve described by the poles P for increasing ω_1. $\zeta_P=\beta^{\frac{1}{2}}=x_P+iy_P$.

tance r. Here is the place where the approximations made in Section 1 prove unreliable: The radius a of the filament may be extremely small, but nevertheless, the inner proper frequencies always range from $\sqrt{2}\omega_H$ (r large) to $2\omega_H$ ($r=a$).

Figure 1 shows the motion of the point β in the complex plane, when ω varies from zero to infinity. According to Eq. (19)

$$\beta=\frac{1}{\omega_1^2-1-i(\omega_1/Q)}$$

with

$$\omega_1=\omega/\sqrt{2}\omega_H=y/\sqrt{2}, \quad Q=\sqrt{2}\omega_H/s. \quad (21b)$$

The curve starts from $\beta=-1$ for $\omega_1=0$ with a vertical tangent, and then runs upwards, with an almost circular shape. The upper point $\beta=iQ$ corresponds to $\omega_1=1$ while $\omega_1=\infty$ brings the representative point near the origin. The dotted curve corresponds to negative ω_1 and has no meaning in our problem. The damping term s is supposed to be very small, so that the Q factor will be extremely large. Figure 2 shows how the position of the poles $\beta^{\frac{1}{2}}$ varies with the frequency ω. For very low frequency the poles are in $\pm i$, then describe large loops, reach a very large distance $Q^{\frac{1}{2}}$ in the 45° direction (for $\omega_1=1$), and come back to 0 along the real axis, for ω_1 infinite.

The integral (20) is taken along the real axis, from $\zeta=1$ to b^2/a^2 and this path runs below the trajectory followed by the pole. The pole may, however, be very near to it (just above it) when its abscissa x lies between 1 and b^2/a^2 which means approximately

$$2\omega_H \gtrsim \omega \gtrsim \omega_H(2+2a^4/b^4)^{\frac{1}{2}}. \quad (22)$$

In case b is much greater than a the lower limit is very nearly $\sqrt{2}\omega_H$.

The integral (20) may conveniently be split into two parts

$$\int_{\zeta=1}^{\zeta=b^2/a^2} \cdots d\zeta = I_1+I_2,$$

$$I_1=\tfrac{1}{2}\int_1^{b^2/a^2}\frac{2\zeta d\zeta}{\zeta^2-\beta}=\tfrac{1}{2}|\log(\zeta^2-\beta)|_1^{b^2/a^2},$$

$$I_2=-\int_1^{b^2/a^2}\frac{\exp[-i\xi_0(\zeta-1/\zeta)]}{\zeta^2-\beta}\zeta d\zeta. \quad (23)$$

Integral I_1 is the logarithm of imaginary expressions

$$2I_1=\log[(b^4/a^4)-\beta]-\log(1-\beta). \quad (24)$$

Now, as well known, for an imaginary $\varphi=\varphi_r+i\varphi_i$

$$\log\varphi=\log|\varphi|+i\,\text{arctg}\,\varphi_i/\varphi_r, \quad |\varphi|^2=\varphi_r^2+\varphi_i^2.$$

Both terms in (24) are of the following type, with X real (1 or b^4/a^4) and $\beta=\beta_r+i\beta_i$ as in (21b),

$$\log(X-\beta)=\log|X-\beta|+i\,\text{arctg}\frac{\beta_i}{\beta_r-X}$$

$$=\log|X-\beta|+i\psi.$$

The ψ angles are indicated on Fig. 1, hence,

$$2I_1=\log\left|\frac{b^4/a^4-\beta}{1-\beta}\right|+i\theta, \quad \theta=\psi_2-\psi_1.$$

As noticed before, the damping coefficient s is very small, which means that Q is a *very large quantity*, and we assume

$$Q\gg b^4/a^4; \quad \beta\approx\beta_r, \quad \beta_i\approx 0. \quad (24a)$$

Figure 1 shows then that the angle θ is very small, except when the point P comes very near the integration path (conditions 22), in

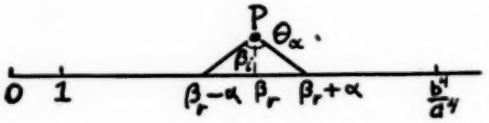

FIG. 3.

which case θ is practically equal to π. Finally

$$2I_1=\log\left|\frac{b^4/a^4-\beta_r}{1-\beta_r}\right|+i[\pi]; \tag{24b}$$

$[\pi]$ for conditions (22) only.

Turning now to the I_2 integral, in (23), we notice that the coefficient ξ_0 is large, so that the exponential oscillates very rapidly, which will practically result in cancelling the integration wherever the $\zeta/(\zeta^2-\beta)$ factor is a slowly varying function of ζ. Hence the most important part of the integral comes from the neighborhood of the poles $\zeta_P=\pm\beta^{\frac{1}{2}}$. As shown on Fig. 2, the pole with the plus sign may come near the integration path, which runs from 1 to b^2/a^2 along the real axis.

Two cases must be distinguished:

A—pole near the integration path, but outside of it.

$$\beta=\beta_r+i\beta_i \quad \text{and} \quad \beta_r\leqslant 1 \quad \text{or} \quad \beta_r\geqslant b^4/a^4.$$

B—pole near the integration path, and inside of it, which corresponds to conditions (22).

$$1<\beta_r<b^4/a^4.$$

Case *B* needs a special discussion before it can be reduced to a similar situation as in case *A*. We shall, in case *B*, divide the integration into 3 parts:

$$\begin{aligned}
&\text{I.} && 1\leqslant\zeta^2\leqslant\beta_r-\alpha && \beta_i \text{ negligible,}\\
&\text{II.} && \beta_r-\alpha\leqslant\zeta^2\leqslant\beta_r+\alpha && \text{exponential practically constant,}\\
&\text{III.} && \beta_r+\alpha\leqslant\zeta^2\leqslant b^4/a^4 && \beta_i \text{ negligible.}
\end{aligned} \tag{25}$$

α is a small quantity, which is chosen such as to satisfy the two following conditions:

$$\beta_i\ll\alpha\ll\frac{2\sqrt{\beta_r}}{\xi_0(1+1/\beta_r)}. \tag{25a}$$

The first inequality $\beta_i\ll\alpha$ enables one to neglect β_i in both intervals I and III where one has

$$\begin{aligned}
&\zeta^2-\beta=\zeta^2-\beta_r-i\beta_i\approx\zeta^2-\beta_r\\
&|\zeta^2-\beta_r|\geqslant\alpha\gg\beta_i.
\end{aligned} \tag{26}$$

The second inequality results in the fact that the exponential is practically constant inside the second interval where

$$\begin{aligned}
&\zeta=\sqrt{\beta_r}(1+\epsilon), \quad 1/\zeta=(1-\epsilon)/\sqrt{\beta_r},\\
&\zeta^2\approx\beta_r(1+2\epsilon),\\
&\xi_0[\zeta-(1/\zeta)]=\xi_0[\sqrt{\beta_r}-(1/\sqrt{\beta_r})]\\
&\qquad+\xi_0\epsilon[\sqrt{\beta_r}+(1/\sqrt{\beta_r})].
\end{aligned} \tag{27}$$

The exponential is practically constant and the ϵ term can be dropped if

$$\epsilon\xi_0[\sqrt{\beta_r}+(1/\sqrt{\beta_r})]\ll 1,$$

but the interval II is defined by

$$|\zeta^2-\beta_r|\leqslant\alpha \quad \text{or} \quad 2\beta_r|\epsilon|\leqslant\alpha,$$

and the inequality on ϵ is certainly satisfied if

$$\xi_0[\sqrt{\beta_r}+(1/\sqrt{\beta_r})](\alpha/2\beta_r)\ll 1,$$

which is the second condition stated in (25a). These conditions (25a) can be satisfied only if

$$\frac{\beta_i}{\sqrt{\beta_r}}\ll\frac{2}{\xi_0[1+(1/\beta_r)]} \tag{28}$$

and this will result in a condition to be fulfilled by the damping coefficient s or the Q factor. According to (21b) and (16)

$$\beta_r=\frac{\omega_1^2-1}{(\omega_1^2-1)^2+\omega_1^2/Q^2}\approx\frac{1}{\omega_1^2-1},$$

$$\beta_i=\frac{\omega_1/Q}{(\omega_1^2-1)^2+\omega_1^2/Q^2}\approx\frac{\omega_1}{Q(\omega_1^2-1)},$$

in which $1/Q^2$ is neglected.

$$\xi_0=\frac{\omega}{2\omega_H}\frac{a^2}{L^2}=\frac{\omega_1 a^2}{\sqrt{2}L^2}\gg 1.$$

Hence condition (28) yields

$$Q\gg\frac{\omega_1^4 a^2}{(\omega_1^2-1)^{\frac{1}{2}}2\sqrt{2}L^2}. \tag{29}$$

When condition *B* (that the pole be inside the interval of integration) is satisfied, the reduced frequency ω_1 lies between 1 and $\sqrt{2}$. On the other hand, ξ_0 is large, which means $L^2\ll a^2$, and condition (29) proves that Q must be very large in order to make our approximations reasonable.

This was always our general assumption. At any rate, conditions (24b) and (29) both postulate a very large Q value and extremely small damping coefficient s, which corresponds to actual conditions in magnetrons.

As a result of this discussion, we are left with the following integrals to calculate (case B, conditions 22):

$$I_2=-\int_1^{(\beta_r-\alpha)^{\frac{1}{2}}}-\int_{(\beta_r+\alpha)^{\frac{1}{2}}}^{b^2/a^2}\exp\left[-i\xi_0(\zeta-1/\zeta)\right]\frac{\zeta d\zeta}{\zeta^2-\beta_r}$$
$$-\exp\left[-i\xi_0(\sqrt{\beta_r}-1/\sqrt{\beta_r})\right]\int_{(\beta_r-\alpha)^{\frac{1}{2}}}^{(\beta_r+\alpha)^{\frac{1}{2}}}\frac{\zeta d\zeta}{\zeta^2-\beta_r-i\beta_i}. \quad (30)$$

The first two integrals correspond to cases I and III and the last one to case II. Let us first notice that we can add to the first two integrals an additional one, taken from $(\beta_r-\alpha)^{\frac{1}{2}}$ to $(\beta_r+\alpha)^{\frac{1}{2}}$ (on the interval II) and which is practically zero.

$$\int_{(\beta_r-\alpha)^{\frac{1}{2}}}^{(\beta_r+\alpha)^{\frac{1}{2}}}\exp\left[-i\xi_0(\zeta-1/\zeta)\right]\frac{\zeta d\zeta}{\zeta^2-\beta_r}\approx\exp\left(-i\xi_0[\sqrt{\beta_r}-(1/\sqrt{\beta_r})]\right)\int_{(\beta_r-\alpha)^{\frac{1}{2}}}^{(\beta_r+\alpha)^{\frac{1}{2}}}\frac{\zeta d\zeta}{\zeta^2-\beta_r}$$
$$=\tfrac{1}{2}\exp\left(-i\xi_0[\sqrt{\beta_r}-(1/\sqrt{\beta_r})]\right)\log|\alpha/\alpha|.$$

According to (27), the exponential is constant in this interval, hence the integral reduces to a logarithm, which is now taken on real quantities and yields $\log|\alpha/\alpha|=\log 1=0$. Integral (30) can thus be written

$$I_2=-\int_1^{b^2/a^2}\exp\left(-i\xi_0[\zeta-(1/\zeta)]\right)\frac{\zeta d\zeta}{\zeta^2-\beta_r}-\exp\left(-i\xi_0[\sqrt{\beta_r}-(1/\sqrt{\beta_r})]\right)\int_{(\beta_r-\alpha)^{\frac{1}{2}}}^{(\beta_r+\alpha)^{\frac{1}{2}}}\frac{\zeta d\zeta}{\zeta^2-\beta_r-i\beta_i}. \quad (31)$$

The last integral is again a logarithm, but contains an imaginary part β_i; it is similar to I_1 [Eq. (23)] but with different limits and yields

$$\int_{(\beta_r-\alpha)^{\frac{1}{2}}}^{(\beta_r+\alpha)^{\frac{1}{2}}}\frac{\zeta d\zeta}{\zeta^2-\beta_r-i\beta_i}=\tfrac{1}{2}\log\left|\frac{\alpha-i\beta_i}{\alpha+i\beta_i}\right|+\frac{i}{2}\theta_\alpha.$$

The angle θ_α, as shown on Fig. 3, is given by

$$tg(\theta_\alpha/2)=\alpha/\beta_i\gg 1, \quad \tfrac{1}{2}\theta_\alpha\approx\tfrac{1}{2}\pi,$$

according to the inequalities (25a), while the first log is zero. Summarizing these results we may write

$$I_2=-\int_1^{b^2/a^2}\exp\left(-i\xi_0[\zeta-(1/\zeta)]\right)\frac{\zeta d\zeta}{\zeta^2-\beta_r}-\left[\frac{i\pi}{2}\exp\left(-i\xi_0[\sqrt{\beta_r}-(1/\sqrt{\beta_r})]\right)\right], \quad (32)$$

where the last term inside the brackets has to be used only when conditions (22) (case B) are fulfilled.

We are left now with the problem of estimating the contribution of the first integral, where all the difficulties related with the imaginary part in the denominator have been excluded. This first integral now keeps the same type in both cases A and B.

As already noticed, the exponential oscillates very rapidly, and this practically cancels most of the integral, but for the neighborhood of the pole $\zeta_P=\beta_r^{\frac{1}{2}}$. Near this point we may conveniently use the following expansions:

$$\zeta=\sqrt{\beta_r}(1+\epsilon), \quad \zeta-1/\zeta=\sqrt{\beta_r}(1+\epsilon)-(1-\epsilon)/\sqrt{\beta_r},$$

$$I_2=-\tfrac{1}{2}\exp\left(-i\xi_0[\sqrt{\beta_r}-(1/\sqrt{\beta_r})]\right)\int_{\epsilon_1}^{\epsilon_2}\exp\left(-i\xi_0\epsilon[\sqrt{\beta_r}+(1/\sqrt{\beta_r})]\right)\frac{d\epsilon}{\epsilon}$$

$$=-\tfrac{1}{2}\exp\left(-i\xi_0[\sqrt{\beta_r}-(1/\sqrt{\beta_r})]\right)\int_{\eta_1}^{\eta_2}e^{-i\eta}\frac{d\eta}{\eta} \tag{33}$$

with $\eta=\xi_0\epsilon[\sqrt{\beta_r}+(1/\sqrt{\beta_r})]=\xi_0[1+(1/\beta_r)](\zeta-\sqrt{\beta_r})$.

The new integral in η is

$$\int_{\eta_1}^{\eta_2}e^{-i\eta}\frac{d\eta}{\eta}=\int_{\eta_1}^{\eta_2}(\cos\eta-i\sin\eta)\frac{d\eta}{\eta}=-Ci\eta_1+Ci\eta_2+i\,si\eta_1-i\,si\eta_2 \tag{34}$$

according to the usual definitions[4] of integral sines and cosines for positive x

$$Cix=-\int_x^\infty\cos t\frac{dt}{t},\quad six=-\int_x^\infty\sin t\frac{dt}{t}. \tag{35}$$

When x is negative, the same definition may be used for six as the point $x=0$ is no pole for this integral, and the relation holds

$$si(-x)=-\pi-six. \tag{36}$$

For $Ci(-x)$, our integration path runs through the pole, which means that we must take (see reference 4, p. 4)

$$Ci(-x)=Ci(x). \tag{37}$$

Here we shall notice that the additional $-\pi$ term in (36) comes into play only when the lower limit η_1 is negative, which means that conditions (22) (case B) are realized. But then we have also an additional term in (32), and these two terms exactly cancel each other, hence, we obtain the following formula, as a good approximation *for all cases:*

$$I_2=-\tfrac{1}{2}\exp\left(-i\xi_0[\sqrt{\beta_r}-(1/\sqrt{\beta_r})]\right)\{-Ci|\eta_1|+Ci|\eta_2|\pm isi|\eta_1|\mp isi|\eta_2|\}. \tag{38}$$

the lower signs, for the *si* functions, correspond to the case of negative arguments η_1 or η_2.

As well known, the *Ci* and *si* functions become rapidly very small for large values of the argument η

$$\eta\gg1,\quad Ci\eta\approx\frac{\sin\eta}{\eta},\quad si\eta\approx-\frac{\cos\eta}{\eta}. \tag{39}$$

These asymptotic expressions can be used as soon as η is larger than 2π. Now we must keep in mind that the approximate expression (38) for I_2 has been obtained only for small values of ϵ. But a small ϵ may mean a rather large η, according to (33), because ξ_0 is assumed to be large. Furthermore, we must notice that both I_2 and formula (38) become very small for large η and so we may, for practical purposes, assume formula (38) to hold for any value of η, even large. The limits are

$$\begin{aligned}&\zeta_1=1, &&\eta_1=\xi_0[1+(1/\beta_r)](1-\sqrt{\beta_r}),\\ &\zeta_2=b^2/a^2, &&\eta_2=\xi_0[1+(1/\beta_r)][(b^2/a^2)-\sqrt{\beta_r}].\end{aligned} \tag{40}$$

As soon as η_1 and η_2 are none too small (larger than 10), the asymptotic expansions (39) may be used

$$Ci|\eta|\mp isi|\eta|\approx(1/|\eta|)(\sin|\eta|\pm i\cos|\eta|)=(1/\eta)(\sin\eta+i\cos\eta)=(i/\eta)e^{-i\eta}. \tag{41}$$

Hence, the following result may be used only when η_1 or η_2 are not too small.

$$I_2\approx\frac{i}{2}\left\{\frac{1}{\eta_1}\exp\left[-i\xi_0\left(\sqrt{\beta_r}-\frac{1}{\sqrt{\beta_r}}\right)-i\eta_1\right]-\frac{1}{\eta_2}\exp\left[-i\xi_0\left(\sqrt{\beta_r}-\frac{1}{\sqrt{\beta_r}}\right)-i\eta_2\right]\right\}. \tag{42}$$

[4] E. Jahnke and F. Emde, *Tables of Functions* (Teubner, Berlin, 1938), third edition, p. 3.

But, according to the approximations used in (33),

$$\xi_0[\sqrt{\beta_r}-(1/\sqrt{\beta_r})]+\eta_2\approx\xi_0[\zeta_2-(1/\zeta_2)]=\xi_0[(b^2/a^2)-(a^2/b^2)],$$
$$\xi_0[\sqrt{\beta_r}-(1/\sqrt{\beta_r})]+\eta_1\approx\xi_0[\zeta_1-(1/\zeta_1)]=0. \tag{43}$$

Hence,

$$I_2\approx\frac{i}{2\xi_0[1+(1/\beta_r)]}\left[\frac{1}{1-\sqrt{\beta_r}}-\frac{\exp\left[-i\xi_0\{(b^2/a^2)-(a^2/b^2)\}\right]}{(b^2/a^2)-\sqrt{\beta_r}}\right]. \tag{44}$$

Returning now to Z from Eq. (20) and using (24b) and (44) we finally obtain

$$Z\approx\frac{\frac{1}{2}\omega}{2\omega_H^2-\omega^2+is\omega}\left\{i\log\left|\frac{b^4/a^4-\beta_r}{1-\beta_r}\right|-\frac{1}{\xi_0[1+(1/\beta_r)]}\right.$$
$$\left.\times\left[\frac{1}{1-\sqrt{\beta_r}}-\frac{\exp\{-i\xi_0[(b^2/a^2)-(a^2/b^2)]\}}{(b^2/a^2)-\sqrt{\beta_r}}-[\pi]\right]\right\}. \tag{45}$$

The $-[\pi]$ term comes in only when conditions (22) are fulfilled. One should be reminded that formula (45) is valid only for large $\eta_1\eta_2$ which means $\sqrt{\beta_r}$ is very different from 1 or b^2/a^2. Let us here notice the following:

1. s may now be neglected, as very small, its introduction was only necessary for the calculation of residues near the pole. Q is practically infinite, hence,
2. $\beta=\beta_r=-2\omega_H^2/(2\omega_H^2-\omega^2)$, (46)
3. $\xi_0[(b^2/a^2)-(a^2/b^2)]=\omega\tau_{ab}$.

τ_{ab} represents the transit time for electrons running from the cathode a to the anode b.

4. PRACTICAL RESULTS

Let us first assume the magnetron to be operated below its critical conditions, with no current flowing to the anode, which makes ξ_0 infinite and I_2 naught. Formula (45) then reduces to

$$Z\approx\frac{1}{2}\frac{\omega}{2\omega_H^2-\omega^2}\left\{i\log\left|\frac{(b^4/a^4)-\beta}{1-\beta}\right|-[\pi]\right\}, \tag{47}$$

the $[\pi]$ term comes in only when conditions (22) are fulfilled, namely:

$$\omega_H[2+(2a^4/b^4)]^{\frac{1}{2}}\leqslant\omega\leqslant 2\omega_H. \tag{22}$$

This proves that such a magnetron behaves like a pure inductance for low or high frequencies, and like an inductance plus a positive resistance for frequencies defined in (22). The following cases may be considered:

$$\omega\ll\sqrt{2}\omega_H,\quad -\infty\ll\beta<-1. \tag{48a}$$

For such low frequencies the $[\pi]$ term does not come in and

$$Z\approx-\frac{1}{2}\frac{i\omega}{2\omega_H^2-\omega^2}\log\left(\frac{(b^4/a^4)+|\beta|}{1+|\beta|}\right). \tag{49a}$$

$$\omega\gg 2\omega_H,\quad 0<\beta\ll 1. \tag{48b}$$

For very high frequencies the $[\pi]$ term also drops and

$$Z\approx-\frac{1}{2}\frac{i\omega}{2\omega_H^2-\omega^2}\log\left(\frac{b^4}{a^4}\right). \tag{49b}$$

This later case corresponds to the result predicted in Eq. (9) and checks the conclusions of Blewett and Ramo as explained in Section 1.

The formula (47) needs also a special discussion of the behavior near $\sqrt{2}\omega_H$, when the denominator is zero, as shown below. Let us assume $\omega^2=2\omega_H^2+\epsilon$, $\beta=2\omega_H^2/\epsilon$, ϵ small.

$$\frac{(b^4/a^4)-\beta}{1-\beta}=\frac{1-(\epsilon b^4/2\omega_H^2a^4)}{1-(\epsilon/2\omega_H^2)}=1+\frac{\epsilon}{2\omega_H^2}\left(1-\frac{b^4}{a^4}\right).$$

Hence,

$$\log\left|\frac{(b^4/a^4)-\beta}{1-\beta}\right|=\frac{\epsilon}{2\omega_H^2}\left[1-\left(\frac{b^4}{a^4}\right)\right]$$

and

$$Z=-\frac{i}{2}\frac{\omega}{(-\epsilon)}\frac{\epsilon}{2\omega_H^2}\left(1-\frac{b^4}{a^4}\right)=\frac{i}{2\sqrt{2}\omega_H}\left(\frac{b^4}{a^4}-1\right) \tag{50}$$

which remains finite. This shows that these conditions do not lead to any difficulty.

The resistance term in $[\pi]$, which comes in when conditions (22) are fulfilled is positive, as the minus sign before π is compensated by the negative denominator $2\omega_H^2-\omega^2$. It should be explained by the following physical considerations, based on the remarks made at the end of Section 2: When the frequency lies between the limits (22), a certain layer of the electronic space charge oscillates very strongly on resonance conditions and radiates energy outside of the magnetron through both ends of the magnetron.

Let us now assume that the magnetron is operated just above critical conditions, with a small current flowing to the anode and a large but finite ξ_0 value. The complete expressions from (38) must now be taken into consideration but for practical discussions we may use the simplified formula (45). The internal impedance of the magnetron will yield a real part R or resistance, with the following approximate values:

Case I. $\dfrac{b^2}{a^2}<\sqrt{\beta}, \quad 2\omega_H<\omega<\omega_H\left[2+\left(2\dfrac{a^4}{b^4}\right)\right]^{\frac{1}{2}}$

β very large,

$$R\approx\frac{\omega}{2\omega_H^2-\omega^2}\frac{\cos\xi_0[(b^2/a^2)-(a^2/b^2)]}{2\xi_0[1+(1/\beta)][(b^2/a^2)-\sqrt{\beta}]}. \quad (51)$$

Case II. $1<\sqrt{\beta}<b^2/a^2$ (conditions 22),

$$R\approx\frac{\omega}{\omega^2-2\omega_H^2}\left\{\frac{\pi}{2}+\frac{1}{2\xi_0[1+(1/\beta)]}\times\left[\frac{1}{1-\sqrt{\beta}}-\frac{\cos\xi_0[(b^2/a^2)-(a^2/b^2)]}{(b^2/a^2)-\sqrt{\beta}}\right]\right\}. \quad (52)$$

Case III. $\sqrt{\beta}<1, \quad \omega>2\omega_H,$

$$R\approx\frac{\omega}{\omega^2-2\omega_H^2}\frac{1}{2\xi_0[1+(1/\beta)](1-\sqrt{\beta})}. \quad (53)$$

Let us now discuss the sign of the resistance: In cases II and III the resistance is always positive. In case II, Eq. (52), ξ_0 is large and $\sqrt{\beta}$ lies between 1 and b^2/a^2 so that the first term in $\pi/2$, inside the brackets, is by far the most important. In case III, Eq. (53) the result is obviously positive. Hence the discussion is now centered on case I, which shows a certain number of frequency bands with negative resistance, according to the sign of the cosine. The denominator is positive, and we obtain

$$R<0 \quad \text{when} \quad \cos\xi_0(b^2/a^2-a^2/b^2)<0. \quad (54)$$

The negative resistance may reach high values when the frequency is such as to make the denominator D very small. By use of (46.2) we have

$$D=2\xi_0(2\omega_H^2-\omega^2)[1+(1/\beta)][(b^2/a^2)-\sqrt{\beta}]$$
$$=\xi_0(2\omega_H^2-\omega^2)\frac{\omega^2}{\omega_H^2}\left[\left(\frac{b^2}{a^2}\right)-\left(\frac{2\omega_H^2}{\omega^2-2\omega_H^2}\right)^{\frac{1}{2}}\right].$$

This amounts to

$$D=\xi_0(\omega^2/\omega_H^2)(\omega^2-2\omega_H^2)^{\frac{1}{2}}\times[\sqrt{2}\omega_H-(b^2/a^2)(\omega^2-2\omega_H^2)^{\frac{1}{2}}] \quad (55)$$

which is zero for

$$\omega=\sqrt{2}\omega_H \quad (56\text{I})$$

or

$$\omega=\omega_H(2+2a^4/b^4)^{\frac{1}{2}}. \quad (56\text{II})$$

The first case does not seem of real importance, first because the corresponding zero would be avoided by keeping the damping term s as in Eq. (45) and second because the calculations and approximations made in Eq. (33) and following are no more reliable, as for such frequencies the pole runs far away from the integration path, on the line at 45° (Fig. 2). Hence it does not seem that the negative resistance might reach any high value near the frequency (56I).

The second root (56II) is much more important as it means that the frequency ω is just the one which sets into resonance the space charge density near the anode. The conclusion of all this discussion is the following:

One anode magnetrons should yield a number of very narrow frequency bands with negative resistance [Eq. (54)] *for frequencies lying just below the limit* (56II).

This checks the general conclusion of a former paper (Magnetron. I). One should notice here that the negative resistance R does not become infinite on the limit (56II), as Eq. (51) seems to indicate. Near this limit, the approximate formula (45) should not be used any more, as it rests on the use of asymptotic expansions (39).

One should revert to the original formula (38) with integral sines and cosines, thus avoiding infinite R values.

5. PLANE MAGNETRON

As an example of application of the general theory, the case of the plane magnetron will be briefly discussed. This case is obtained as the limit of a cylindrical magnetron when the radius a of the filament is increased to infinity, while the distance $d=b-a$ between filament and anode is kept constant. Hence

$$a\to\infty, \quad b=a+d=a(1+p_b). \tag{57}$$

A point at a distance r from the center will be defined by a parameter p:

$$r=a(1+p) \tag{58}$$

in which $p=(r-a)/a$ is small. The angular velocity of the electrons is given by Eq. (15) of "Magnetron. I" which now reads

$$\dot\theta=\omega_H[1-(a^2/r^2)]=\omega_H(1-1/(1+p)^2)$$
$$\approx\omega_H(2p-3p^2\cdots). \tag{59}$$

This means that the tangential velocity becomes

$$\dot x=r\dot\theta=2a\omega_H p(1+p)(1-\tfrac{3}{2}p)\approx 2\omega_H a p(1-\tfrac{1}{2}p).$$

Denoting y the distance $r-a$ from the surface of the cathode, we obtain

$$\dot x=2\omega_H y[1-(y/2a)]. \tag{60}$$

For the plane magnetron ($a\to\infty$) the x velocity increases proportionately to the distance y from the cathode.

Under critical conditions (no current on the anode), the space charge density is given by Eq. (25) of "Magnetron. I":

$$\rho=\frac{m\omega_H^2}{2\pi e}\left(1+\frac{a^4}{r^4}\right)\approx\frac{m\omega_H^2}{\pi e}(1-2p), \tag{61}$$

which on the limit of a plane magnetron ($p=0$), is a constant. In a plane magnetron (of infinite length) operated under critical conditions, there is a uniform space charge density (61) between the plane cathode and the plane anode. These charges have no perpendicular component of velocity ($\dot y=0$) and move parallel to the electrodes with a velocity $\dot x$ given by Eq. (60). The voltage V is obtained from Eq. (23) of "Magnetron. I."

$$V_0(r)=-\frac{m\omega_H^2}{2e}\left[r-\left(\frac{a^2}{r}\right)\right]^2$$
$$=-\frac{m\omega_H^2}{2e}a^2\left(1+p-\frac{1}{1+p}\right)^2\approx\frac{2m\omega_H^2}{e}a^2p^2(1-p)$$

or

$$V_0(y)=\frac{2m\omega_H^2}{e}y^2\left(1-\frac{y}{a}\right). \tag{62}$$

This yields the anode voltage $V(b)$ when $y=d$ is inserted in the formula. When the total electric charge Q between the electrodes is computed, it comes out to be

$$Q=-V_0L/2\pi d, \tag{63}$$

L is the length measured along the x axis, and the calculation refers to a unit length of the filament. The plane magnetron thus yields a capacity twice as large as a plane condenser of same dimensions.

Such a plane magnetron can be used for sustaining oscillations, and the discussion of the preceding section shows that it should oscillate in the neighborhood of the frequency

$$\omega=2\omega_H, \quad \frac{b}{a}\longrightarrow 1, \tag{64}$$

which corresponds to the proper frequency of vibration for the electronic layers near the filament, as emphasized in Section 1.

It is a pleasant duty for me to thank Professor Le Corbeiller for many helpful criticisms and suggestions.

Letters to the Editor

PROMPT publication of brief reports of important discoveries in physics may be secured by addressing them to this department. The closing date for this department is the third of the month. Because of the late closing date for the section no proof can be shown to authors. The Board of Editors does not hold itself responsible for the opinions expressed by the correspondents. Communications should not in general exceed 600 words in length.

Thermal Equilibrium Between Elementary Particles

GLEB WATAGHIN
Department of Physics, University of Sao Paulo, Brazil
January 2, 1943

RECENT investigations by C. F. Weiszäcker,[1] S. Chandrasekhar,[2] and L. R. Henrich on the prestellar stage of the universe, based on the actual distribution of chemical elements and on the theory of thermal reactions between nuclei and elementary particles, induce me to publish further remarks on an earlier study[3] of thermal equilibrium between elementary particles at extremely high temperatures.

The chief feature of the statistical equilibrium at temperatures $T>8\times10^{9}$°C ($\kappa T>2mc^2$, where m is the mass of the electron) is the production of pairs by photons having energy $h\nu>2mc^2$. In these conditions (as was stated in the above-mentioned papers) the energy of the rest mass mc^2 takes part in the exchanges of thermal energy and, by increasing the temperature, the total inertial or gravitational mass of the created pairs increases also proportionally to T^3. An exact calculation of the constants of degeneracy which appear in these new statistical conditions leads us to the following conclusions: At temperatures $T>2mc^2/\kappa$, the concentrations n^+ and n^- of positrons and electrons and N of photons with $h\nu>2mc^2$ are nearly equal (as in the energetic cascade showers)

$$n^+\sim n^-\sim N\sim(16\pi/c^3h^3)(\kappa T)^3.$$

The constant of degeneracy α which appears in the formulae:

$$n^-=\frac{8\pi}{c^3h^3}(\kappa T)^3\int_{x_0}^{\infty}\frac{(x^2-x_0^2)^{\frac{1}{2}}x\,dx}{e^{-\alpha+x}+1},$$

$$n^+=\frac{8\pi}{c^3h^3}(\kappa T)^3\int_{x_0}^{\infty}\frac{(x^2-x_0^2)^{\frac{1}{2}}x\,dx}{e^{\alpha+x}+1},$$

where $x_0=mc^2/\kappa T$, $x=E/\kappa T$, and E is the total relativistic energy component, is given approximately by: $n^+/n^-\leqq e^{-2\alpha}$ or, in the case $\alpha\ll1$, $\alpha\sim(n^--n^+)/(n^-+n^+)$.

In the case of thermal equilibrium between protons, neutrons, electrons, and photons, the general formulae obtained for a constant number of heavy particles lead to the result that at temperatures $\gtrsim(1/\kappa)2mc^2$, at which $\alpha\lesssim1$ and $n^+\gtrsim n^-$ is greater than the concentration of heavy particles, the number of protons is nearly equal to the number of neutrons. The statistical laws above-mentioned suffer an alteration at temperatures $T\gtrsim6\times10^{12}$° if the definition of distinguishable and independent quantum states is altered in a manner proposed by the author,[4] so that the asymptotic number of states in an interval $(p, p+dp)$ is $(8\pi V/h^3)g(p)p^2dp$, where $g(p)$ is a "cut off factor."

An entirely new situation appears in the conditions in which the total energy of the assembly is so high that the average kinetic energy $\bar{E}$ of a proton or neutron is $\bar{E}\gg\mu c^2\sim10^9$ ev, where μ is the rest mass of the meson. In these conditions, as seems to follow from the experimental evidence on cosmic rays, the high energy primaries give rise to the creation of particles by explosion showers, producing groups of mesons, electrons, photons, and neutrinos, and in each of such collisions a considerable amount of primary energy can be transformed into neutrinos (through meson decay or directly). On the basis of the theory of these collisions proposed recently by the author,[5] we must expect that no equilibrium condition is possible in these cases and that the idea of a temperature $\kappa T\gg2\mu c^2$ cannot be introduced in the usual way in an assembly of heavy particles. One must expect a rapid transformation of the energy of the heavy particles into the energy of the created ones. The kinetic energy of the proton results divided among a great number of particles of average kinetic energy $\sim2\mu c^2$ and is simultaneously transformed into the energy of the rest mass (μc^2) of the created particles and into the gravitational energy.

One of the most important features of the collisions in which many particles are simultaneously created (including mesons and neutrinos) is the irreversibility, due to the vanishing probability for the inverse processes. This probability depends obviously on the cross section for a nearly simultaneous collision of n particles of energy $\sim2\mu c^2$, which decreases rapidly with increasing n. If the number of created particles is proportional to the primary energy measured in the frame of the center of masses, the inverse transition to the high energy states has a probability which tends to 0 with increasing energy E. So the equilibrium is practically impossible, because the conditions of detailed balance cannot be fulfilled in an assembly of elementary particles having plausible concentrations.

If the property of creation of groups of particles in the high energy collisions is not only limited to the heavy particles (as we want to assume), we are led to the conclusion that the value $T_c\sim(1/\kappa)2\mu c^2\sim6\times10^{12}$ degrees of the temperature indicates a separation between two different types of thermal processes, the usual one well below T_c and the others in which a statistical equilibrium is practically impossible and in which the creation of mesons and neutrinos constitutes the dominant feature of the collision process. Instead of the neutrino hypothesis one can abandon the conservation laws of energy and momentum. Then, for instance, the disappearance of a great amount of energy in β-processes and decay processes would produce a decrease of the intensity of gravitational forces and thus an increase of gravitational energy (in accordance with a well-known suggestion of Landau).

[1] C. F. Weiszäcker, Zeits. f. Physik. **38**, 176 (1937); **39**, 633 (1938).
[2] S. Chandrasekhar, Astrophys. J. **95**, 288 (March, 1942).
[3] Phil. Mag. **17**, 910 (May, 1934); Comptes rendus, 909 (March 11, 1935).
[4] G. Wataghin, Nature **142**, 393 (1938).
[5] G. Wataghin, Symposium on Cosmic Rays, Rio de Janeiro (August, 1941), An. Acad. Brasil. Sci. (Dec. 1942).

Proceedings of the American Physical Society

Meeting at Los Angeles, California, December 29, 1942

THE 252nd meeting of the American Physical Society was held in the University of California at Los Angeles, on Tuesday, December 29, 1942. The attendance at the two sessions varied from 40 to 45, which is greater than anticipated, in view of the trying conditions under which the meeting was held. Most of those in attendance had luncheon together, Tuesday noon, in the faculty dining room of Kerckhoff Hall.

Of the 18 papers whose abstracts are given below, only one, No. 7, was read by title. Professor S. J. Barnett gave a detailed account of his own extensive researches in the field of gyromagnetism. This was an invited paper, given at the close of the morning session. By previous arrangement, and with the consent of the society, Professor Millikan expanded paper No. 11 into a half-hour invited paper.

R. T. Birge
Local Secretary for the Pacific Coast

Abstracts of Contributed Papers

1. The Polarization of the Absorption Spectra of Neodymium Ions in Crystals. Robert W. Krueger, *Douglas Aircraft Company*, and E. L. Kinsey, *University of California at Los Angeles.*—It has been discovered that many of the sharp electronic lines in the absorption spectrum of crystals containing neodymium ions are polarized. Photographs were taken of the absorption spectra of neodymium ions in crystals of $NdCl_3 \cdot 6H_2O$ and $Nd(BrO_3)_3 \cdot 9H_2O$ cut in various directions with respect to the crystallographic axes, using polarized light. The polarization effect has been successfully explained by the assumption of a perturbing field having the symmetry of the arrangement of the water molecules surrounding the neodymium ion. This field produces a splitting of each unperturbed energy level into a number of component levels equal to the number of irreducible representations of the symmetry group contained in a reducible representation presented by the $2J+1$ unperturbed eigenfunctions corresponding to the unperturbed energy level. When the mixing of unperturbed eigenfunctions to produce a perturbed one is simple, polarization effects become pronounced. Knowing the correct mixing from group theory, one can predict polarizations, using the correct selection rules which are found to be those for forced electric dipole radiation. The splitting and polarization effects observed in at least four groups of lines in the bromate spectrum substantiate the theory very well.

2. On the Heat Transfer from Radiating Gases to Water Tubes of a Boiler. R. M. Langer and G. Potapenko, *California Institute of Technology.*—The transfer of heat from radiating gases to water tubes of a heat exchanger depends upon the arrangement of tubes, because this arrangement determines the "radiant path length," i.e., the average thickness of gas layer which a tube faces. The theory developed allows one to calculate the radiant path length for any arrangement of tubes. The application of the theory to the case of water tube boilers permits a complete physical analysis of heat exchange in such boilers and leads to the following general formula showing the temperature of gases at any point along the pipes:

$$2xF=\left\{\left(\frac{T^2(0)}{T^2(x)}-1\right)-\tfrac{2}{3}A\left(\frac{T^3(0)}{T^3(x)}-1\right)+\cdots\right\},$$

where x is the distance along the boiler under consideration, F is the fraction of the heat content of the entering gases which is absorbed in the first unit of length. $T(x)$ and $T(0)$ are the gas temperatures at a point x and at $x=0$, respectively. A is the ratio of the convective to the radiative heat transfer coefficient. In the part of the boiler where the radiative heat transfer predominates, A is small and only the first term in the brackets needs to be considered. If ΔT is the temperature rise due to combustion of the fuel gases and if the efficiency of boiler of a length x is $E(x)$ then $T(0)-T(x)=E(x)\Delta T$. The quantities F, A, and ΔT can be calculated for any given set of operating conditions and so it is possible to calculate the length of a boiler for any desired efficiency E, and vice versa.

3. The Production of Photons Relative to Ionization by Collision in a Townsend Gap. Ronald Geballe, *University of California.*—Measurements were made in a Townsend gap to determine the average number of photons liberated by an electron for each secondary electron it liberates. Gases used included H_2, N_2, A, and air. In H_2, this number was found to decrease rapidly with increasing ratio of field strength to gas pressure, in the range from 50 to 150 volts/cm/mm, and at pressures of the order of one millimeter. Determination of the absolute number of photons per electron depends on the unknown efficiency of the photoelectric cell used to count the photons. However,

this number is estimated as of order unity. In H_2, the effective radiation has an absorption coefficient of 0.55 ± 0.2 cm^{-1} at a pressure of one millimeter of mercury. This large coefficient indicates that only those photons of rather high energy were counted. There is corroborative evidence that the brass surface of the photoelectric cell had a high work function. Thus only high energy photons would be expected to register. Photoelectric currents in the other gases were too small to be measured with the available apparatus. It thus appears that these gases have absorption coefficients for the effective radiation even higher than that found in H_2.

4. The Magnetic Properties of Iron-Cerium Alloys. J. R. CLARK,* S. T. PAN, AND A. R. KAUFMANN, *Massachusetts Institute of Technology.*—The susceptibility and magnetization of iron-cerium alloys containing 1.07 to 37.8 atomic percent (0.44 to 19.8 weight percent) iron have been measured in fields up to 35,000 gauss and at temperatures from 77°K to 1200°K. The structure of the alloys has been investigated by means of x-ray diffraction patterns recorded at 77°K, 195°K, and 300°K. The alloys containing up to about 30 atomic percent iron have a ferromagnetic Curie point at about 275°K; the alloy containing 37.8 atomic percent iron has a ferromagnetic Curie point at about 475°K. Below 275°K the intercept magnetization increases with decreasing temperature and increasing iron content, but there is an abrupt change in the magnetic properties between 150°K and 100°K. At 150°K the alloys are readily saturated; but below 100°K the susceptibility is field-dependent in fields up to 35,000 gauss, the field-dependency being most pronounced in the higher iron-content alloys. The appearance of new lines and a change in the relative intensities of the face-centered cubic lines at 77°K indicate a structural change in the 1.07 atomic percent iron alloy. This transformation is not apparent in the alloys containing more iron. The Curie points observed are believed to be due to intermediate phases of the Fe-Ce system. The relation between the structural and magnetic transformations at low temperature requires further investigation.

* Now at Stanford University.

5. Theoretical Dependence of Continuous X-Ray Intensity and Polarization upon Several Experimental Parameters. PAUL KIRKPATRICK, *Stanford University.*—The Sommerfeld theory of the continuous x-ray spectrum from thin or atomic targets has been put by Weinstock into a form which makes computation feasible. Encouraged by certain agreements between this theory and our experiments, computations have been conducted of the dependence of intensity and polarization upon target atomic number, radiation frequency, bombardment energy, and spatial distribution. The computations are still laborious, requiring about six hours of the work of a skilled computer per calculated point. They make possible for the first time the visualization of the principal features of the spectrum. Curves and space models are used to display the functional relations disclosed.

6. Direct and Fluorescence Excitation of the L_{III} Level in Thick Targets of Thorium. BURR G. BURBANK, *Stanford University.* (*Introduced by Paul Kirkpatrick.*)—X-rays from an oil-cooled thorium target were analyzed by a Bragg spectrometer, the intensities at the peak of the $L\alpha$ line and in its continuous background at both sides being measured. The line intensity was partly produced by direct cathode electron ionization of the thorium atoms and partly by ionization produced by absorption of the thorium continuous spectrum. To determine the ratio of these components auxiliary measurements were performed in which the thorium target was covered by a foil of palladium thick enough to prevent direct ionization of the thorium and to provide a palladium continuous spectrum sufficiently intense to excite a measurable intensity of Th $L\alpha$ by photoelectric ionization. From measurement of this purely indirect line excitation the indirect component with pure thorium targets was computed by a procedure taking account of the relative continuous background intensities in the two experiments. The ratio of the number of $L\alpha$ line quanta produced by direct electron collision to the number produced by fluorescence for normally emergent x-rays from a thick thorium target was found to be 2.8 for 40-kv electrons. Determinations were made in the range from 40 to 100 kv.

7. Inelastic Scattering of Slow Neutrons. ROBERT WEINSTOCK, *Stanford University.*—The first-order (single phonon emission or absorption) inelastic scattering cross section for neutrons by polycrystals has been calculated. The Born approximation and the Fermi (δ-function) interaction between slow neutrons and bound nuclei are employed. In the preliminary work, attention is limited to spin-free nuclei, and both isotopic disorder and magnetic interaction are neglected. The Debye approximation of a constant sound velocity is used. The ratio of the probability of a first-order process to zero order (elastic) is found to be roughly of the order of neutron mass divided by scattering nucleus mass. At temperatures high compared with the Debye temperature of the scatterer, however, the inelastic cross section may become larger than this ratio indicates. Computations carried out for Fe scattering room temperature neutrons show a rise from three percent at 151°K to 27 percent at 1000°K for the ratio of (first order) inelastic to elastic scattering cross section. The sum of these cross sections, however, varies only slightly over this temperature range. Future work will take into account both isotopic disorder and magnetic interaction.

8. Dimensional Characteristics of the Large Scale Condensations of Matter in the Universe. F. ZWICKY, *California Institute of Technology.*—It is one of the most fundamental facts of observation that the large scale distribution of matter is very far from uniform. Clusters of nebulae, nebulae, and stars the dimensions of which are of the order 10^{25} cm, 10^{22} cm, and 10^{11} cm, respectively, represent the most conspicuous condensations on a cosmic scale. A complete theory of the structures of these condensations is lacking because it involves the statistical mechanics of cooperative gravitational systems, a discipline which has

not yet been developed. General considerations coupled with dimensional analysis show that the "structural length" α for clusters of nebulae and for nebulae must be of the order $k(\bar{\epsilon}_k/\Gamma\rho_0)^{\frac{1}{2}}$ where $\bar{\epsilon}_k$ is the average kinetic energy per unit mass of all the matter in the universe, ρ_0 its average density, Γ the universal gravitational constant, and k a dimensionless constant. For individual clusters of matter which are in stationary equilibrium k assumes the value $(12\pi)^{-\frac{1}{2}}$ if ρ_0 denotes the central density. These conclusions are checked through a comparison with the data obtained on the three large clusters of nebulae in Coma, in Perseus, and in Hydra.

9. Static Charges Produced on Moving Rubber-Tired Vehicles. S. S. MACKEOWN AND VICTOR WOUK, *California Institute of Technology.*—The current flowing from an automobile whose rear wheels were turning on a dynamometer was measured. These results show that the total current generated is proportional to speed, independent of load or tire pressure. Measurements made when the tires were made semi-conducting and with a series resistance suggest a simple equivalent electric circuit that is consistent with the experimental results. Approximate values of the constants of this equivalent circuit were obtained. Constant currents as high as 4 microamperes were obtained at a speed corresponding to 40 miles per hour. These results were checked by road tests. The tires are sufficiently conducting to discharge the automobile in a short time after the car is stopped.

10. Preliminary Energy Distribution Curve of Cosmic Rays. L. KATZ, R. V. ADAMS, JR., AND W. E. DEEDS, *California Institute of Technology. (Introduced by C. D. Anderson.)*—Several test runs have been made with the twenty-four inch, vertical cloud chamber at a field strength of approximately 5000 gauss. A preliminary energy distribution curve has been made, on the basis of measurements of 107 tracks, with energies ranging from 100 Mev to 31,000 Mev. Altogether, there were 54 tracks of negative particles, 51 of positive particles, and 2 of doubtful sign. In the region above 5000 Mev there were 5 negatives, 9 positives, and 2 doubtful cases. The tentative curve shows several secondary maxima, including one at 1700 Mev, which may or may not be due to statistical variation.

11. The Origin of Cosmic Rays. ROBERT A. MILLIKAN, H. VICTOR NEHER, AND WILLIAM H. PICKERING, *California Institute of Technology.*—The authors had predicted that since their hypothetical silicon-annihilation rays should have enough energy (13.2 bev) to get through the earth's magnetic field at the equator in Peru, though not in India, there should be found both at sea level and at all altitudes in the Americas a very long plateau of uniform, vertical cosmic-ray intensities extending north from Peru clear up about to the magnetic latitude of Victoria, Mexico (32.8° N Mag.). There the strong band due to the annihilation of the oxygen atom (computed energy 7.5 billion electron volts) should first begin to be able to break vertically through the earth's magnetic field. This prediction and others deducible from the hypothesis were experimentally tested in Mexico and the United States in December, 1940, with no results as yet found anywhere at variance with the atom-annihilation hypothesis.

12. An Improved Cosmic-Ray Radio Sonde. WILLIAM H. PICKERING, *California Institute of Technology.*—A description will be given of the cosmic-ray radio sonde used for the measurements described in the preceding paper (No. 11). The chief difference between this and the preceding instrument lies in the method used to scale down the counts. This is now done at the receiving station. The transmitted pulses are made sufficiently short to avoid any loss of efficiency at high counting rates.

13. Mesotron Mass and Heavy Tracks on Mt. Evans. CARL E. NIELSEN AND WILSON M. POWELL, *University of California.*—A cloud chamber in a 2500 oersted field was so operated that diffuse tracks permitting ionization measurement by droplet count were photographed. A few slow mesotrons with ionization and curvature suitable for mass determination were observed in the approximately 7000 photographs taken at 14,100 ft. and the 1500 at 12,700 ft. Preliminary measurement of two of the best tracks indicates a mass of about 200 electron masses; the mass is determinable from each track to within ± 15 percent. There were observed also many heavily ionized tracks made by protons or heavier particles—several such appear in each hundred photographs. A count is being made of the relative frequency of these heavy tracks at the two elevations; the decrease with elevation is not conspicuous.

14. Collision Electrons Accompanying Mesotrons in Lead at 10,000 Feet. WAYNE E. HAZEN, *University of California. (Introduced by R. B. Brode.)*—A cylindrical cloud chamber (30 by 30 cm) containing eight 0.6 cm lead plates was expanded at random. Two thousand of the photographs have been studied for the production of knock-on electrons in the lead. In these photographs 4540 particles traversed at least three plates without multiplication but only 4570 traversals were classified as suitable for the observation of knock-on electrons. Since 340 electrons were observed, of which only 2.5 percent passed through another 0.6 cm of lead, the plates were thick enough to establish equilibrium. Ten percent of the knock-on electrons were noticeably scattered in the gas and therefore had energies less than 10^8 ev. There were two cases of small showers accompanying mesotrons out of the lead, one of three and the other of four particles. From the above data the probability that a collision electron accompanies a mesotron in lead is 7.5 ± 0.5 percent. Seren[1] found 9.7 percent for the probability that a collision electron with $E>4\times 10^8$ ev accompanies a mesotron in lead at sea level. The difference is probably a consequence of the higher mean energy for mesotrons at sea level.

[1] L. Seren, Phys. Rev. 62, 204 (1942).

15. Optical Constants of Electron Microscopes. L. MARTON AND R. G. E. HUTTER, *Stanford University.*—In electron microscopical work it has been previously assumed that the field of the objective lens which extends

beyond the specimen into the region between it and the condenser lens is not strong enough to exert an appreciable converging effect on the illuminating beam of electrons. Recent calculations of Glaser[1] and Dosse[2] show that if the object is placed at a distance from the lens where the spherical aberration becomes a minimum, the converging effect is far from negligible. Taking into account the necessary corrections for such an extended objective field and with a minimum of assumptions, several optical constants of the electron microscope are recalculated. For the new values thus obtained, the resolution of the instrument is calculated and the role of the limiting factors discussed.

[1] Zeits. f. Physik 117, 285 (1941).
[2] Zeits. f. Physik 117, 316 (1941).

16. The Influence Function for a Cubic Lattice. H. BATEMAN, *California Institute of Technology.*—In 1912 Born and Kármán studied the periodic solutions of a differential difference equation analogous to the wave equation for a homogeneous isotropic medium. An expression is now found for the disturbance produced when one member of an elastic lattice system is given an initial displacement or velocity.

17. Theory of Elastic Oscillations in Plates and Shells. PAUL S. EPSTEIN, *California Institute of Technology.*—The assumptions forming the foundation of the classical theory of plates and shells are open to the objection of being arbitrary. A new theory meeting this objection is offered and carried through for the following cases: (1) with respect to terms of zero order in the thickness of the shell (h), for shells of any shape; (2) with respect to terms of second order in h, for circularly cylindric shells (including, as a special case, plane parallel plates). The zero-order terms turn out to be identical with those resulting from the classical theory, while the second-order terms are different. The new theory gives a satisfactory account of torsional oscillations which cause difficulties in the classical theory.

18. Continuous Radiation in Prismatic X-Ray Spectra. PAUL KIRKPATRICK, *Stanford University.*—In determining e/m by x-ray reflection and refraction[1] Stauss observed in his prismatic x-ray spectrograms unexpected refraction between the $K\alpha$ lines of Mo and the undeviated beam. He was inclined to attribute this radiation to imperfection of the surfaces of his quartz prism. Pardue[2] while investigating the dispersion of x-rays in calcite noticed the same effect and attributed it to refracted continuous spectrum radiation of wave-length less than that of the molybdenum lines. The band possessed a sharp edge on the *long wave* side which he thought might be a result of a deposit of tungsten on the molybdenum target. It is shown in the present work, using a glass prism, that the band is indeed continuous radiation since it responds appropriately to voltage and filtration variations. The sharp edge on the long wave side is found to be a photographic effect caused by the K discontinuity of the silver in the film.

[1] H. E. Stauss, Phys. Rev. **36**, 1101 (1930).
[2] L. A. Pardue, Phys. Rev. **38**, 1808 (1931).

AUTHOR INDEX TO ABSTRACTS OF PAPERS PRESENTED AT THE LOS ANGELES MEETING

Adams, R. V., Jr.—see Katz, L.

Bateman, H.—No. 16
Burbank, Burr G.—No. 6

Clark, J. R., S. T. Pan, and A. R. Kaufman—No. 4

Deeds, W. E.—see Katz, L.

Epstein, Paul S.—No. 17

Geballe, Ronald—No. 3

Hazen, Wayne E.—No. 14
Hutter, R. G. E.—see Marton, L.

Katz, L., R. V. Adams, Jr., and W. E. Deeds—No. 10
Kaufman, A. R.—see Clark, J. R.
Kinsey, E. L.—see Krueger, Robert W.
Kirkpatrick, Paul—Nos. 5 and 18
Krueger, Robert W. and E. L. Kinsey—No. 1

Langer, R. M. and G. Potapenko—No. 2

MacKeown, S. S. and Victor Wouk—No. 9
Marton, L. and R. G. E. Hutter—No. 15
Millikan, Robert A., H. Victor Neher, and William H. Pickering—No. 11

Neher, H. Victor—see Millikan, Robert A.
Nielsen, Carl E. and Wilson M. Powell—No. 13

Pan, S. T.—see Clark, J. R.
Pickering, William H.—No. 12
—— see Millikan, Robert A.
Potapenko, G.—see R. M. Langer
Powell, Wilson M.—see Nielsen, Carl E.

Weinstock, Robert—No. 7
Wouk, Victor—see MacKeown, S. S.

Zwicky, F.—No. 8